Università degli Studi di Napoli
Federico II

Tesi di Dottorato di Ricerca in
Tecnologie Innovative per Materiali Sensori ed Imaging
XVII ciclo

New frontiers in liquid crystal photonics:
from active Bragg gratings to mirrorless lasing

Antigone Marino

Napoli, Dicembre 2004

This thesis work has been performed at
Soft Matter Optics Lab of the
Physical Science Department
"Federico II" University of Naples

antigone@na.infn.it
http://people.na.infn.it/~antigone

Contents

Acknowledgments

Writing down this thesis the past three years passed through my mind, and with them all the people involved.

My special thanks go, first and foremost, to Professor Abbate, who followed my research with judgement, giving me the freedom to act on my way, and at the same time supporting my decisions and stimulating my work with wide and interesting discussions.

I would like to thank Francesco (I should say Dr. Vita). When he started in our laboratory he was my first thesis student, and now he is the first person with whom I share my scientific doubts. I'm further grateful to Dr. Tkachenko for the intense participation he showed in my work.

I never will forget the months spent in Ohio working beside Professor Palffy-Muhoray at the Liquid Crystal Institute (LCI) of Kent State University, dreaming of my country, but also appreciating the American way of making scientific research.

I also would like to acknowledge the Italian Liquid Crystal Society (SICL) for the opportunity I had to meet other scientists with whom I exchanged information and most of all new ideas to pursue this project's aim. Among them I would like to mention Professor Umeton and his coworkers from University of Calabria for the materials they provided me.

Curiosity and creativity have been playing a significant role in this thesis. That is why the sincerest thanks go to all the people near me who stimulated my creativity, believing in its importance: my family and my friends.

Introduction

In the last decades the telecommunication world has undergone an highest development. The request of faster and more widespread communications, due to the larger number of users, mostly day by bay more exigent, opens the way to the research of the most innovative, operative and cost-effective technology to implement this request. Since several years, optical fibers have supplanted traditional systems, like cable, satellite and radio-link, yielding the transmission more reliable and faster. Nevertheless, the performances of the fiber network are not utilized enough, because of the signal processing at the network nodes. This task, in fact, is carried out by electronic devices, which require a signal conversion from optical to electric, the elaboration of the signal itself, and at least a new conversion into an optical signal, in order to reinsert it in the fiber. These steps strongly limit the network performances, in terms of losses and speed. Hence, the challenge for companies and research groups worldwide is to render "optical" not only the signal transmission, but also its processing, reducing the fiber coupling losses and making the transmission speeder [1].

To reach this aim, a strong competition among different technologies has started and a winning comprehensive one is not already established. The technologies in question are Lithium Niobate ($LiNbO_3$), Micro-electro-mechanical systems (MEMS), bubbles, thermo-optic switching, Liquid Crystals and others.

The idea to use Liquid Crystals (LCs) dates back to the 70's: after the first impressive success of LC materials in the display area, scientists thought to exploit the large electrooptic coefficient, the high birefringence and the low-viscosity liquid nature of LCs in the design of

photonic devices. Interesting results showed that the capability of LCs to affect the light propagation in guided systems could be used to realize devices for the optical signal processing. But these results were abandoned (now we should say "frozen") because the drawbacks, mainly in terms of optical losses, were too relevant to foresee an effective technological development.

During the 90's this idea was resumed. Owing to the progress in soft matter science and technology, the recent scientific advances in LCs-based photonic devices have had a first non-negligible influence in real applications and in the market. A number of companies in U.S. are already offering few LCs-based photonic devices and also few European ones are interested in developing such components.

In this perspective, the aim of my PhD research was to realize optoelectronic devices having functionalities of interest for optical communication systems using as active materials liquid crystals. The first chapter of this thesis outlines the wonderful properties of LCs, and their exploitation in the telecom world, giving also some LCs-based telecom devices examples. The work focuses the attention on two innovative devices: the first one is an active Bragg grating realized with a composite liquid crystal and polymer material, and the second one is a distributed feedback laser realized with cholesteric liquid crystals.

An active Bragg grating filter is a key component for the realization of several devices for Dense Wavelength Division Multiplexing (DWDM) systems, like switches, add-and-drop systems, beam deflectors or routers. For instance, one of the easiest way to realize an optical multiplexing/de-multiplexing device is to integrate one or several switchable gratings in a guiding system such as a fiber or a waveguide.

An holographic grating can be written by an interference pattern over a composite liquid crystal and polymer material. Choosing the suitable parameters, like the pitch, the thickness, and the average refractive index, the grating can be written in order to observe the Bragg condition. Gratings observing this condition are called Bragg gratings. As LCs are active materials, using an external field, or changing the temperature,

the grating average refractive index can be modulated and the diffraction properties of the active Bragg grating can be changed and driven.

Using different recipes, several groups obtained gratings, whose operating mode is based on the same physical phenomenon, but yield to different features.

In this thesis I give an optical characterization of a new kind of active Bragg grating, called POLICRYPS, both in the visible range, at $\lambda = 632{:}8\text{nm}$, and in the near infrared (NIR), at $\lambda = 1550\text{nm}$, that is the C-band of the 3^{rd} window for optical communications. The samples have been kindly provided by the Professor C. Umeton group from University of Calabria, developers of this new device, in the frame of a running Italian National Research Project (PRIN), in which I am involved.

The name POLICRYPS stands for "Polymer Liquid Crystal Stripes". In fact, the device is composed by a sequence of homogeneously aligned LC layers separated by isotropic polymer walls. The optical contrast between the two series of stripes gives rise to the diffraction grating: it is electrically switchable because the application of an electric voltage drives the LC stripes in an optical state, whose constants are almost matched with those of the isotropic stripes. This switching effect can be obtained also by a temperature variation. From the beginning, these gratings have been designed to work in the visible, but their characterization in the NIR has been a compulsory task for the optimization of the telecom device.

Measurements had been performed with both stationary and dynamic electric fields to outline their diffraction efficiency, the switching voltage, the switching temperature, the angular response, the losses and the dynamical response. These results not only show the good operation of the device at both wavelength, but also point out some peculiar features of the POLICRYPS material, like the non negligible weight that forces at the interface between polymer and liquid crystal might have. Compared to others kind of active Bragg gratings, like Holographic Polymer Dispersed Liquid Crystal (HPDLC), POLICRYPS gratings show smaller switching voltage, higher efficiency and a faster electrooptical

response. Nevertheless, there are some drawbacks, like a strong dependence on the light polarization. In this thesis the second and the third chapters are focused respectively on the theory of holographic gratings and on POLICRYPS gratings.

The second device handled in this research project is a distributed feedback (DFB) laser made of cholesteric liquid crystals.

DWDM systems impose stringent requirements on laser: first and foremost a dynamic single mode operation, a narrow linewidth, low threshold and high speed. Several laser structures have been designed to achieve single mode operation and among them the most promising seems to be the DFB laser operation.

In general, the resonator structure of a laser provides the feedback necessary for the build-up of oscillations. If the medium shows a spatial variation of the refractive index, this feedback mechanism can be distributed inside the medium: the feedback is provided by backward Bragg scattering, and moreover the grating-like nature of the device provides a filter mechanism which restricts the oscillation to a narrow spectral range.

Cholestric Liquid Crystals (CLCs) show a periodic spatial variation of the refractive index. These are chiral nematic liquid crystals: due to chirality, the direction of the average molecular orientation varies linearly with the position, giving rise to a self-assembling helicoidal structure. Adding a suitable fluorescent dye inside the CLC and pumping the mixture we can have a mirrorless laser emission. The cholesteric acts like a distributed cavity and the dye as active material. Such a mirrorless laser has the advantage to be self-assembling and easy to integrate into fiber as fiber sensor.

In order to optimize the lasing conditions, I have studied the dependence of the lasing threshold on the dye concentration and sample thickness, carrying out the possible physical process responsible for the observed behaviour. The fourth and the fifth chapters offer respectively a survey on the propagation of light in cholesteric LCs and on the threshold effect in cholesteric liquid crystal.

The two studied devices have many points in common. Both exploit the periodicity of the soft material they are made of: in the Active Bragg grating this periodicity is realized through a polymerization process, while in the DFB laser it is self-assembly. Both are easy to integrate in fibers becuase they are realized with soft material. The performances of both can be driven by a temperature change, or by an external electric force. Finally, I outline the possibility to realize a tunable distributed feedback laser inside a dye-doped active Bragg grating, combining the properties of the two studied devices.

Every day we are witness, but without too much consciousness, of one of the most innovative technology realized during our century: the liquid crystal display. This widespread application of liquid crystal has attracted a larger and larger number of scientists to study this mysterious state of matter. In my opinion, Liquid Crystals are the proof that a research that is at the same time basic research and applied research is possible.

Papers

Papers included in this thesis

- **PAPER I**
  Policryps Characterization in the Near Infrared ,
  G. Abbate, A. Marino, F. Vita,
  Mol. Cryst. and Liq. Cryst., 398, 269 (2003).

- **PAPER II**
  Dynamical Behaviour of Policryps Gratings,
  A. Marino, F. Vita, V. Tkachenko, R. Caputo, C. Umeton, A. Veltri, G. Abbate,
  Eur. Phys. J. E, 15, 47-52 (2004);
  Electronic Liquid Crystal Communications, 2004/Jan/29.

- **PAPER III**
  Lasing Thresholds of Cholesteric Liquid Crystals Lasers,
  W. Cao, A. Marino, G. Abbate, P. Palffy-Muhoray, B. Taheri,
  accepted for publication in Mol. Cryst. and Liq. Cryst.;
  Electronic Liquid Crystal Communications, 2004/Oct/16.

- **PAPER IV**
  Mueller-Matrix Characterization of Liquid Crystals,
  J. N. Hilfiker, C. M. Herzinger, T. Wagner, A.Marino, G. Delgais, and G. Abbate,
  Thin Solid Films, 455-456, 591 (2004).

- **PAPER V**
  Spectroscopic Ellipsometry Study of Liquid Crystal and Polymeric Thin Films in Visible and Near Infrared,
  V. Tkachenko, A. Marino, F. Vita, F. D'Amore, L. De Stefano, M. Malinconico, M. Rippa, G. Abbate,
  Eur. Phys. J. E, 14, 185-192 (2004);
  Electronic Liquid Crystal Communications, 2004/Feb/26.

Papers on liquid crystal photonics not contained in this thesis

- *Dynamical Electro-optical Characterization of Policryps Gratings,*
  G. Abbate, A. Marino, F. Vita
  Acta Phys. Polon., A, 103, 177 (2003).
- *ZLI-1695 Liquid Crystal Anisotropy Characterization in the Near Infrared by Generalized Ellipsometry*,
  G. Abbate, G. Del Gais, L. De Stefano, A. Marino, T. Wagner,
  Mol. Cryst. and Liq. Cryst. , 398 249 (2003).
- *Policryps Characterization in the Near Infrared*,
  G. Abbate, A. Marino, F. Vita,
  Mol. Cryst and Liq. Cryst., 398, 269 (2003).

Chapter 1

Liquid Crystals

Most people are familiar with liquid crystals world, but not many of them have dwelled upon this strange name. If they did, the common reaction was “how can a crystal be liquid!”. It can be.

Liquid crystals (LC) are thought like material, even if they are not. This mistake rise from the fact that they are used in common objects like displays and they are presented from the commercial market like materials. To be correct (or more physicist) the “liquid crystal” is a phase of the matter, like the solid, the liquid, the gas and the plasma phases. The liquid crystal phase is an intermediate phase between the solid and the liquid. Only some materials presents these phases, hence these materials are improperly named Liquid Crystals.

Solids, liquids, and gases respond to electric and magnetic fields, but the responsce is minimal even when strong fields are applied. Liquid Crystals, on the contrary, respond to even weak electric and magnetic fields with significant structural changes.

Liquid crystals have been known since 1888 when F. Reinitzer found two melting points in the materials cholesterol benzoate and cholesterol acetate, but it was not until the late 1960’s that the development of applications utilizing liquid crystals started. Today liquid crystals displays (LCDs) are very common and almost everyone own or use a liquid crystal device. In a near future we will certainly see liquid crystals in a diversity of new products, like rolled up displays, light modulators,

switches, optical components, and probably applications that have not been thought yet!

1.1 Liquid Crystal Phases

The states of matter are distinguishable for the different amounts of order of the material molecules. The solid state consists of a rigid arrangement of molecules: they are constrained to occupy a specific position and they are oriented in a specific way. The molecules might vibrate, but the highly ordered arrangement is maintained. This arrangement causes the large attractive forces between individual molecules to add them together. Hence, it takes large external forces to disrupt the structure. Unlike in the liquid phase the molecules neither occupy a specific average position nor remain oriented in a particular orientation. The amount of order is therefore much less than in a solid. Attractive forces still exist, but the random motion of molecules does not allow the forces between individual molecules to add together. That's why a liquid maintains a constant density, even if it takes the shape of its container.

Summarizing we can say that a solid possesses *positional order*, that is molecules are constrained to occupy only certain positions. Moreover it possessed *orientational order*, because molecules in these specific positions are constrained in the ways they orient themselves with respect to another. When solid melts to liquid, both types of orders are completely lost.

However, during this transition can happen that the positional order is lost, but some of the orientational order remains: the liquid crystal phase possesses orientational order and not positional order (Figure 1.1).

Liquid Crystals are anisotropic organic material: their constituent molecules are fairly rigid, elongated objects. For pure systems, phase transitions are most easily induced by varying the temperature, these systems are called *thermotropic liquid crystals*; for systems of rods in

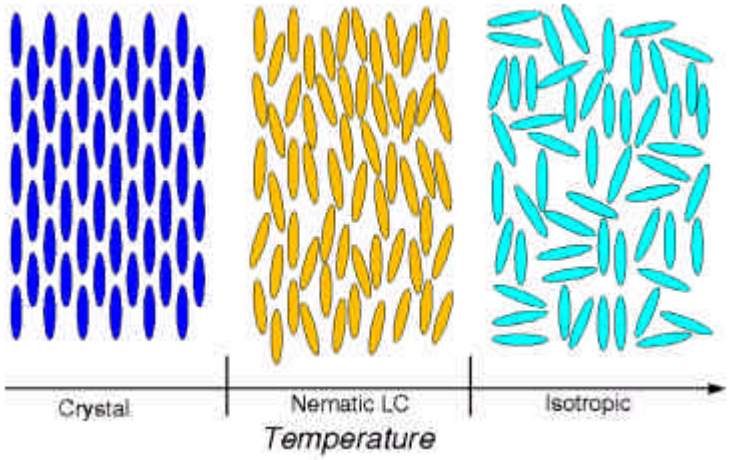

Figure 1.1. The Liquid Crystal phase appears between the Solid and the Liquid: increasing the temperature the positional order is lost, while the orientational remains.

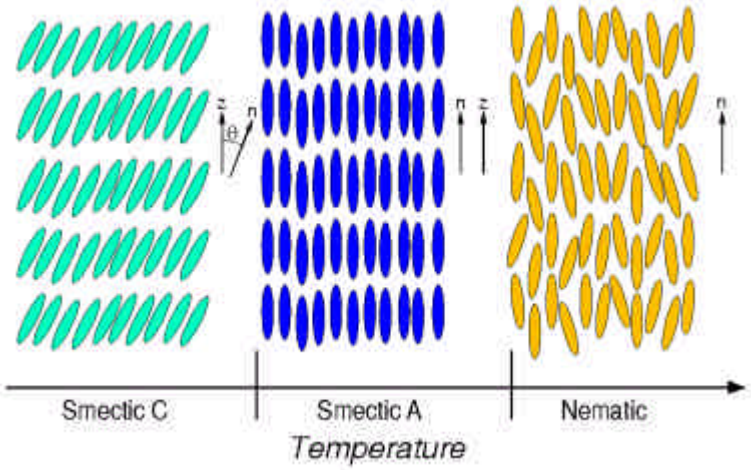

Figure 1.2. Phase sequence for a Liquid Crystal material. The degree of order decreases with increasing the temperature. Liquid crystals materials commonly do not exhibit all the phases shown in figure.

solution, phase transitions are most easily induced by varying the concentration of rods, these are called *lyotropic liquid crystals*. In the present work, only thermotropic LCs are considered.

The geometrical anisotropy of LC molecules gives rise to various liquid crystal mesophases, all of them characterized by a different degree of positional order. In general, the order of the subsequent phases decreases with increasing the temperature, going from the crystal phases to the isotropic phase passing through the Smectic C, Smectic A and Nematic (Figure 1.2):

- The least ordered liquid crystal phase is the *Nematic* (N) phase where the molecules have no positional order but long range orientational order. Here all the molecules tend to align with their long axes in a preferred direction described by the unit vector $\mathbf{b}$ called the *molecular director*. The nematic is a uniaxial medium where the states $\mathbf{b}$ and $-\mathbf{b}$ are indistinguishable (see Figure 1.2c).

$$\mathbf{b} \equiv -\mathbf{b} \tag{1.1}$$

- A higher degree of order is found in *Smectic* liquid crystals. In addition to the orientational order of the director, there is also positional ordering of the molecules in at least one dimension, i.e. the molecules are ordered in layers.

  - In the *Smectic A* phase (SmA) the director is perpendicular to the smectic layers and parallel to the smectic layer normal z (see Figure 1.2b).
  - In the *Smectic C* phase (SmC) the director is tilted with respect to the smectic layer normal (see Figure 1.2b). The angle between z and $\mathbf{b}$ is called the tilt angle.

Many other mesophases exist, like the *Smectic B* (SmB) in which the layers are not entirely liquid, and the molecules tend to arrange hexago-

nally. Liquid crystals materials commonly do not exhibit all this mesophases. Summarizing we can say that for thermotropic liquid crystal material displaying all these phases, the phase sequence with increasing the temperature is

Crystalline ! SmB ! SmC ! SmA ! N ! Isotropic

1.1.1 Chiral Liquid Crystal Phases

We can have liquid crystals with chiral molecules: we remind that a chiral object is one which is not superposable on its mirror image. In that case there will be a tendency of forming a helicoidal structure and new mesophases need to be defined:

- A nematic phase with chiral molecules becomes distorted in a helical structure. The director rotates around an axis, named the helix axis, being everywhere perpendicular to it. The pitch of the helix is a full turn through $360^{\pm}$, and, due to the invariance condition of Equation (1.1), the period of the helix is half of the value of the pitch (Figure 1.3a). Chiral nematics (N*)[1] are called cholesterics[2].
- In the chiral Smectic A (SmA*) there is no helical distortion. In fact, if the molecules were to form a helix with the director perpendicular to the helix axis, the smectic layers should necessarily break, and this will require a big amount of energy. That's why does not usually occur, and the SmA* phase is geometrically indistinguishable from the SmA, but they present different physical properties.

[1] The * stays for chiral.

[2] If the twisting power is very strong in the cholesteric phase, other phases called blue phases may appear between the cholesteric and the isotropic. In the blue phases there is a twist of the medium in more than one dimension. Liquid crystal appears organized in disclination lines filling the space in a cubic structure. The lattice constant of the blue phases is of the order of the wavelength of visible light, that is why they are called "blue".

² In the chiral Smectic C (SmC*) helical distortion appears, with the helix axis parallel to the smectic layer normal (Figure 1.3b). In this phase, since molecules are tilted with respect to the smectic layer normal **k**, the system has an other degree of freedom: the direction of the tilt plane, specified from **b** and **k**.

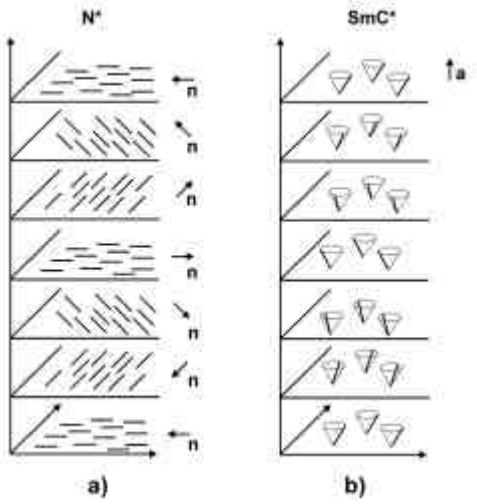

Figure 1.3. Chirality and Liquid Crystals: a) chiral nematic, also called Cholesteric (N*); b) Chiral Smectic C (SmC*).

1.2 Physics of Nematic LCs

As said before, in Nematic Liquid Crystals (NLCs) the centres of gravity of the molecules have no long-range order. However, there is some orientational order, all the rod-like molecules tend to align in a preferred direction described by the *molecular director*.

Let us label c the rod axis, and take the average direction of alignment of the molecules n along the z-axis. We shall define c by its polar

angles μ and $'$ where

$$\begin{aligned} c_x &= \sin\mu\cos' \\ c_y &= \sin\mu\sin' \\ c_z &= \cos\mu \end{aligned}$$

The state of alignment of a nematic can be described by the function $f(\mu;')d\text{-}$, which is the probability of finding rods in a small solid angle $d\text{-} = \sin\mu d\mu d'$ around the direction $(\mu;')$. To describe properly the features of a nematic, $f(\mu;')$ might have some requirements:

1) it must be independent of $'$, because of the cylindrical symmetry about n;
2) $f(\mu) = f(¼ ¡ \mu)$, due to the equivalence between n and $¡n$.

Instead of using the full function $f(\mu)$, one prefers to use only one related numerical parameter. The average value

$$\langle\cos\mu\rangle = \langle c¢n\rangle = \int f(\mu)\cos\mu d\text{-},$$

cannot be used: in fact, it vanishes identically because for the second property. The first non-zero multipole is the quadrupole [2], defined as

$$S = \frac{1}{2}\left\langle 3\cos^2\mu ¡ 1\right\rangle = \int f(\mu)\frac{1}{2}\left(3\cos^2\mu ¡ 1\right)d\text{-}.$$

- If all the molecules are parallel to the z, it means $\mu = 0;¼$, thus $\cos\mu = §1$ and $S = 1$.
- If they are oriented perpendicular to z, it means $\mu = ¼=2$, and $S = 1=2$.
- If orientations is random, $f(\mu)$ is independent of μ; we would have $\langle\cos^2\mu\rangle = \frac{1}{3}$ and $S = 0$.

Clearly $f(\mu)$, and so S, critically depends on temperature.

1.2.1 The Continuum Theory

In the previous section we have considered a macroscopically uniform medium, in which n and S are independent on their position in the space. This approximation is not always true. Let us, now, consider a macroscopically small but microscopically large volume inside the bulk of a liquid crystal. The volume contains a sufficiently large number of molecules so that long-range molecular order and the director are well defined in that region. If we divide the liquid crystal in such small volumes with an orientational direction in each of them we can define this direction at any point in the medium as long as we in fact relate every point with a small region of space. The liquid crystal is then treated as a continuous medium.

At a given temperature T, the $n(r)$ distribution of a liquid crystal can be found describing by system by its free energy density, imposing the boundary conditions, and minimizing the free energy density. Hence, the main part of the procedure is to find the right expression of the free energy density F_d.

The deformation of the liquid crystal is just a change in molecular orientation, and not in molecular density, i.e. the deformations are gradients in the director field. For most of the situation of interest the distance l over which significant changes of the director field occur are much larger than the molecular dimension a (typically $l \gtrsim 1\mu m$, while $a \approx 20$). So the deformation free energy density F_d may be written in terms of director deformation ∇n. We expect that:

- F_d goes to zero when $\nabla n = 0$;
- F_d is a even function in n, because $n \equiv -n$;
- F_d has not linear terms in ∇n; in fact, they will contradict the previous requirement or they will not respect the cylindrical symmetry;

- F_d has not terms in the form $\nabla \mathbf{u}$, with $\mathbf{u}$ generic vectorial field; in fact these terms would describe only a surface free energy and not the volume free energy (that is because $\int \nabla \mathbf{u}\,dr = \int \mathbf{u}\,d\sigma$).

Afterwards these considerations the deformation free energy density may be written in the form

$$F_d = \frac{1}{2}k_{11}(\nabla \mathbf{n})^2 + \frac{1}{2}k_{22}(\mathbf{n}\cdot\nabla\times\mathbf{n})^2 + \frac{1}{2}k_{33}(\mathbf{n}\times\nabla\times\mathbf{n})^2, \quad (1.3)$$

Which is the fundamental formula of the continuum theory for nematics. The three constant k_{ii} are elastic constant for splay, twist and bend deformations. All possible deformations of the liquid crystal can be described as a combination of these three basic ones (see Figure 1.4).

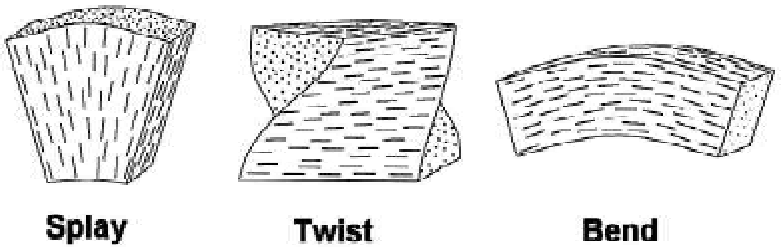

Figure 1.4. The three basic types of elastic deformation in a nematic liquid crystal: splay, twist and bend.

Equation (1.3) is a little bit complex for a practical use. A useful approximation is to assume all the elastic constants equal

$$k_{11} = k_{22} = k_{33} = k$$

This is called one-constant approximation which gives a more simple form of the free energy density

$$F_d = \frac{1}{2}k\left[(\nabla \mathbf{n})^2 + (\nabla \times \mathbf{n})^2\right]. \quad (1.4)$$

Equation (1.4) defining the distortion energies in the bulk of the nematic phase must be, in principle, supplemented by a description of the energies associated with the surface of the sample. In most practical conditions, in fact, the surface forces are strong enough to impose a well-defined direction of the director at the surface; this is what we call strong anchoring.

Instead of minimizing the sum bulk plus surface energies, it is sufficient to minimize only the bulk terms, with fixed boundary conditions for n.

To find the equilibrium condition we have to minimize F_d with respect to director deformation ∇n and its derivatives, imposing the condition that $|n|^2 = 1$. Using the Lagrange Multiplier Method, we have to minimize

$$F_d = \int_V \mathcal{F}_d(n_\alpha; \partial_\beta n_\alpha) - \lambda |n|^2 \, dr,$$

where λ is a Lagrange Multiplier, and $\partial_\alpha = \frac{\partial}{\partial x_\alpha}$. Assuming the stationary condition under small variations of the director coordinates n_α and their derivatives $\partial_\beta n_\alpha$, we obtain

$$\delta F_d = \int_V \left(\frac{\partial F_d}{\partial n_\alpha} \delta n_\alpha + \sum_\beta \frac{\partial F_d}{\partial(\partial_\beta n_\alpha)} \delta(\partial_\beta n_\alpha) - 2\lambda n_\alpha \delta n_\alpha \right) dr = 0. \tag{1.5}$$

The second term inside the integral can be calculated inverting the derivation, integrating per parts and letting the surface terms go to zero (strong anchoring hypothesis):

$$\begin{aligned}
\int_V \frac{\partial F_d}{\partial(\partial_\beta n_\alpha)} \delta(\partial_\beta n_\alpha) dr &= \int_V \frac{\partial F_d}{\partial(\partial_\beta n_\alpha)} \partial_\beta(\delta n_\alpha) dr \\
&= \frac{\partial F_d}{\partial(\partial_\beta n_\alpha)} \delta n_\alpha \Big|_{\partial V} - \int_V \partial_\beta \left[\frac{\partial F_d}{\partial(\partial_\beta n_\alpha)} \right] \delta n_\alpha dr \\
&= - \int_V \partial_\beta \left[\frac{\partial F_d}{\partial(\partial_\beta n_\alpha)} \right] \delta n_\alpha dr.
\end{aligned}$$

Substituting in equation (1.5),

$$\pm F_d = \int_V \pm n_\alpha \left(\frac{\partial F_d}{\partial n_\alpha} - \sum_\beta \partial_\beta \frac{\partial F_d}{\partial(\partial_\beta n_\alpha)} - 2\lambda n_\alpha \right) dr = 0.$$

This must be true for every variations $\pm n_\alpha$, so

$$\frac{\partial F_d}{\partial n_\alpha} - \sum_\beta \partial_\beta \frac{\partial F_d}{\partial(\partial_\beta n_\alpha)} = 2\lambda n_\alpha. \qquad (1.6)$$

It is usual to define

$$h_\alpha = \frac{\partial F_d}{\partial n_\alpha} - \sum_\beta \partial_\beta \frac{\partial F_d}{\partial(\partial_\beta n_\alpha)},$$

which are the components of the vector $\mathbf{h}$, called *molecular field*. In this way equation (1.6) establish that at the equilibrium the director $\mathbf{n}$ is, point by point, parallel to the molecular field $\mathbf{h}$.

Equation (1.6) may also be interpreted in terms of torques: $\mathbf{n}$ is adimensional, while $\mathbf{h}$ is a force per length over volume. Hence, $\mathbf{h}$ can be related to the density of moment that acts on $\mathbf{n}$. So one can define

$$\zeta_{el} = \mathbf{n} \times \mathbf{h}$$

called elastic *torque*. The equilibrium equation become

$$\zeta_{el} = 0$$

1.2.2 External Field Effects

Liquid crystals respond to even weak electric and magnetic field with significant structural changes, showing a redistribution of the molecular director. The ordered structures of anisotropic molecules make the macroscopic physical properties also anisotropic. Because of the anisotropy, the dielectric permittivity and the magnetic permeability de-

pend on the direction in which they are measured, so the electric and magnetic fields are

$$D_i = \varepsilon_{ij} E_j \tag{1.7a}$$
$$B_i = \mu_{ij} H_j = (\delta_{ij} + 4\pi\chi_{ij}) H_j \tag{1.7b}$$

where $\mu = 1 + 4\pi\chi$.
Because of the cylindrical symmetry around n, the tensors ε_{ij} and χ_{ij} can be written in the form

$$\varepsilon_{ij} = \varepsilon_\perp \delta_{ij} + \varepsilon_a n_i n_j$$
$$\chi_{ij} = \chi_\perp \delta_{ij} + \chi_a n_i n_j$$

Introducing this in equations (1.7a) and (1.7b), we have

$$D = \varepsilon_\perp E + \Delta\varepsilon (n \cdot E) n$$
$$B = (1 + 4\pi\chi_\perp) H + 4\pi \Delta\chi (n \cdot H) n$$

where $\Delta\varepsilon = \varepsilon_a - \varepsilon_\perp$ and $\Delta\chi = \chi_a - \chi_\perp$ are the dielectric anisotropy and the magnetic anisotropy respectively.

The electromagnetic energy density is

$$W = \frac{1}{8\pi}(E \cdot D + H \cdot B)$$

To obtain the total free energy density in presence of external fields, we have to add this term to the deformation free energy density

$$F_{TOT} = F_d + W$$

Because one can express

$$dW = \frac{1}{4\pi}(E \cdot dD + H \cdot dB)$$

F_{TOT} is, therefore, a function of the independent variable D and B, of the temperature T and the volume V: the equilibrium is reached minimizing F_{TOT} with T, V, D and B constant.

In order to work with E and H constant, we define the new potential G

$$G = F - \frac{1}{4\pi}(E \cdot D + H \cdot B) = F - W$$

which is a function of E, H, T and V. Analogously to the situation without fields, we find that the molecular director is everywhere parallel to a molecular field, given by the sum of a distortion term, an electric term and a magnetic one:

$$h = h_d + h_e + h_m = h_d + \frac{\varepsilon_a}{4\pi}(n \cdot E)E + \chi_a(n \cdot H)H.$$

We can define the *electric torque* and the *magnetic torque*,

$$\tau_e = n \times h_e = \frac{\varepsilon_a}{4\pi}(n \cdot E)(n \times E)$$
$$\tau_m = n \times h_m = \chi_a(n \cdot H)(n \times H)$$

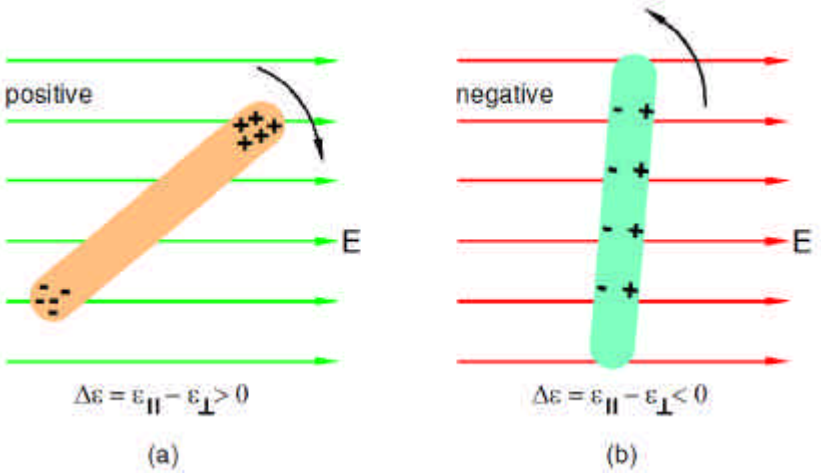

Figure 1.5. Orientation of an electric dipole by an electric field. In (a) the dipole is along the long axis of the molecule while in (b) it lies across the long axis. The presence of the electric field causes rotation of the molecule as shown by the curved arrows.

At equilibrium

$$¿_d + ¿_e + ¿_m = 0.$$

Nematic liquid crystals might show both positive and negative value of the dielectric anisotropy:

- if $¢" > 0$, the molecular director tends to dispose parallel to electric field, Figure 1.5a;
- if $¢" < 0$, the molecular director tends to dispose perpendicular to electric field, Figure 1.5b.

The magnetic anisotropy $¢Â$ is almost always positive, and the molecular director tends to align parallel to the magnetic field.

1.2.3 Alignment

The term alignment, or texture, refers to the orientation of liquid crystal molecules in the vicinity of a surface.

Liquid crystals are usually confined between closely spaced plates with an alignment layer that forces the direction of the molecules near the surface:

- planar alignment, the director aligns parallel to the cell surface, see Figure 1.6a.
- homeotropic alignment, the molecular director is perpendicular to the cell surface, see Figure 1.6b;

1.2.4 Freédericksz Transition

Consider what happens when a small amount of nematic liquid crystal is placed between two pieces of glass that have been treated to pro-

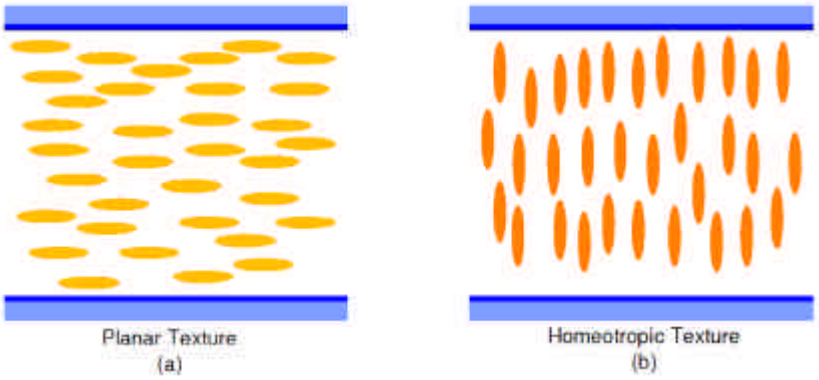

Figure 1.6. LC alignments inside a cell: (a) planar alignment; (b) homeotropic alignment.

duce alignment of the director parallel to the surface (Figure 1.7a). Near the two glass surfaces, the director is constrained to point in certain direction (parallel to the surface). Now imagine that the NLC has positive anisotropy, $\Delta\varepsilon > 0$, and an electric or magnetic field is applied perpendicular to the glass surfaces: the field tends to orient the director parallel to the field. The molecules near the surface are not very free to reorient with the field like the one in the middle of the cell. The electric or magnetic field thus causes the director to change its orientation most in the middle, with diminishing change closer to the surfaces. This deformed structure is shown in Figure 1.7b. The most interesting aspect of this deformation is that it does not occur gradually as the strength of the field is gradually increased. For fields with strengths below a certain value, the LC remains undeformed. Then at some threshold value of the field, the deformation begins and then gets as the field strength is increased. The transition from an undeformed structure to a deformed one at a certain value of the field is called *Freédericksz transition*. It is not a phase transition, but only a geometrical transition.

- if $E < E_{critical}$ no reorientation occurs;

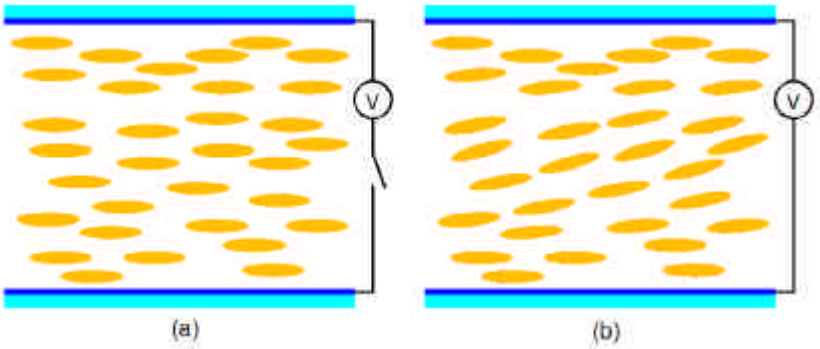

Figure 1.7. Freedericksz transition: cell has planar alignment. When the field is below the threshold the liquid crystal orientation is given by the alignment (a); above the threshold the field tends to align the director perpendicular to the surfaces (b).

- if $E > E_c$, reorientation has a behaviour shown in Figure 1.8. It is a second order transition.

With a cell of thickness d and strong anchoring, it is possible to demonstrate [2] that

$$E_c = \frac{1}{d}\sqrt{\frac{4\pi^3}{\varepsilon_a}k_i},$$

with $i = 1$ if the alignment passes from the planar to the homeotropic, $i = 2$ if the alignment remains planar but orthogonal to the initial one, $i = 3$ for the passage from homeotropic to planar. It is interesting that the field is proportional to d^{i-1}, so if we consider that the voltage to apply is $V = Ed$, one has that the critical voltage is independent to the cell thickness:

$$V_c = \sqrt{\frac{4\pi^3}{\varepsilon_a}k_i}.$$

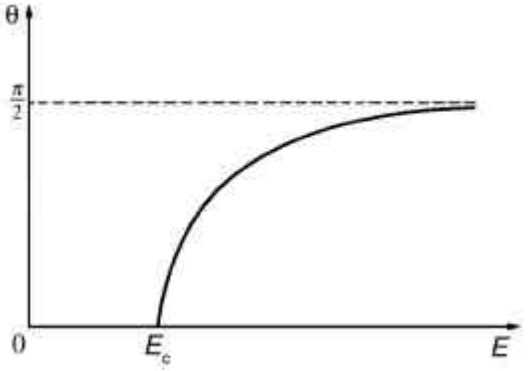

Figure 1.8. Freedericksz transition

1.3 Light and Liquid Crystals

The optical properties of liquid crystals are one of the most interesting and certainly the most beautiful features of the phase. How LCs effect light is also the basis for just about all the applications of liquid crystals. Two aspects are extremely relevant:

- due to anisotropy, light propagates in different way with respect to the molecular director orientation;
- light itself can reorient the liquid crystal, because light is an electro-magnetic field, and this reorientation of the LC modify the propagation of light giving arise to non-linear optical effect. This situation will not be discussed in this thesis.

1.3.1 Propagation in Anisotropic Media

Let us consider a plane wave $e^{i(kr - \omega t)}$ linearly polarized, where ω is its frequency, $k = \frac{\omega}{c} n s$ the wave vector, and n the refractive index of the medium, and s the unit vector normal to the wave front. The Maxwell

equantions are

$$k \pounds H = -\frac{\omega}{c} D \tag{1.11a}$$

$$k \pounds E = \frac{\omega}{c} B \tag{1.11b}$$

$$k \cdot D = 0 \tag{1.11c}$$

$$k \cdot B = 0 \tag{1.11d}$$

where the constitutive equations are

$$D_i = \varepsilon_{ij} E_j \tag{1.12}$$

$$B_i = \mu_{ij} H_j \tag{1.13}$$

To study the optical properties of the medium we can neglect the effects due to the magnetic permeability, in fact $\mu_{ij} \approx \delta_{ij}$, and equation (1.13) becomes

$$B = H \tag{1.14}$$

From equations (1.11c), (1.11d) and (1.14) descends that D, H and k make a tern of orthogonal vector. Equation (1.12) establishes that D is not in general parallel to E, and so the Poynting vector, proportional to $E \pounds H$, is not parallel to k. In other words, in anisotropic media the energy flux, which determines the propagation direction is not oriented in the same direction as the wave front propagation.
From equations (1.11a) and (1.11b), using also equation (1.14), we get

$$\frac{\omega^2}{c^2} D = -k \pounds (k \pounds E) = k^2 E - k(k \cdot E)$$

that, using equation (1.12), after same algebra, becomes

$$\sum_j (k_i k_j + \frac{\omega^2}{c^2} \varepsilon_{ij} - k^2 \delta_{ij}) E_j = 0$$

This is a three equations system with three unknown quantities. It has non-null solutions only if

$$\det(k_i k_j + \frac{\omega^2}{c^2}\varepsilon_{ij} - k^2\delta_{ij}) = 0$$

Letting $p = ns$,

$$\det(p_i p_j + \varepsilon_{ij} - n^2\delta_{ij}) = 0 \tag{1.15}$$

Equation (1.15), called *Fresnel Equation*, has solutions $\pm n_1$ and $\pm n_2$, where the sign $+$ and $-$ correspond to the two propagation directions. For an arbitrary direction, there are two independent wave with phase velocity c/n_1 and c/n_2.

1.3.2 Uniaxial Media

Commonly the tenson ε_{ij} is real (for transparent material like LC) and symmetric [3]. The reference system in which this tensor ε_{ij} is diagonalizable defines the *princial axis* of the system. If one element of the diagonal is different from the other two that are egual, the medium is said to be *uniaxial*. The axis relative the diagonal element different from the other two is called the *optic axis*, because the optical properties of the material are invariant under rotations around this axis. If all the diagonal elements are different, the medium is *biaxial*.

Nematic LC are uniaxial, and the optic axis is the molecular director.

Let us take z parallel to the optic axis, the tensor ε_{ij} of a NCL is

$$\varepsilon_{ij} = \begin{pmatrix} \varepsilon_\perp & 0 & 0 \\ 0 & \varepsilon_\perp & 0 \\ 0 & 0 & \varepsilon_\parallel \end{pmatrix} \tag{1.16}$$

The propagation direction of the wave is given by the unit vector $s = s(\mu; \varphi)$. Because of the symmetry around z, φ can be chosen $\varphi = 0$, that means we are considering a wave propagating in the plane $x - z$. Under these conditions $s = (\sin\mu; 0; \cos\mu)$, introducing in equation (1.15) with

the (1.16), we get the new Fresnel equation

$$(n^2 - \varepsilon_\perp)(\varepsilon_\perp \varepsilon_\parallel - n^2 \varepsilon_\parallel \cos^2\theta - n^2 \varepsilon_\perp \sin^2\theta) = 0$$

which has the two solutions

$$\begin{aligned} n_o &= \sqrt{\varepsilon_\perp} \\ n_e(\theta) &= \frac{n_o n_e}{\sqrt{n_e^2 \cos^2\theta + n_o^2 \sin^2\theta}} = \sqrt{\varepsilon_\parallel} \end{aligned}$$

Corresponding to these solutions there are two values of the wavevector:

$$\begin{aligned} k_1 &= \frac{\omega}{c} n_o \\ k_2 &= \frac{\omega}{c} n_e(\theta) \end{aligned}$$

A linearly polarized light wave propagating perpendicular to the optic axis and its E-vector parallel to the optic axis sees the refractive index n_e: the wave is called *extraordinary* wave. If the E-vector is perpendicular to the optic axis, the wave sees the refractive index n_o the wave is *ordinary*. If the E-vector makes some angle with the optic axis, the wave is split up into two waves, which simultaneously propagate through the medium with different speeds. Hence, an optically anisotropic medium is said to be birefringent, and the birefringence is

$$\Delta n = n_\parallel - n_\perp$$

In liquid crystals the birefringence is typically $0.1 \sim 0.2$, an extremely high value compared with other materials.

1.4 Ferroelectric Liquid Crystal

A polar material is one in which local dipoles exist on a microscopic level: if the dipoles are macroscopically ordered in a same direction by

the presence of an external field the material is said to be *piezoelectric*; if they order spontaneously, in absence of external field, the material is called *pyroelectric*.

A *ferroelectric* material is a special case of a pyroelectric in which the polarization is switchable and has two stable states. A liquid crystal showing a macroscopic spontaneous polarization P_s is called *Ferroelectric Liquid Crystal* (FLC).

For symmetry reasons and from the fact that $\mathbf{b} = -\mathbf{b}$, a spontaneous local polarization can only exist in chiral tilted smectic phase, for instance in the SmC*. Moreover, this local non vanishing polarization P_s can exist only in a direction perpendicular to the director n, and orthogonal to the normal to the smectic layers a; this means that each smectic layer has a non vanishing polarization. But, due to the helicoidal structure arising from the chirality of the molecules every macroscopic polarization is cancelled out (see Fig. 1.9a).

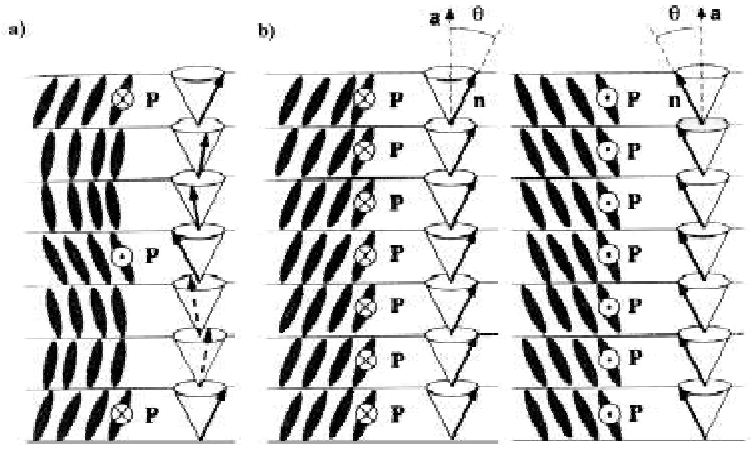

Figure 1.9. Ferroelectric Liquid Crystals: a) the SmC* phase. The polarization vector, coupled rigidly with the diretor, rotates with it plane by plane; b) in the SSFLC configuration the helix has been unwound, the director can occupy only two stable states, which have parallel polarization but in opposite directions.

However, in thin cells (few microns) where the pitch is large compared to the cell thickness and the helical ordering is suppressed by the liquid crystal-surface interactions a macroscopic polarization may be present (see Fig. 1.9b). The surface conditions may be such that the director is confined to the plane of the surface in so-called bookself geometry, with the smectic layers perpendicular to the surfaces (planer alignment). This allows for only two possible stable orientations for n, corresponding to the intersection between the plane of the surface and the smectic C* cone. Hence, those positions make an angle of 2μ, where μ is the cone angle of the SmC* phase, and regions with one or the other orientation has a spontaneous polarization up or down respectively (see Fig. 1.10).

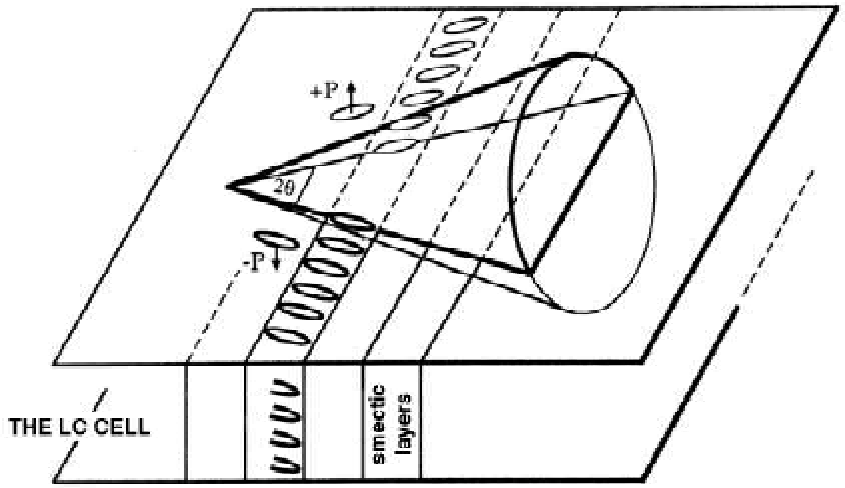

Figure 1.10. The SSFLC configuration: smectic layers are perpendicular to the surfaces. This allows for only two possible stable orientations for the director, corresponding to the intersection between the plane of the surface and the smectic C* cone.

The director may be switched between the two stable states by means of an electric field applied across the cell. The field makes the director switch into the states corresponding to the polarization being parallel to the field and since the two states are stable we have a ferroelectric system called *Surface Stabilized Ferroelectric Liquid Crystals* (SSFLC). The interaction between the macroscopic polarization P and the electric field is given by the torque

$$\tau_F = P \times E$$

which reorients the molecules between the two states rotating them of 2μ. What is really important to mention is that the coupling of FLC with the electric field is much more intense that the one of nematics: the first is a linear response, it means that it depends on the sign of E; the second is quadratic, and it is not affected of the E sign. That is why ferroelectric liquid crystal are faster than nematics, thus their utilization is prefered in telecom applications.

1.5 Liquid Crystals and Telecommunications

In order to satisfy the companies request, academic groups are testing the possibility to make optical not only the signals transmission but also their processing at the network nodes.

Different systems and devices to build up optical systems may require different technologies so that a strong competition is open and a winning comprehensive technology is not already established. In this section a survey of the situation is given.

Technologies based on inorganic materials, such as *Lithium Niobate* ($LiNbO_3$), either by using electro-optic effect or acousto-optic effect, do not allow for optical switch matrices with many inputs and many outputs. In fact, a large number of them is paid in terms of too high insertion losses, crosstalk and too large dimensions in the order of several mm^2 per device.

Micro-electro-mechanical systems (MEMS) based on vertical torsion micro-mirrors on Si substrate are a good solution to implement large switching matrices but this advantage is often paid in terms of high driving voltages of about 80 V, switching times of about $1ms$ or longer and tight fabrication constraints with limitation due to diffraction of light in free space.

Another proposed approach consists in the so called *bubble-switch* in which total internal reflection is obtained by switching refractive index of a substance, when it goes from vapour to liquid phase, placed at cross-point between silica waveguides. In this technology the drawback is due to the bubbles dimension: in fact, to maintain the state of a bubble, it is necessay to maintain their dimensions in a certain range, and this can bring to high losses and high driving currents.

Another approach is based on *thermo-optic effect* which can be used in passive materials such as glass and was largely exploited to make space-division optical switches with Mach-Zehnder interferometer configuration based on planar lightwave circuit technology, which employs silica-based waveguides on silicon, but with high driving power of the order of 0.4 W. Silica based technology is suitable for both large optical and electronic integration, low propagation loss, and low fiber coupling loss thanks to compatibility with single-mode optical fibers index. Fabrication technology of silica-based waveguides is well consolidated, it consists in SiO_2 deposition on Si, either by flame hydrolysis (FHD) developed at NTT laboratories or high pressure thermal oxidation developed at ATT Bells Labs and LETI, in combination with plasma enhanced chemical vapour deposition to deposit a doped silica layer with slightly higher refractive to make the core waveguide and a final cladding on top of it. Lithography and reactive ion etching processes are used to sculpt optical channel waveguides. Waveguide optical refractive index can be tailored to meet fiber index matching requirements, low bend losses, etc., by controlling dopant concentration. In particular a variety of optical waveguide elements can be designed and realised such as: simple straight optical waveguided, X and Y junctions, MZIs,

bends, directional couplers. Multi/demultiplexers, waveguide gratings routers, based on arrayed waveguide gratings (AWG), have been successfully demonstrated and are commercially available. Several fabrication foundries offer prototype service to make silica on silicon novel devices, designed by customers.

In this work I screen the use of liquid crystals: because of their refractive index close to silica, their high electro-optic effect and their birefringence, LCs seem to be a good material for the optical signal processing.

The idea to use Liquid Crystals (LCs) dates back to the 70's: after the first impressive success of LC materials in the display area, scientists thought to exploit them in the design of photonic devices. Interesting results showed that the capability of LCs to affect the light propagation in guided systems could be used to realize devices for the optical signal processing. But these results were abandoned because the drawbacks, mainly in terms of optical losses, were too relevant to foresee an effective technological development.

During the 90's this idea was resumed. Owing to the progress in soft matter science and technology, the recent scientific advances in LCs-based photonic devices have had a first non-negligible influence in real applications and in the market. A number of companies, spin-offs and also medium-size enterprises, in US are already offering few LC based photonic devices (e.g. Spectraswitch, Meadowlark, Displaytech) and also few European ones are interested in developing such components (Jenoptik-Germany, Nemoptic-France, Calctec-Italy) and want to afford the challenge with competing technologies[3].

The advantages of using liquid crystals are many:

- they are transparent, hence they exibit a low absorption;
- their birefringence is typically $0{:}1 \div 0{:}2$, an extremely high value compared with other materials;

[3] In the webgraphy some web-site references of the mentioned companies are given.

- they can by driven by low electric field (let's say few Volts);
- their low-viscosity liquid nature makes them easy to integrate;
- they are cheap;
- companies are already to handle them, because of their widespread in the display market;
- they show so many mesophases and composites, that they are adaptable to the required device necessities.

Drawbacks in the use of Liquid Crystals is mainly due to scattering losses and to responce times:

- scattering losses are due to spatial fluctuations of the material optical constants. It is possible to minimize these losses improving the medium homogeneity through a high alignment quality or using thin LCs layers;
- nematic liquid crystals show response time of milliseconds, while ferroelectric of microseconds. Compared with other technologies, like Lithium Niobate, they are slower. In fact, the responce to an electric field is not of electric nature, but it is the time needed to reorient all the molecules in the medium. Nevertheless in optical signal processing devices response times are not always asked to be faster.

Since several years, the *Integrated Optics Lab* of *Federico II University of Naples*, coordinated by *Professor G. Abbate*, and with whom I work, is developing telecom applications of Liquid Crystals. I report here some devices designed in the past years, in order to give an idea of how liquid crystals properties can be exploited.

1.5.1 A Liquid Crystal Based Deflector

On of the easiest Liquid Crystal based device for telecom applications is a beam switch/deflector in a planar waveguide. It is a slab polymeric waveguide showing a LC filled basin (Figure 1.11). It is composed of four layers:

1) a *glass* substrate of $1mm$ thickness;
2) a thin *Indium Tin Oxide* (ITO), $\gg 20nm$, used as electrode to apply an electric field to the LC;
3) a *buffer* layer, used to isolate the field propagating in the waveguide from the ITO layer;
4) a guiding layer, *core* ;

A small rectangular basin is etched by photolithography over the guiding layer: this basin long axis is tilted of an appropriate angle with respect to the light propagation direction. Being etched in the core, the basin bottom is just the buffer layer. Once that the basin has been filled with LC, another glass cover is added to the structure to plug the basin: this glass cover has a planar alignment layer, so that the LC molecules will be oriented in the same plane of the waveguide[4], and another ITO substrate that acts as second electrode.

If the electric field is polarized parallel to the waveguide plane and orthogonal to the propagation direction, the device can work both with nematic or ferroelectric liquid crystals. In the former the molecules are aligned along the field polarization direction, so that light sees the extraordinary index if no electric field is applied to the LC, and the ordinary index otherwise. In the latter, the molecular director has only two stable positions, both parallel to the waveguide plane, but making a different angle with the propagating direction.

[4] In this multilayer the alignment is given only from the glass cover; in fact, the other side of the LC cell is given by the buffer, which has got no alignment. However, if the cell thickness (in this case the basin deepness) is few micron, the alignment can be good enough, even if given only by one side.

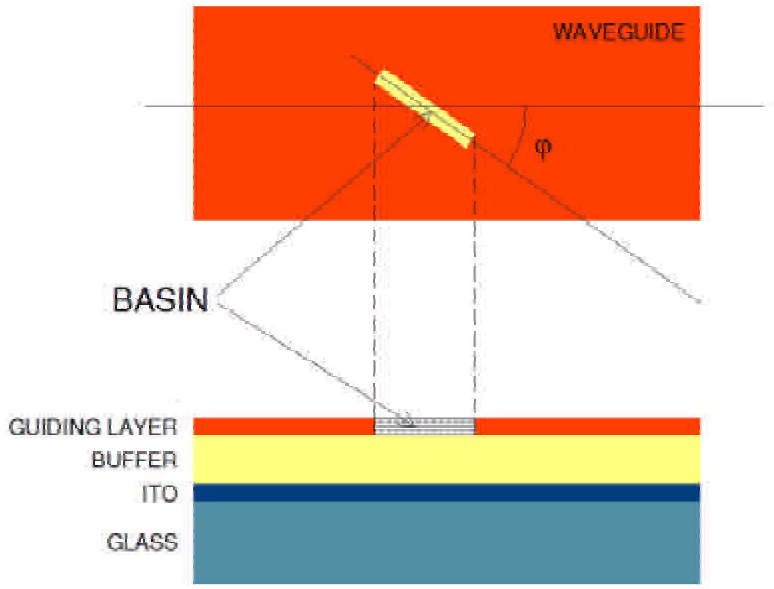

Figure 1.11. A Liquid Crystal baser device: a beam deflector realized with a liquid crystal filled basin incised inside a planar waveguide.

The main idea of this device is to choose the proper parameters so that if no electric field is applied, the light sees a liquid crystal refractive index equal to the one of the guiding layer. If this happens, the signal will continue its propagation inside the waveguide without seeing the basin. On the other hand, if we apply the field, we induce a reorientation of the liquid crystals and a consequent decrease of the refractive index, up to induce total reflection at the waveguide-basin interface. If this happens the beam will continue to propagate in the waveguide, but deflected in a different direction.

We label n_{high} and n_{low} respectively the higher and the lower value showed by the liquid crystal inside the basin. The conditions to impose to the constructive parameters of the device are really simple:

- in the transmission state, the high refractive index value is matched with the value of the index in the core of the polymeric waveguide, $n_{guiding}$, so that the basin does not affect the straight propagation inside the waveguide:

$$n_{high} = n_{guiding}$$

- in the reflection state, the light beam experiences a total internal reflection at the basin interface and is deflected correspondingly. This happens if the angle between propagating direction and the normal to the interface, $'$, is bigger than the critical angle $'_c$:

$$' \geq '_c = \arcsin\frac{n_{low}}{N}, \tag{1.19}$$

where N is the mode index, which is different from $n_{guiding}$ if we consider the not straight propagation of the beam inside the waveguide. In general $N > n_{guiding} = n_{high}$, hence equation (1.19) becomes

$$' \geq '_c > \arcsin\frac{n_{low}}{n_{high}}.$$

In a nematic liquid crystal $n_{low} = n_o$ and $n_{high} = n_e$. In a ferroelectric it depends on the tilt angle. Using ferroelectric LCs instead of nematic will improve the time response of the deflector up to $10 - 100\,\mu s$, instead of several ms as the usual nematic LC response.

1.5.2 A Tunable Bragg Grating

The second device is an electrically tunable Bragg Grating Filter (BGF): it device is based on a Bragg grating in planar waveguide with a liquid crystal overlayer, which allows to change the spectral behaviour of the device. The device (Figure 1.12) is a sol-gel waveguide: on a common glass substrate, a thin ITO layer has been deposited as electrode. Over the ITO a sol-gel deposition has been realized as guiding

film. A Bragg grating has been written on the waveguide by means of holographic exposure followed by a reactive ion etching. The grating is finally covered by a LC cladding, another ITO electrode layer and the glass.

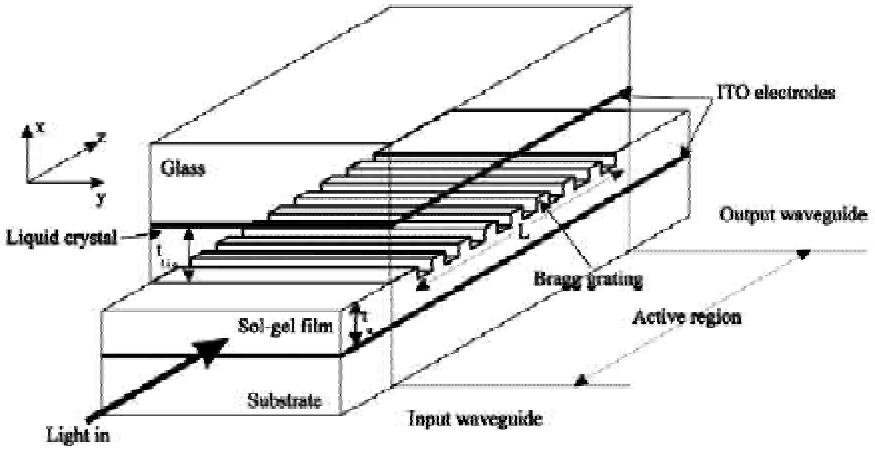

Figure 1.12. A tunable filter based on a Bragg grating in planar waveguide with a liquid crystal overlayer.

The Bragg grating exhibits a behaviour equivalent to a wavelength selective mirror. The reflectivity is maximum at the Bragg wavelength λ_B, depending both on the physical characteristics of the guiding structure and on the geometrical characteristics of the Bragg grating:

$$\lambda_B = 2n_{eff}\Lambda \tag{1.20}$$

where n_{eff} is the effective refractive index of the guided mode and Λ is the grating period. According to equation (1.20), any change of the effective refractive index involves a change in the spectral response of the device. The molecular reorientation of the liquid crystal can be induced applying an electrical field between the two ITO electrodes. This reorientation implies a change of the refractive index of the cover of the

active region and consequently a change of the effective refractive index of the guided mode. Thus, if a laser beam propagates along the device, a field induced modulation of the laser intensity at the output of the device can be achieved by a proper design of the grating period.

Choosing a nematic liquid crystal the device acts like a tunable filter: applying a voltage the liquid crystal experiences a continuous reorientation of its molecules, which provides a continuous variation of the effective refractive index.

Choosing a ferroelectric liquid crystal and exploiting its bistability, the device can act as a switch: in fact, to the two stable states of the liquid crystal correspond two values of the effective refractive index and so two wavelength.

Chapter 2

Holographic Gratings

A switchable diffraction grating is a key component for the realization of several devices used in the chain of optical communication networks, such as switches, Add-and-Drop systems, beam deflectors, routers.

Modern transport networks not only provide the physical transfer of information, but must do it in an efficient way, with the flexibility to change information quickly and appropriately among a broad number of interconnections. To achieve this, the principle of multiplexing has been introduced [1]: *"Don't look at the details when this is not required: group small entities in larger entities"*. The basis principle of a Wavelength Division Multiplexing (WDM) line system is just this: all the singals travel simultaneously into the fiber, each one of them modulated by a wavelength. In this way the large transmission band of fibers is better expoited, and more information can travel in the net. Hence, one will modulate different light sources, each having a different wavelength, with an electricl signal. In order to multiplex the different signals together in a single fiber a wavelength multiplexer is used. The multiplexed signal is then transmitted in the fiber to the far end of the link, where the different wavelengths will be separated or demultiplexed againg. After demultiplexing, different detectors may convert the individual optical signals to electric signals, or may directly process the individual wavelength signals and connect to another WDM line system.

At first, wavelength-division multiplexing was used with only two wavelengths, $1310nm$ and $1550nm$. However, this was suitable only for limited applications. Dense Wavelength Division Multiplexing (DWDM) in an attempt to make optimum use of the Erbium-Doped Fiber Amplifier's (EDFA[5]) gain band, $1530nm$ to $1570nm$ to carry tens of different signals in that wavelegth range. A number of signals coming from different transmitters with different centerwavelengths are combined into one fiber using an optical multiplexerand amplified almost equally using an Erbium-Doped Fiber Amplifier. The aim of DWDM is to increase the fiberoptic cable capacity by packing up to 100 high speed data channels to one fiber optic cable. The International Telecommunication Union (ITU) Recommendation G.692 specifies $100GHz=0:8nm$ channel spacing on $32nm$ grid centered at $193:1THz=1552:52nm$ (preliminary standards works are specifying $50GHz$ and $25GHz$ spacing).

Bragg Diffraction Filters are the basic element of several WDM devices: depending on its pitch $¤$ and its refractive index n, a Bragg grating will select a wavelength corresponding to the Bragg wavelentgh, $¸_B = 2n¤$. For instance, if we send to a Bragg grating a wavelengths group it will transmitt all of them except $¸_B$, if the grating works in reflection. Hence, a reflective Bragg grating works exactly as a selective mirror (see Figure 2.1a). If the Bragg grating works in transmission, the Bragg wavelength will be diffracted of a certain angle (given by the Bragg condition $sin #_B = ¸(2¤)^{i1}$): driving somehow the grating parameters, like the refractive index, this angle can be modulated, and the grating can act like a switch (see Figure 2.1b).

One of the easiest way to realize an optical multiplexing or demultiplexing device is to integrate one or several switchable gratings in a guiding system such as a fiber or a waveguide [4]: as you can see in Figure 2.2 every grating acts on a wavelength, which can be for example added or removed from the packet.

[5] Erbium-Doped Fiber Amplifiers (EDFA) are optical fibers doped with the rare earth element, erbium, which can amplify light in the $1550nm$ region when pumped by an external light source.

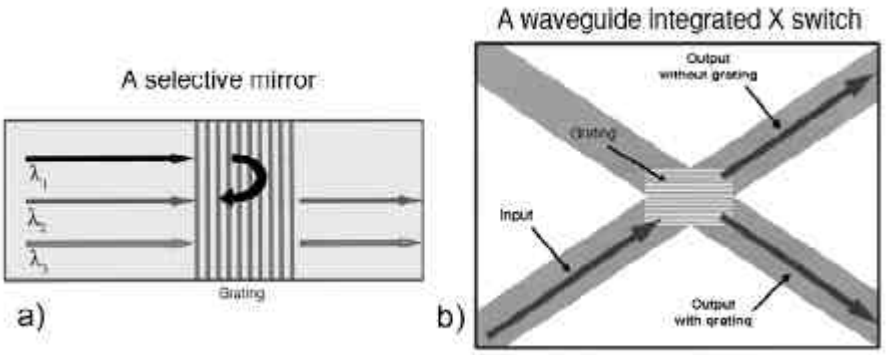

Figure 2.1. Bragg gratings for optical devices: a) a selective wavelength mirror; b) a switch.

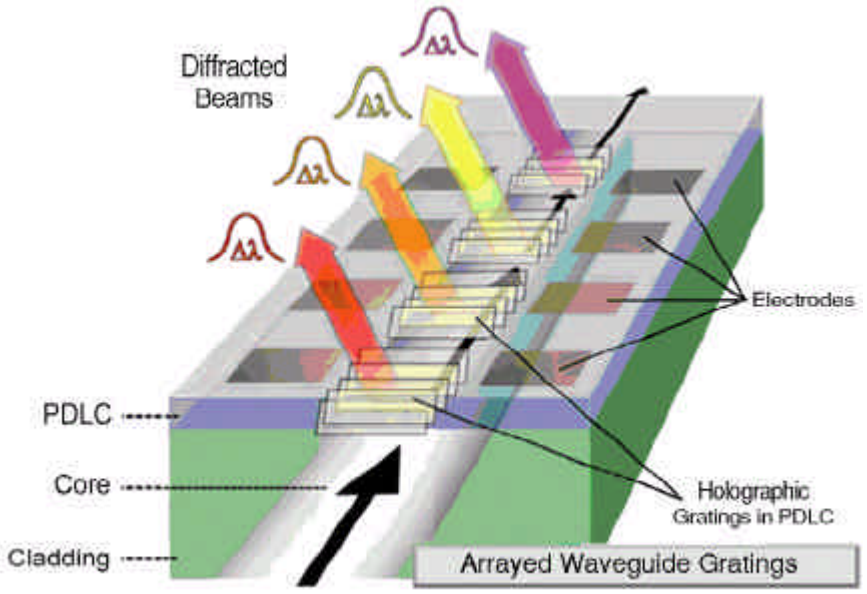

Figure 2.2. A succession of tunable Bragg gratings integrated in a waveguide acts as an optical multiplexing/de-multiplexing device.

Laser-induced formation of diffraction gratings in polymer-Liquid Crystals (LC) composites is an item of increasing interest, from both a scientifical and technical point of view, for several reasons: as said in the previous chapter, this is mainly due to their high electrooptical effect, their high integrability and their transparency.

In this chapter a short outline on holographic gratings will be given.

In a conventional recording technique, such as photography, a three dimensional scene is recorded by an optical system on a light sensitive surface. The system records the intensity distribution in the original scene, but all information on the relative phases of the light waves from different points is lost. What we have is only a bidimensional image of the scene.

In order not to lose this information, the main idea of holography is to record both the amplitude and the phase of the light scattered by the object. Since all recording media respond only to intensity, it is necessary to convert the phase information into variations of intensity. This is done by using coherent illumination, like laser light. The final product that we have is a hologram recorded on flat surface, which produces a three dimensional image.

Without going into the theory of optical holography [6], I will briefly discuss the different types of holographic gratings that can be recorded by an interference pattern of laser light [7].

2.1 Classification of Holographic Gratings

Holographic gratings can be classified in different typologies, each one characterized by a proper geometry and efficiency.

A first characterization can be done with respect to the effect that a grating produce on the incident light:

- a grating showing a periodic variation of the refractive index produces a phase modulation of the incident ray, that is why we talk about *phase grating*;
- a periodicity in the absorption coefficient produces a modulation of the incident light amplitude, and we talk about *amplitude grating*.

A second characteristic, which has relevant consequences in the grating features, is the thickness of the recording medium. We might have:

- *thin holograms*, when the thickness of the recording material is small compared with the average spacing of the interference fringes;
- *thick holograms* or *volume holograms*, if the medium thickness is bigger than the fringes spacing.

Theoretically both of this geometries can be designed with the fringes perpendicular to the grating plane (*transmission gratings*) or parallel (*reflection gratings*). But when the grating thickness is negligible, like in thin gratings, the only configuration we might have is with the fringes perpendicular to the grating plane (see Figure 2.3).

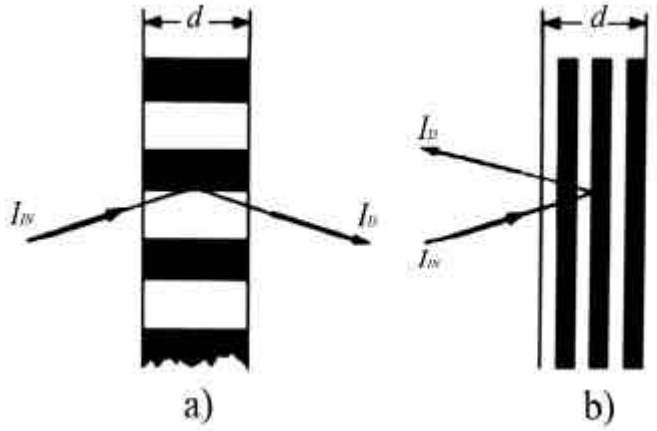

Figure 2.3. Holographic Gratings: (a) in transmission and (b) in reflection.

Based on these three classifications we can have six types of holograms:

1) thin phase holograms, working in transmission;
2) thin amplitude holograms, working in transmission;
3) thick phase holograms, working in transmission;
4) thick phase holograms, working in reflection;
5) thick amplitude holograms, working in transmission;
6) thick amplitude holograms, working in reflection.

As we will briefly see at the end of this section, one of the differences among these geometries is in the diffraction efficiency of the granting [6]. Moreover different thickness gratings work in different diffraction regimes: thin holograms in the Raman-Nath regime, while volume grating in the Bragg regime. Afterwards criteria to distinguish gratings typologies are extremely useful.

The distinction between these two regimes is commonly made on the basis of a parameter Q which is defined by the relation

$$Q = \frac{2\lambda d}{n_0 \Lambda^2}$$

where Λ is the grating pitch, n_0 the average refractive index, and d the thickness.

- If $Q < 1$, the grating thickness is small compared with the pitch and we talk about *Raman-Nath regime*. The diffraction maxima are given by the equation

$$\sin\theta_m = m\frac{\lambda}{\Lambda} \pm \sin\theta_i \qquad (2.1)$$

where m is the diffraction order, θ_i is the incident angle, and θ_m of the m-order diffracted ray. The sign of $\sin\theta_i$ is $-$ if the two rays stay on the same side of the normal to the grating, and $+$ otherwise.

Such a thin grating diffracts the incident wave into a large number of orders.

- If $Q > 1$, the grating is thick. Equation (2.1) still occurs, but the diffracted intensity is maximum only when the incident angle and the first diffracted order coincide. In such situation we have

$$\sin \#_B = \frac{\text{ب}}{2¤}$$

known as the *Bragg condition*. For such gratings the only orders are the zero and the first diffracted order.

As we will see in the next chapter, the active Bragg grating studied in this thesis are volume phase gratings working in transmission.

2.1.1 Thin Holograms

If the thickness of the recording material is small compared with the average spacing of the interference fringes, the hologram can be classified as a thin hologram. As said before, they can work only in transmission.

Let ¤ be the grating pitch, the z-axis perpendicular to the surfaces of the medium, and the x-axis perdpendicular to the fringes. We consider the grating infinite along the y-axis. Such a hologram exhibit a spatially varying complex amplitude transmittance:

$$T(x) = ¿(x)e^{\,i\,iÁ(x)}$$

where $¿(x) = |T(x)| \in [0;1]$. If incident light is a plane wave like

$$E(x;z) = E_0 e^{\,i\,ikr}$$

with $k = k_x\hat{x} + k_z\hat{z}$ wavevector, the transmitted wave will be a plane wave

$$E(x;z) = ¿(x)E_0 e^{\,i\,i(kr+Á(x))} \tag{2.2}$$

In a *amplitude hologram* $\acute{A} = const$, while $¿(x)$ varies over the hologram. If we assume that the resulting amplitude transmittance is linearly related to the intensity in the interference pattern, the amplitude transmittence of the grating can be written as

$$¿(x) = ¿_0 + ¢¿ \cos Kx \tag{2.3}$$

where $¿_0$ is the average amplitude transimittence of the grating, $¢¿$ is the amplitude of the spatial variation of $¿(x)$ and

$$K = \frac{2¼}{¤}$$

is the grating wave vector. Expanding equation (2.3), equation (2.2) becomes

$$E(x;z) = E_0 e^{\,i\,ik_z z}\left[¿_0 e^{\,i\,ik_x x} + \frac{¢¿}{2}\left(e^{\,i\,i(k_x+K)x} + e^{\,i\,i(k_x\,¡\,K)x}\right)¢\right] \tag{2.4}$$

The diffracted field appears as the superimposition of three waves (diffraction orders) of wavevector k_n, propagating in three distinct directions connected from a relation which express the wave vector conservation

$$k_n = k + Kî$$

From equation (2.4) we find that the intensity of the first diffracted order is $|E_0|^2\left(\frac{¢¿}{2}\right)^2$. Since $¿(x)$ is limited to the range [0,1] the maximum value is reached for $¢¿ = 1=2$; that means the maximum amplitude in each of the diffracted orders is one fourth of that in the wave used to illuminate the hologram, so that the peak diffraction efficiency is

$$´_{max} = \frac{1}{16} = 6{:}25\%$$

In a *phase hologram* $¿(x) = 1$, so that the compex amplitude transmittance is $T(x) = e^{\,i\,iÁ(x)}$. If the phase shift produced by the recording medium is linearly proportional to the intensity in the interference pat-

tern,

$$\acute{A}(x) = \acute{A}_0 + ¢\acute{A}\cos Kx$$

and equation (2.2) becomes

$$E(x;z) = E_0 e^{¡ ikr} e^{¡ i\acute{A}_0} e^{¡ i¢\acute{A}\cos Kx} \tag{2.5}$$

The last factor can be expanded as a Fourier series,

$$e^{¡ i¢\acute{A}\cos Kx} = \sum_{n=¡1}^{\infty} i^n J_n(¢\acute{A})\, e^{inKx}$$

where J_n is the Bessel function of the first kind of order n. Introducing it into equation (2.5),

$$E(x;z) = E_0 e^{¡ ik_z z} e^{¡ i\acute{A}_0} \sum_{n=¡1}^{\infty} i^n J_n(¢\acute{A})\, e^{¡ i(k_x x ¡ nKx)}$$

Such a modulation diffracts a wave incident into a large number of orders, each one of them with intensity $|E_0|^2 J_n^2(¢\acute{A})$. According to the properties of Bessel function, the maximum diffraction efficiency is

$$´_{max} = J_1^2(¢\acute{A}) \simeq 33{:}9\%$$

2.2 The Coupled Wave Theory for Thick Holograms

In 1969, Herwig Kogelnik published an interesting article analysing the diffraction of light by thick gratings with a theory known as the coupled wave theory [8]. Such theory can predict the maximum possible efficiencies of the various thick holograms. Consider a coordinate system (see Figure 2.4) in which the z-axis is perpendicular to the surfaces of the recording medium and the x-axis is in the plane of incidence, while the fringe planes are oriented perpendicular to the plane of incidence.

The grating vector K is perpendicular to the fringe planes, and makes an angle $\tilde{A}$ with the z-axis:

- $\tilde{A} = 0^{\pm}$ in transmission gratings;
- $\tilde{A} = 90^{\pm}$ in reflection gratings.

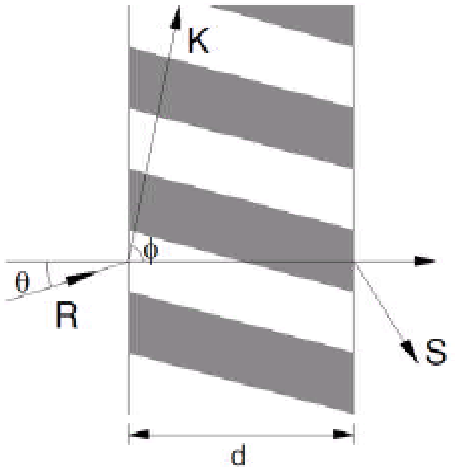

Figure 2.4. Model of a thick hologram with slanted fringes.

The volume record of the holographic interference pattern usually takes the form of a spatial modulation of the absorption constant or the refractive index of the medium, or both. For semplicity, here the analysis is restricted to the holographic record of sinusoidal fringe patterns:

$$n = n_0 + n_1 \cos K \cdot x$$
$$® = ®_0 + ®_1 \cos K \cdot x$$

where x is the radius vector $x = (x; y; z)$, n_1 and $®_1$ are the amplitudes of the spatial modulation, n_0 is the average refractive index and $®_0$ is the average absorption constant. The coupled wave theory assumes monochromatic light incident on the grating at or near the Bragg angle: following the Kogelnik's paper, I will start from light polarized perpendic-

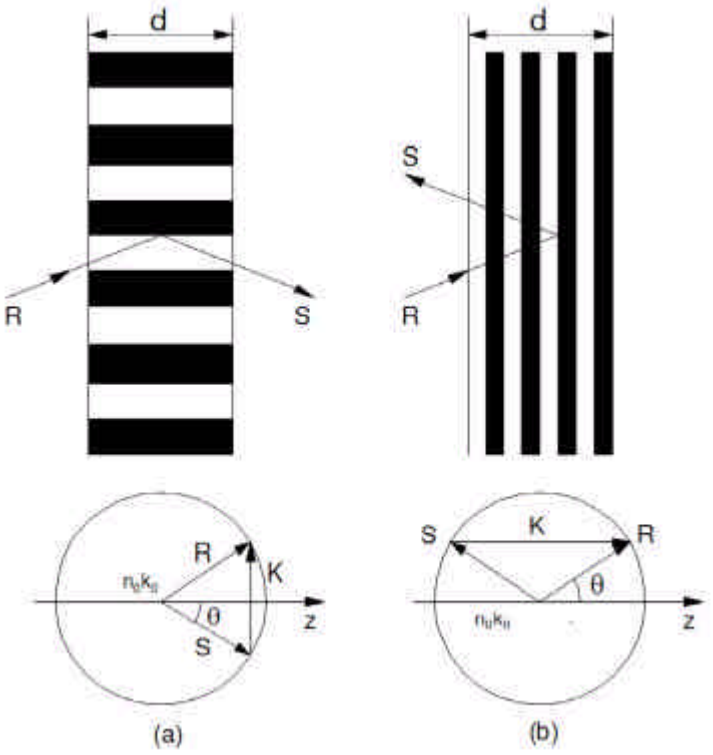

Figure 2.5. Volume transmission (a) and reflection gratings (b) and their associated vector diagrams for Bragg incidence.

ular to the plane of incidence and after I will generalize to parallel polarization. If the medium thickness is large enought, only two waves in the grating need to be taken into consideration: the incoming reference wave R and the outgoing signal wave S. Only these two waves obey the Bragg condition, the other diffraction orders violete it strongly, so they are severely attenuated and can be neglected.

Wave propagation in the grating is described by the scalar wave equation

$$\nabla^2 E + k^2 E = 0 \qquad (2.6)$$

where E is the complex amplitude $E(x;z)$ of the y-component of the electric field, which is assumed to be independent of y and to oscillate with an angular frequency $!$; k is the spatially varying propagation constant in the grating, related to n and $®$. In his paper Kogelnik assumed that the absorption per wavelength, as well as the relative variations in refractive index of the medium, are small (which is true in almost every practical case) so that

$$\begin{aligned} n_0 k_0 &\grave{A} ®_0 \\ n_0 k_0 &\grave{A} ®_1 \\ n_0 &\grave{A} n_1 \end{aligned}$$

Where $k_0 = 2¼=¸$, and $¸$ is the wavelength in free space. Under the above conditions, the propagation constant can be written in the form

$$k^2 = {}^{-2} ¡ 2i®^{-} + 4 \cdot {}^{-} \cos K ¢ x \qquad (2.7)$$

where ${}^{-} = n_0 k_0 = 2¼n_0 = ¸$ is the average propagation constant, and $\cdot$ is the coupling constant defined as

$$\cdot = \frac{¼n_1}{¸} ¡ i\frac{®_1}{2}$$

This coupling constant is the central parameter in the coupled wave theory, it describes the coupling between the reference wave R and the signal wave S. If $\cdot = 0$, there is no coupling and, therefore, there is no diffraction. The spatial modulation indicated by n_1 or $®_1$ forms a grating which couples the two waves R and S, and leads to an exchange of energy between them. As a resull of this energy interchange, or because of an energy loss from absorption, the complex amplitudes $R(z)$ and $S(z)$ of these waves vary along z. The total electric field in the grating is the superposition of the fields due to these two waves:

$$E = R(z)e^{\,i\,i½¢x} + S(z)e^{\,i\,i¾¢x} \qquad (2.8)$$

where ½ and ¾ are the propagation vectors for the two waves; they contain the information about the propagation constant and the directions

of propagation of R and S. The quantity ½ is assumed to be equal to the propagation vector of the free space reference wave in absence of coupling, while ¾ is determined by the grating and is related to ½ and to the grating vector K by the expression

$$¾ = ½ ¡ K \tag{2.9}$$

which has the appearance of a conservation of momentum equation. Figure 2.6a shows the vectors of interest and their orientation:

$$½ = \begin{pmatrix} ½_x \\ ½_y \\ ½_z \end{pmatrix} = -\begin{pmatrix} 0 \\ \sin\# \\ \cos\# \end{pmatrix}$$

$$¾ = \begin{pmatrix} ¾_x \\ ¾_y \\ ¾_z \end{pmatrix} = -\begin{pmatrix} 0 \\ \sin\# ¡ \frac{K}{-}\sin Ã \\ \cos\# ¡ \frac{K}{-}\cos Ã \end{pmatrix}$$

The vector relation (2.9) is shown in Figure 2.6: the general case is shown in Figure 2.6a, where the Bragg condition is not met and the length of ¾ differs from -; figure 2.6b shows the same diagram for incidence at the Bragg angle $\#_0$. In this special case, the lengths of both ½ and ¾ are equal to the free propagation constant $n_0 k_0$, and the Bragg condition, which can be written in the form

$$\cos(Ã ¡ \#_0) = \frac{k}{2n_0 k_0}$$

is obeyed.

For a fixed wavelength the Bragg condition is violater by angular deviations ¢# from the Bragg angle $\#_0$. For a fixed angle of incidence a similar violation takes place for changes ¢¸ from the correct wavelegth $¸_0$. Differentiating the Bragg condition, we obtain

$$\frac{d\#_0}{d¸_0} = \frac{K}{4¼n_0}\sin(Ã ¡ \#_0)$$

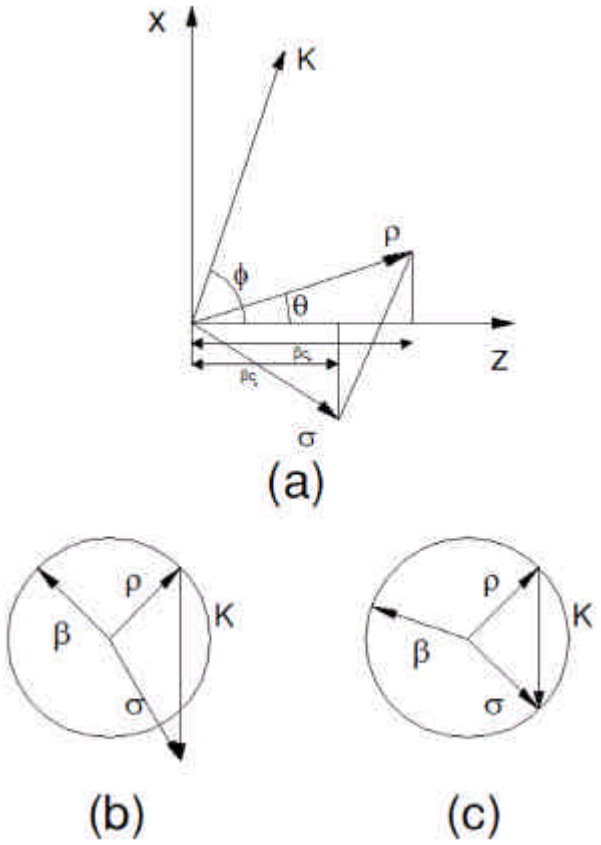

Figure 2.6. Vector diagrams: a) the relation emong the propagation vector and the grating vector; b) conservation of the momentum near the Bragg condition; c) conservation of the momentum at the Bragg incidence.

equation from which follows that there is a close relation between the angular sensitivity and the wave length sensitivity of thick hologram grating. In fact, small changes in the angle of incidence or the wavelength have similar effects.

To express the # and ¸ connection. Kogelnik introduced a new parameter for evaluating the effects of deviations from the Bragg condition. He introduced the dephasing measure ³ defined as

$$³ \equiv \frac{(—^2 - ¾^2)}{2—} = K\cos(Ã - #) - \frac{K^2}{4¼n_0}¸, \tag{2.10}$$

which has been expressed in this form using equation (2.9). A Taylor series expansion of equation (2.10) yields the following expression of ³ for small deviation ¢# and ¢¸ from the Bragg condition,

$$³ = ¢#K\sin(Ã - #_0) - ¢¸\frac{K^2}{4¼n_0}$$

To derive the coupled wave equations, (2.6) and (3.1) are combined, and (2.8) and (2.9) are inserted. Then, the terms involving equal exponentials ($e^{-i½¢x}$ and $e^{-i¾¢x}$) are compared,

$$\begin{aligned} R'' - 2iR'½_z - 2i®—R + 2·—S &= 0 \\ S'' - 2iS'¾_z - 2i®—S + (—^2 - ¾^2)S + 2·—R &= 0 \end{aligned}$$

where the primes indicate differentiation with respect to z. If it is assumed that the energy interchange between S and R, as well as the energy absorption in the medium are slow, the second differetials R'' and S'' can be neglected [8]. The coupled wave equation can be rewritten in the form

$$\begin{aligned} c_R R' + ®R &= -i·S \\ c_S S' + (® + i³)S &= -i·R \end{aligned} \tag{2.11}$$

where the abbreviations c_R and c_S (see Figure 2.6) stand for the expressions

$$c_R = \frac{½_z}{—} = \cos\#$$

$$c_S = \frac{\partial z}{\partial} = \cos\# \; ¡ \; \frac{K}{=} \cos Ã$$

The coupled wave equations (2.11) show that the amplitude of a wave changes along z because of coupling to the other wave ($\cdot R; \cdot S$) or absorption ($®R; ®S$). For deviations from the Bragg condition, S is forced out of synchronism with R, due to the term involving $³S$, and the interaction decreases.

2.2.1 Solution of the Coupled Wave Equations

The general solution of the couples wave equations is

$$R(z) = r_1 e^{°_1 z} + r_2 e^{°_2 z} \qquad (2.12a)$$

$$S(z) = s_1 e^{°_1 z} + s_2 e^{°_2 z} \qquad (2.12b)$$

where r_i and s_i are constants which depend on the boundary conditions. If we insert equations (2.12a) and (2.12b) into (2.11) we find

$$\begin{cases} (c_R °_i + ®) r_i = ¡ i \cdot s_i \\ (c_S °_i + ® + i³) s_i = ¡ i \cdot r_i \end{cases} \qquad (2.13)$$

The boundary conditions for a *transmission grating* are $R(0) = 1$ and $S(0) = 0$. By equations (2.12a) and (2.12b) it follows immediately that

$$\begin{cases} r_1 + r_2 = 1 \\ s_1 + s_2 = 0 \end{cases}$$

Combining these relations with equations (2.13), we find

$$s_1 = ¡ s_2 = ¡ i \frac{\cdot}{c_s (°_1 ¡ °_2)}$$

and we can have the expression for the amplitude of the signal wave at the output of the grating

$$S(d) = i \frac{\cdot}{c_s (°_1 ¡ °_2)} £ e^{°_2 d} ¡ e^{°_1 d} ¤$$

This is a general expression, which is valid for all types of thick transmission holograms including the case of off-Bragg incidence, lossy gratings and slanted fringe planes. All these cases are detailed in the original paper of Kogelnik [8].

For a *reflection grating* the boundary conditions are $R(0) = 1$ and $S(d) = 0$. Hence,

$$\begin{cases} r_1 + r_2 = 1 \\ s_1 e^{-\gamma_1 d} + s_2 e^{-\gamma_2 d} = 0 \end{cases}$$

The relation for s_1 and s_2 can be written in the form

$$\begin{aligned} s_1 \left[e^{-\gamma_2 d} - e^{-\gamma_1 d} \right] &= (s_1 + s_2)\, e^{-\gamma_2 d} \\ s_2 \left[e^{-\gamma_2 d} - e^{-\gamma_1 d} \right] &= -(s_1 + s_2)\, e^{-\gamma_1 d} \end{aligned}$$

Then we can sum equations (2.13) for $i = 1$ and $i = 2$,

$$-i\kappa (r_1 + r_2) = -i\kappa = (s_1 + s_2)(\alpha + i\delta) + c_S (\gamma_1 s_1 + \gamma_2 s_2)$$

After some algebra we finally arrive at the result for the amplitude $S(0)$ of the output signal of a reflection hologram,

$$S(0) = (s_1 + s_2) = -i\kappa \cdot \frac{1}{\alpha + i\delta + c_S \frac{\gamma_1 e^{-\gamma_2 d} - \gamma_2 e^{-\gamma_1 d}}{e^{-\gamma_2 d} - e^{-\gamma_1 d}}}$$

In his paper Kogelnik defines the diffraction efficiency η as

$$\eta = \frac{|c_S|}{c_R} S S^*$$

where S is the complex amplitude of the output signal for a reference wave R incident with unit amplitude. Defined in this way, η is the fraction of the incident light power which is difffracted into the signal wave: S is equal to $S(d)$ for transmission holograms and equal to $S(0)$ for reflection holograms. If the fringes are not slanted, $\tilde{A} = 0$, so $c_S = c_R$ and the diffraction efficiency is

$$\eta = S S^* = |S|^2$$

Volume Transmission Phase Gratings

In lossless phase gratings $\alpha_0 = \alpha_1 = 0$ and the coupling constant is $\cdot = \pi n_1/\lambda$. Diffraction is caused by spatial variation of the refractive index, the amplitude is then

$$S(d) = -ie^{-i\hat{A}} \frac{\sin\sqrt{\mathbb{C}^2 + \hat{A}^2}}{\sqrt{1 + \frac{\hat{A}^2}{\mathbb{C}^2}}}$$

where

$$\mathbb{C} = \frac{\pi n_1}{\lambda} \frac{d}{\cos\theta} \text{ and } \hat{A} = \frac{\Delta\theta d}{2\cos\theta}$$

At the Bragg angle $\Delta\theta = 0$, so that $\hat{A} = 0$ and

$$S(d) = -i\sin\mathbb{C}$$

The diffraction efficiency is then

$$\eta = |S|^2 = \sin^2\mathbb{C} = \sin^2\frac{\pi\delta n d}{\lambda\cos\theta}$$

As either d the thickness, or n_1 the variation of the refractive index increases, the diffraction efficiency increases until the modulation parameter $\mathbb{C} = \pi/2$. At this point $\eta = 1 = 100\%$ (see Table 2.1), and all the energy is in the diffracted beam. When $\mathbb{C}$ increases beyond this point, energy is coupled back into the incident wave and η drops.

If $\alpha_0 \neq 0$, hence for a lossy phase grating, the diffracted amplitude at the Bragg angle is

$$S(d) = -ie^{-i\frac{\alpha_0 d}{\cos\theta}}\sin\mathbb{C}$$

The additional exponential term decreases the peak diffraction efficiency.

Volume Transmission Amplitude Gratings

In an amplitude grating, the refractive index does not vary, so that $n_1 = 0$. However, the absorption constant varies with an amplitude α_1

about its mean value α_0. In this case, the coupling constant $\xi = -i\alpha_1/2$, and the diffracted amplitude is

$$S(d) = -e^{i\frac{\alpha_0 d}{\cos\theta}} e^{i\delta} \frac{\sinh\sqrt{\gamma_\alpha^2 + \delta^2}}{\sqrt{1 + \frac{\delta^2}{\gamma_\alpha^2}}}$$

where

$$\gamma_\alpha = \frac{\alpha_1 d}{2\cos\theta} \text{ and } \delta = \frac{\pi d}{2\cos\theta}$$

For incidence at the Bragg angle, $\delta = 0$ and the diffraction efficiency can be written as

$$\eta = e^{i\frac{2\alpha_0 d}{\cos\theta_0}} \sinh^2 \frac{\alpha_1 d}{2\cos\theta_0}$$

The diffracted amplitude increases with α_1, but since negative values of the absorption are excluded, $\alpha_1 \geq \alpha_0$. The highest diffraction efficiency is therefore obtained when $\alpha_1 = \alpha_0$, for a value $\alpha_1 d\cos\theta_0 = \ln 3$; this maximum has the value (see Table 2.1)

$$\eta = \frac{1}{27} = 0.037 = 3.7\%$$

Volume Reflection Phase Gratings

In reflection holograms the recorded fringe planes are parallel to the surfaces of the recording medium, and the signal appears as a reflection of the reference wave (see Figure 2.5). In a lossless phase grating $\alpha_0 = \alpha_1 = 0$ and the coupling constant is $\xi = \pi n_1/\lambda$. The diffracted amplitude is given by the expression

$$S(0) = i\left[-i\frac{\delta_r}{\gamma_r} + \sqrt{1 - \frac{\delta_r^2}{\gamma_r^2}} \coth\sqrt{\gamma_r^2 - \delta_r^2}\right]^{-1}$$

where

$$\gamma_r = \frac{\pi n_1 d}{\lambda\cos\theta} \text{ and } \delta_r = \frac{\pi d}{2\cos\theta}$$

The diffraction efficiency can be written as

$$\eta = \left[1 + \frac{1 - \frac{\hat{A}_r^2}{\nu_r^2}}{\sinh^2\sqrt{\nu_r^2 - \hat{A}_r^2}}\right]^{-1}$$

For a wave incident at the Bragg angle, $\hat{A}_r = 0$,

$$\eta = \tanh^2 \frac{\pi n_1 d}{\lambda \cos\theta_0}$$

so it increases asymptotically to $\eta = 1 = 100\%$ (see Table 2.1) as the value of ν_r increases.

Volume Reflection Amplitude Gratings

Finally we consider $n_1 = 0$, while α_1 and α_0 are finite. The amplitude of the diffracted wave leaving the hologram is then

$$S(0) = -\left[\frac{\hat{A}_{r\alpha}}{\nu_{r\alpha}} + \sqrt{\left(\frac{\hat{A}_{r\alpha}}{\nu_{r\alpha}}\right)^2 - 1}\coth\sqrt{\hat{A}_{r\alpha}^2 - \nu_{r\alpha}^2}\right]^{-1}$$

where

$$\nu_{r\alpha} = \frac{\alpha_1 d}{2\cos\theta} \text{ and } \hat{A}_{r\alpha} = \frac{\alpha_0 d}{\cos\theta_0} - i\frac{\xi d}{2\cos\theta_0}$$

If the incident wave is at the Bragg angle, $\xi = 0$ and $\hat{A}_{r\alpha}/\nu_{r\alpha} = 2\alpha_0/\alpha_1$, so

$$S(0) = -\left[\frac{2\alpha_0}{\alpha_1} + \sqrt{\frac{4\alpha_0^2}{\alpha_1^2} - 1}\coth\left(\frac{d}{\cos\theta_0}\sqrt{\alpha_0^2 - \alpha_1^2/4}\right)\right]^{-1}$$

When the modulation is maximum, $\alpha_1 = \alpha_0$ the maximum diffraction efficiency is (see Table 2.1)

$$\eta = \frac{1}{\left[2 + \sqrt{3}\right]^2} = 0.072 = 7.2\%$$

2.2.2 Validity of the theory

The maximum diffraction efficiencies that can be obtained with the six types of gratings studied are summarized in Table 2.1.

	Modulation	
Type	Phase	Amplitude
Thin Transmission	33.9%	6.25%
Volume Transmission	100%	3.7%
Volume Reflection	100%	7.2%

Table 2.1. Maximum theoreticl diffraction efficiency for different types of grating

Kogelnik's coupled wave theory is applicable under several assumptions that makes the analysis possible: the spatial modulation of the refractive index and the absorption constant is sinusoidal; there is as a slow energy interchange and only a small absorption loss per wavelength between the two coupled waves; there is the same average index for the region inside and outside the gratings boundaries; light incidence is at or near the Bragg angle and only two diffraction orders which obey to the Bragg condition at least approximately are retained in the analysis. The other diffraction orders are neglected.
Finally, the obtained results where based on the assumption that incident light is polarized perpendicular to the plane of incidence, however Kogelnik showed [8] that these results are the same when the light is polarized in the plane of incidence, provided a new expression for the coupling constant $\cdot$,

$$\cdot_q = \text{¡} \cdot \cos 2(\#_0 \text{¡} \tilde{A})$$

All the results are still valid for parallel polarization if $\cdot$ is replaced by $\cdot_q$.

More accurate theories for the diffraction of light by volume holograms have been developed in the last years. In 1981 Gaylord and Moharam [21] gave an exact definition of a thick grating. To be more pre-

cise, the condition to be fullfilled is not only

$$Q = \frac{K^2 d}{2\pi n} > 1$$

but also

$$\rho = \frac{K}{\alpha^2 n''} > 10$$

where $n'' = \Delta n$ for dielectric gratings and $n'' = \Delta\alpha/2\pi$ for absorption gratings. If the two above conditions are not strictly fullfilled the diffraction may be described by a mixture of Bragg and Raman-Nat regime.

Moreover, the coupled wave theory is widely used to describe thick, isotropic gratings. Howevere an extension of the theory to optically anisotropic materials is needed when dealing with samples showing a strong polarization dependent behaviour or when accurate results are desiderated. The advent of materials with strong birefringence, such as liquid crystal, ordered polymers or organic crystals in the field of volume holography asked for a novel consideration of the anisotropy effects. This was given by Montemezzani and Zgonik in 1997 [22]. In these materials the isotropic Bragg diffraction is strongly affected by the optical anisotropy. The main reason lies in the difference between the energy propagation direction and the wave-front normal. However, without entering in the details, the given notions on the coupled wave theroy seem to me to be enough to understand the diffraction in active Bragg gratings, which is the topic of the next chapter.

The diffraction gratings analyzed in this thesis are Volume Transmission Phase Gratings. In the next chapter their operation mode will be showed.

Chapter 3

Active Bragg Grating

A number of different technologies have been proposed for realizing switchable diffraction gratings, including, quite recently, technologies based on Liquid Crystals (LC) materials. Laser-induced formation of holographic diffraction gratings in polymer-Liquid Crystals (LC) composites has been realized by several research groups [5][9].

At present, the most common process to get these polymer-LC composite gratings is realizing the so-called H-PDLC (Holographic PDLC) [10][11]. It consists in the alternate sequence of isotropic stripes of a polymer-LC mixture followed by stripes of anisotropic PDLC material: the optical contrast between the two series of stripes gives rise to the diffraction grating. It is electrically-switchable because the application of an electric voltage drives the PDLC stripes in an optical state, whose constants are almost matched with those of the isotropic stripes. Thus, under the application of the electric voltage the H-PDLC becomes a homogeneous layer and the grating disappears (see Appendix A).

In this thesis we will focalize our attention on a specific grating, realized by University of Calabria. The authors named this devices POLICRYPS.

3.1 Polymer-LC Composites Diffraction Gratings

Following the same scheme of laser-induced formation of holographic diffraction gratings, a new process has been proposed for the realization of diffraction gratings with polymer-LC composites. The resulting material has been named by the authors POLICRYPS, name that stands for "POlymer LIquid CRYstals Polymer Stripes" [12][13]. It is composed by a sequence of homogeneously aligned LC layers separated by isotropic polymer walls having thickness of the same order as the LC ones (see Figure 3.1).

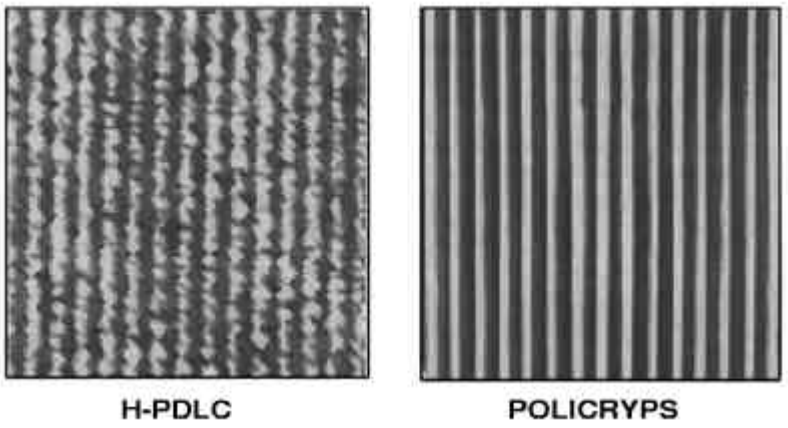

Figure 3.1. SEM microscope images of PDLC and Policryps gratings

From a morphological point of view, the biggest difference between H-PDLCs and POLICRYPS is the following. In the former, in the UV-illuminated regions, a light-induced phase separation process creates LC droplets embedded in a polymer matrix, while the dark regions remain in the form of isotropic LC-polymer mixture (see Figure 3.1a). In the latter material, no phase separation happens within the illuminated regions, instead, under particular conditions, it happens between the illuminated and non-illuminated regions, so that one component (namely polymer) is almost totally confined within illuminated regions and the

other component (namely LC) within non-illuminated regions, resulting in the geometry depicted in Figure 3.1b.

One essential feature that these composite materials must exhibit, in order to be attractive for telecom applications, consists in their transparency in both the ON and the OFF states. This constraint imposes an upper limit to the size of the droplets in the PDLC; in fact droplet size of the order of the light wavelength gives rise to significant scattering losses. For this reason, nano-PDLC with droplet size of the order of $100nm$ have been developed by different authors[10][11]. Nano-PDLC may show a very high diffraction efficiency and good transparency having however as a drawback a quite large driving voltage, increasing with decreasing droplet size. Due to their morphology, being a stack of uniform and transparent layers, POLICRYPS samples are inherently transparent.

One of the aims of the present work was to give an optical characterization of some POLICRYPS samples both in the visible range, at $\lambda = 633nm$, and in the near IR, at $\lambda = 1550nm$ that is the C-band of the 3^{rd} window for optical communications [14][15][16]. It is worth noting that very few optical characterizations have been performed until now at telecom wavelengths on LC materials and in particular on polymer-LC composites. In our opinion, this lack of necessary data and the consequent uncertainty on working performances might be one reason for the limited present utilization of these materials in devices and systems for optical networks.

The studied samples have been kindly provided by the group that has developed POLICRYPS at the University of Calabria, in the frame of a running Italian National Research Project [18]. The whole production process has been for many years patent pending, since only few months the authors had the opportunity to publish it [19][20]. Their winning idea was to avoid the formation of a separate Nematic Liquid Crystals (NLC) phase and consequently the growing of NLC droplets, during the polymerization process. In this way they obtained only a macroscopic phase separation that is an almost complete redistribution of nematic

and monomer components inside the sample. The standard procedure to obtain POLICRYPS gratings consists of three steps:

1) the photoinitiator-monomer-NLC mixture is heated up to a temperature above the Nematic-Isotropic transition. This cunning prevents the appearance of a nematic phase during the curing process;
2) the sample is illuminated with an interference pattern of curing UV radiation;
3) after the curing radiation is switched off and the polymerization process has come to an end, the sample temperature is kept down below the Isotropic-Nematic transition point.

For further information on POLICRYPS production process I suggest their inventors lectures [12][13][19][20].

3.2 POLICRYPS Operating Model

Measurements had been performed on three different samples labelled as HCB-25, HCB-31, and HCB-3, respectively. They were made starting from the same initial mixture, a solution of 30% liquid crystal (5CB, provided by Merck) in a commercially available pre-polymer (Norland Optical Adhesive NOA-65). This blend was injected by capillarity into a cell realised with two ITO coated glasses separated by Mylar spacers. These samples were heated over the Nematic-Isotropic phase transition temperature of the LC component and cured by a UV laser interference pattern ($\lambda = 351nm$, $I = 10 \div 100mW/cm^2$).

Samples differ only in two geometrical parameters, the pitch Λ and the thickness d[6], that are reported in Table 3.2; in the volume of the sample, fringes are disposed, in both cases, perpendicularly to the cell glasses.

[6] The grating pitch is defined as usual and the grating depth is the distance between the two glass plates.

Acronym	HE-3	HCB-25	HCB-31
Liquid Crystal	5CB	5CB	5CB
Grating Pitch (^{1}m)	0.6	1.34	1.34
Grating depth (^{1}m)	12.0	7.8	8.8

Table 3.2. Samples Characteristics

The behaviour of the grating is strictly dependent on the incident beam polarization: it is possible to reach the diffraction condition only with a p-polarized wave. The reason should be found in the molecular orientation inside the LC layers. First, let's recall that at $\lambda = 633nm$ and $25^{\pm}C$ the polymer NOA-65 refractive index is $n_p = 1{:}56$ and the values for 5CB indices are $n_o = 1{:}53$ and $n_e = 1{:}71$, respectively; in the isotropic phase ($35^{\pm}$C) 5CB refractive index is $n_{iso} = 1{:}57$. Now, the polarization dependence clearly indicates that, without any applied field, the molecular director is not randomly distributed in POLICRYPS, as is for instance in a PDLC sample. For light impinging at quasi-normal incidence, no grating formation (OFF-state) for s-polarized wave has been observed, thus the LC regions must exhibit a refractive index value close to the polymeric one, as the ordinary index is. Instead, a p-polarized wave experiences a phase grating, thus the index seen in the LC layers must be quite different from the polymeric one, then closer to the LC extraordinary index value than in the previous case. This behaviour suggests that the most likely unperturbed molecular orientation within the LC layers is along the plane of incidence and orthogonal to the polymeric walls as shown in Figure 3.2. This molecular orientation inside the grating explain the POLICRYPS operating model, described in Figure 3.2: when p-polarized light impinges on the sample at a small angle, it experiences a LC refractive index close to n_e, without any applied external field, and close to n_o, with an applied electric field that fully reorients the LC director. Being $n_p \simeq n_o << n_e$, by means of the external voltage we can switch from a diffraction state (ON state, when a high index mismatch is achieved between adjacent fringes) to a transmission state (OFF state, obtained when the LC refractive index matches

polymer one)[7]. On the other hand, POLICRYPS cannot operate properly with s-polarized light, because in this case, it is the ordinary wave that propagates through the sample and, with or without applied electric field, it sees always the LC ordinary refractive index.

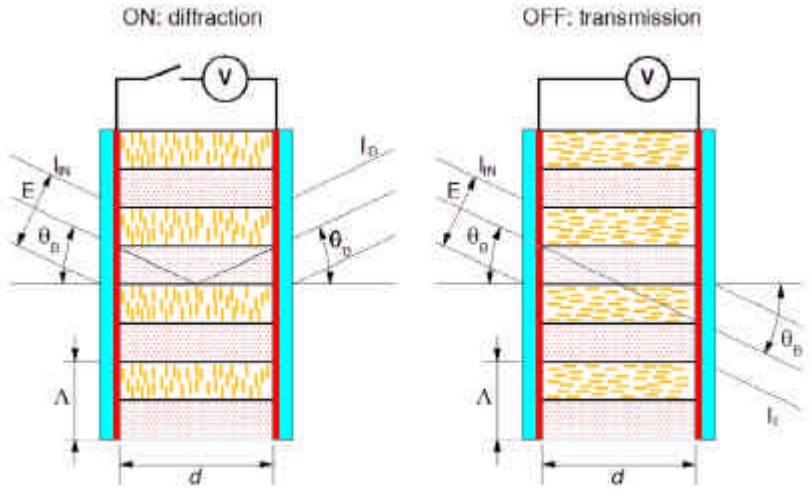

Figure 3.2. POLICRYPS Operating Model

3.3 Measurement

Measurements had been performed with both stationary and dynamic electric fields to fully characterize the samples with red light and near infrared light. In this work only the most important graphs are reported, just to point out the gratings performances.

Static measurements had been performed on HBC-25 and HCB-31 samples. Dynamic measurement on all the samples.

[7] Please notice that here and in the following ON and OFF states are referred to the effectiveness of the diffraction grating and not to the application of the external voltage.

The data analysis for the static measurements will foremost consider two quantities: the diffraction efficiency and the losses.

I set with I_{IN} the intensity of the incident light, with I_T the intensity of the transmitted beam (the zero order), with I_D the intensity of the diffracted ray (the first order), and with I_L the intensity lost because of the reflections between interfaces, diffusion and absorption of the sample.

In all measurements presented in the following and related discussions, the impinging light is always p-polarized, moreover we define the Diffraction Efficiency (DE) as the ratio between the diffracted light intensity and the total light intensity, diffracted plus transmitted, behind the sample:

$$I_{IN} = I_T + I_D + I_L \tag{3.1}$$

The quantity I_L has been calculated by difference between the measured quantities I_{IN}, I_T and I_D. Hence, I_L includes also the intensities of higher diffracted orders. But being in our gratings $Q > 1$ we assume that this effect is negligible.

We define

$$\eta_T = \frac{I_T}{I_{IN}}, \quad \eta_D = \frac{I_D}{I_{IN}}, \quad \alpha = \frac{I_P}{I_{IN}}$$

respectively as the efficiency for the transmitted order, the efficiency for the diffracted order and α the losses. Equation (3.1) becomes

$$1 = \eta_T + \eta_D + \alpha$$

Usually diffraction efficiency is used to name the quantity η_D. By the way, in this work I introduce a new parameter

$$\eta' = \frac{I_D}{I_T + I_D} = \frac{I_D}{I_{IN} - I_P} = \frac{\eta_D}{1 - \alpha},$$

If the losses are negligible, $\alpha = 0$, and η is the diffraction efficiency.

3.3.1 Diffraction Efficiency versus Temperature

The used liquid crystal, 5CB nematic liquid crystal, has a clearing point around $35^{\pm}C$, thus a strong temperature dependence on both n_e and n_o around room temperature. Further considering that 5CB refractive index in the isotropic phase is quite close to the polymeric index n_p, hence a drastic drop of the diffraction efficiency heating the sample from room temperature to over $35^{\pm}C$ is expected. Figure 3.3 shows DE

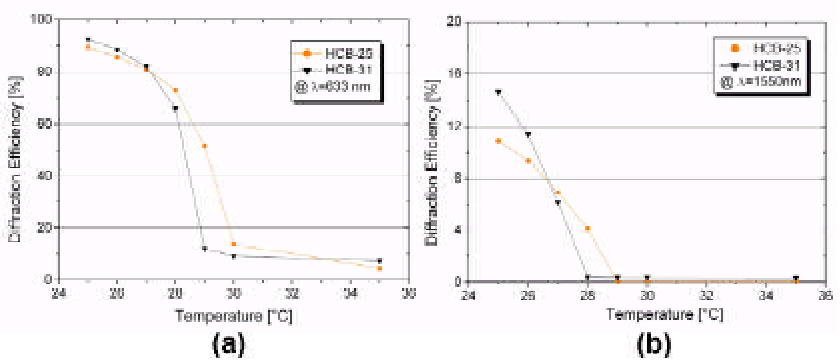

Figure 3.3. DE versus Temperature (a) @ 633nm (b) @1550nm

versus temperature using He-Ne light at $633nm$ and a DFB laser diode at $1550nm$, respectively, for two of the three samples. It should be noted that DE drop off temperature is always less than 5CB clearing temperature indicating a mesophase modification, in particular a reduction of the nematic range, induced in this confined geometry. This loss of nematic behaviour could be ascribed to the effect of impurities certainly present in the LC regions owing to the production process of this composite: a low concentration of unreacted monomers as well as of photoinitiator molecules is still present within LC layers after the phase separation process. Eventually, impurities effect could have been enhanced by effect of confinement. The two samples give quite similar responses. The most significant difference is observed between the curves recorded with red and NIR light. DE, which at $25^{\pm}C$ can arrive over 90% with red

light, hardly reaches 15% with NIR light. It is almost evident that the choice made by the samples producer, concerning the refractive indices values of the materials, was in the direction of optimising performances working with red light.

3.3.2 Diffraction Efficiency versus Applied Voltage

Static measurements had been performed using an AC square voltage at a sufficiently high frequency, say 1kHz, in order to avoid unwanted effects induced by the flow of free ions within the sample. Results

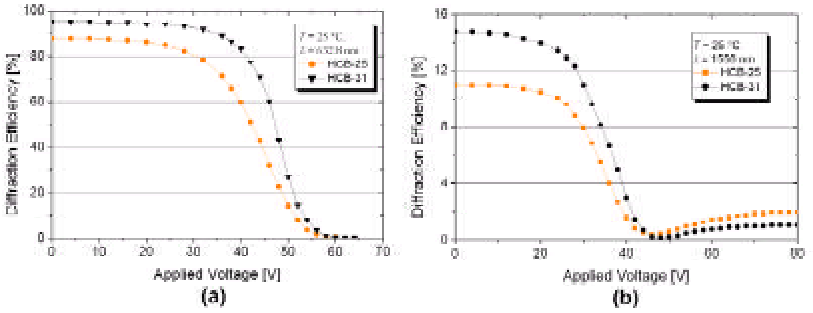

Figure 3.4. DE versus Voltage (a) @ 633nm (b) @1550nm

are shown in Figures 3.4a and 3.4b for red and NIR light, respectively. A very interesting features of POLICRYPS gratings that can be inferred by these results is the switching voltage. Actually, a threshold voltage of around $40V$ was observed with red light in the sample HCB-31 and even less in the HCB-25 one, yielding a threshold field of about $4{:}5V{=}{}^{1}m$ in both cases. This is neither a very low nor a very high field for electric switching of LC-polymer composites, however if we compare it with competing nano-sized H-PDLC's, the POLICRYPS value is by far lower than those commonly observed in nano-PDLC's. Furthermore, it has

been obtained in the very first POLICRYPS samples, not optimised at all for electric performance.

In Figure 3.4b, showing DE versus voltage obtained with NIR light, we notice again the large decrease in the maximum diffraction efficiency. Moreover, a slight decrease in the threshold voltage is observed. A complete switching off is reached for voltage around $45V$; however, further increasing the applied voltage above $50V$ leads to a small "undesired" increase of the diffraction efficiency. We can deduce that, using NIR light, the OFF state of the grating is not reached when the molecular reorientation is completed in the LC regions, as it is in the case of using red light, but instead for some intermediate configuration.

Observations in this and in the previous sub-section consistently confirm that the samples under investigations have fairly good performances at $633nm$, while they are not optimised at $1550nm$. This behaviour was expected and our purpose was exactly a quantitative evaluation of this performance degradation and possibly its correlation with material parameters' variation. In fact, if the three index values, n_e, n_o, n_p, are properly chosen at red wavelength, owing to the great difference between the dispersion curves of the polymeric material and the LC one, they cannot be optimised at the wavelength of $1550nm$.

3.3.3 Angular Selectivity

The angular selectivity is an important parameter for photonic applications. In Figure 3.5, the grating response varying the angle of incidence of the light beam around the Bragg angle is shown. The wide angular response (' $20^{\pm}$) observed at both wavelength, could be a problem for the telecom application. However, it can be affected and tuned by changing the geometry of the grating, especially the grating length, and/or by using the grating in reflection rather than in transmission.

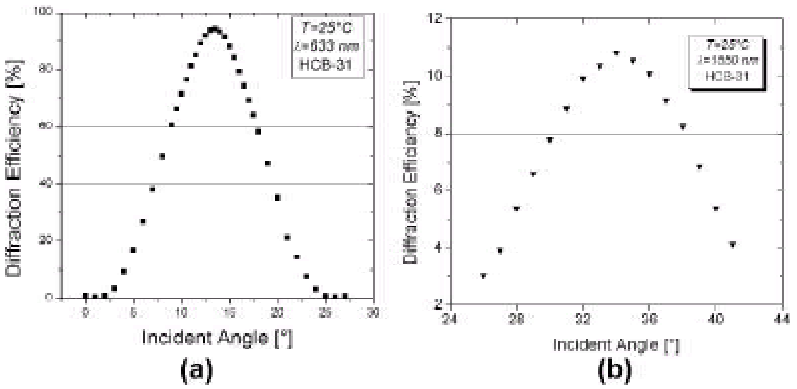

Figure 3.5. DE versus incident angle at 633 nm (a) and 1550 nm (b)

3.3.4 Losses

Table 3.3 summarizes the measured losses at both wavelengths, for the ON and the OFF state. The total losses ° have been divided in two terms

$$° = °_b + °_{s+a}$$

where $°_b$ are losses due to backreflection, and $°_{s+a}$ includes the losses due to scattering and absorption. Losses in the NIR are higher than in the red. The losses due to backreflection can be minimized in the device using an antireflection coating.

¸		´T	´D	°	°b	°s+a
632:8nm	ON	5.8	81.3	12.9	3.1	9.8
	OFF	86.3	0.6	13.1	7.7	5.4
1550nm	ON	67.1	14.7	18.2	4.1	14.1
	OFF	82.8	0.2	17.1	3.8	13.3

Table 3.3. Efficiencies and Losses is POLICRYPS gratings at 632.8nm and 1550nm. Values are expressed as the per cent value of the incident light.

3.3.5 Dynamic

Let us focus the discussion on the dynamical response of POLICRYPS grating to a variable electric field. Obtained results are quite similar on all the sample, thus here only those for HCB-25 are reported. In all the following, the impinging light is always p-polarized. POLICRYPS response times were measured by recording the diffracted beam signal detected by a photodiode. A driving voltage, enough to completely switch off the diffractive device, was applied to the ITO electrodes, using different frequencies in the range $1 ¥ 100Hz$. In order to avoid static electric biasing of the sample all the applied waveform were zero-average. Figure 3.6 shows the oscilloscope image recorded: the applied waveform is shown in the lower part and the optical response in the upper part.

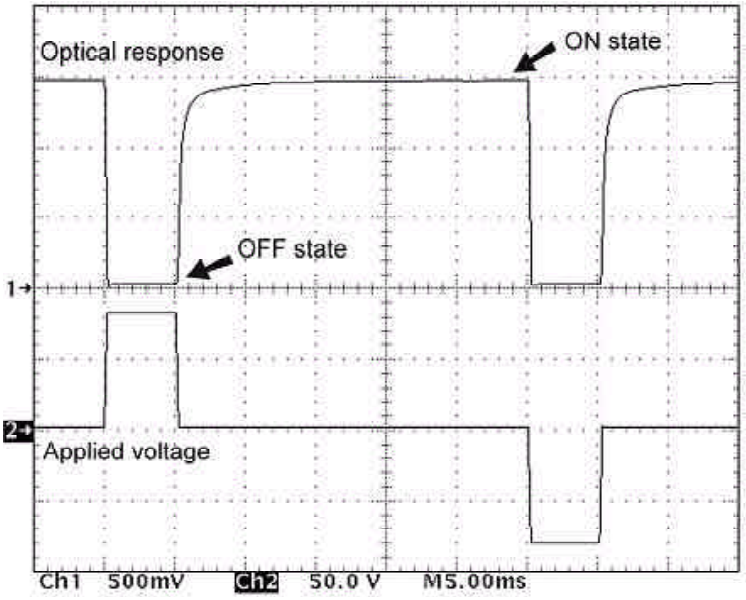

Figure 3.6. Oscilloscope snapshot of the applied field (channel 2) and the diffracted beam optical response (channel 1).

Figure 3.7 shows the oscilloscope image recorded with red light at voltage frequencies of $100Hz$ (3.7a) and $1Hz$ (3.7b), respectively.

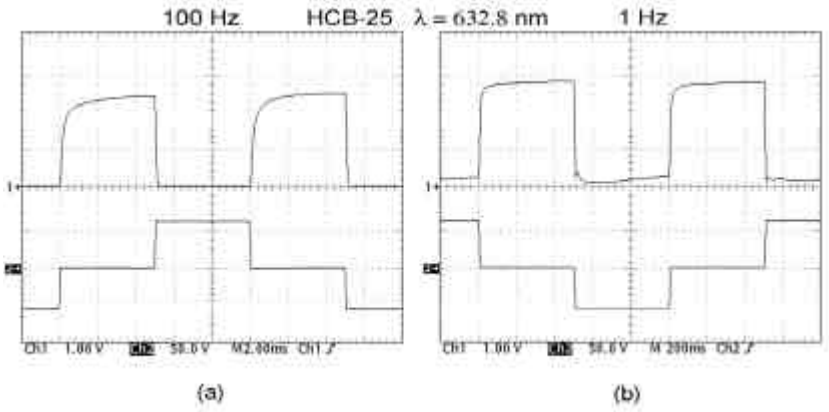

Figure 3.7. Optical response, upper curves, and driving waveform, lower curves, at 633nm. a) voltage frequency 100 Hz; b) 1 Hz

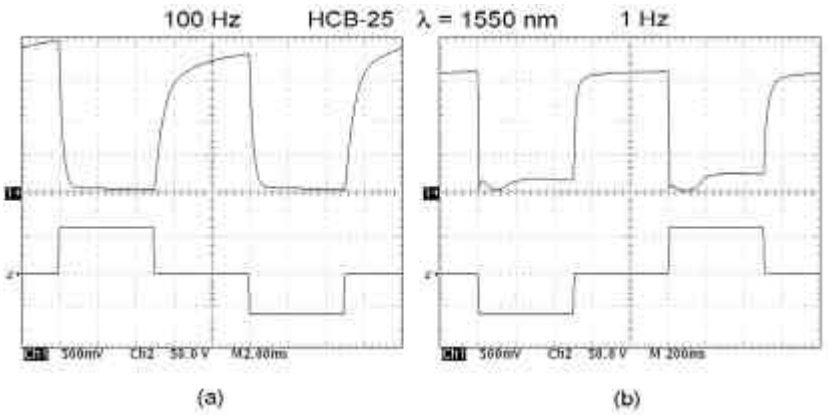

Figure 3.8. Optical response, upper curves, and driving waveform, lower curves, at 1550nm. a) voltage frequency 100 Hz; b) 1 Hz.

Figure 3.8 shows the analogous images recorded with NIR light. In Figures 3.7b and 3.8b, the optical response at 1Hz exhibits an irregular behaviour and even a slight increase with time of the detected signal during the half period corresponding to the OFF state, that is when the applied voltage is different from zero. This was unexpected and probably due to a molecular flow and/or turbulence induced by free charge (ions) motion under the effect of a constant voltage for a quite long time, say 500ms. To overcome this problem, a different waveform was used, in which the previous square voltage at a slow frequency f_1 is further modulated at a faster frequency f_2, in the range $1 \div 10kHz$, the voltage amplitude being fixed at 60V. Generally, liquid crystals have response times too slow to follow such fast driving signal as the ones at frequency f_2, so that the reorientation torque is almost equivalent to that imposed by a constant voltage of same rms value. However, in this way one can get rid of any effect caused by collective ion motion inside the sample.

In Figures 3.9 and 3.10, same pictures captured on the oscilloscope display are reported as in Figures 3.7 and 3.8, but with the double frequency modulation of the waveform[8].

A summary of the most significant results is presented in the Table 3.4. Differences among the achievements at λ_{red} and λ_{NIR} are again evident, despite the fact that molecular reorientation in LC is obviously only driven by electric and elastic forces and must not depend on the light travelling in the sample. However, the response of the diffraction grating is not immediately and only related to the LC molecular director reorientation. It is known that several geometric and optic parameters enter in the determination of a Bragg grating DE, ruled by the so-called Kogelnik formula [21]:

$$DE = \sin^2 \frac{2\pi d \cdot n}{\lambda \cos \theta_B}$$

where

[8] Notice that in Figures 3.9b and 3.10b, recorded with f_1 *=1 Hz*, the modulation at f_2 is not viewable in the waveform, because the ratio f_2/f_1 is too high to let both frequencies be displayed simultaneously; for the same reason the shown amplitude scale (channel 2) is meaningless.

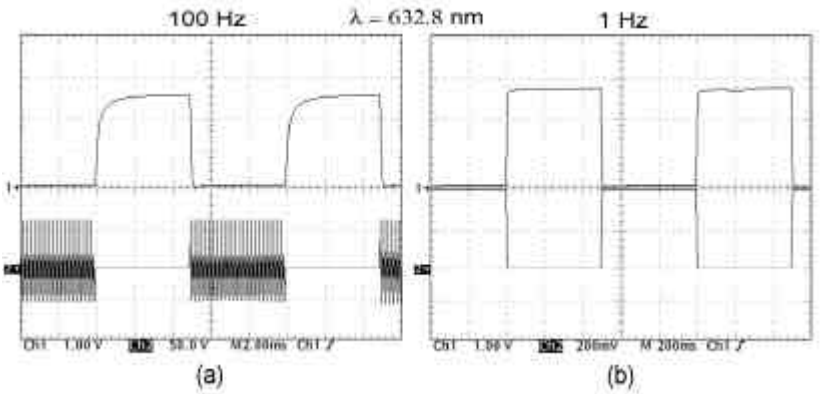

Figure 3.9. a) voltage frequency 100 Hz; b) 1 Hz.

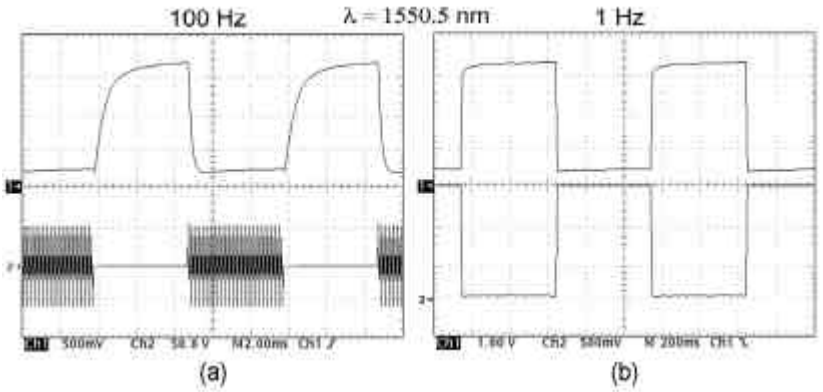

Figure 3.10. a) voltage frequency 100 Hz; b) 1 Hz.

$$2\Lambda \sin\theta_B = \lambda$$

d is the grating depth, Λ the period and Δn the difference between the polymer and the LC refractive index. Refractive index values and refractive index contrast amongst the layers are the most important parameters affecting DE in Kogelnik formula[9]. Unfortunately, not many data about refractive index values at NIR are presently available for LC materials, so that a comprehensive comparison of theoretical predictions and experimental findings has not been performed yet.

Light wavelength λ [nm]	Voltage frequency f_1 [Hz]	Modulation frequency f_2 [Hz]	t_{ON} [μs]	t_{OFF} [μs]
633	1	1000	1300	160
633	10	1000	1000	130
633	100	10000	900	70
1550	1	1000	2800	440
1550	10	10000	3200	320
1550	50	5000	1500	370
1550	100	10000	1300	320

Table 3.4. Response times of Policryps samples

From the last two columns of the Table, it is evident also that t_{OFF} times are one order of magnitude smaller than t_{ON} times, the former being in the hundreds of μs range, and the latter in the ms one. Let's recall that the grating is switched OFF while the electric field is applied and switched ON when it is removed. For that, the torque responsible for molecular reorientation in the LC layers is ruled during switching OFF by the balance between elastic forces and electric ones. In our case, the electric field is quite intense, that is about $4{:}5V/\mu m$, yielding a fast reori-

[9] For anisotropic materials Kogelnik formula has been extended by the theory of Montemezzani and co-workers.

entation. On the other hand, molecular reorientation during switching ON is only due to restoring elastic forces, that is mainly to surface interactions with the polymer layers and the glass substrates. Thus, the observed difference in response times is in agreement at least qualitatively with the physical picture underlying it. However, large fluctuations in the measured t_{ON} times had been observed, not comparable with those observed in t_{OFF} ones. For instance, standard errors in t_{OFF} have been estimated to be about 5%, while standard errors in t_{ON} are even greater than 25%, putting some doubts on the way we have measured them, as the time interval between 10% and 90% values of the maximum light signal detected by the photodiode. Looking more carefully at the switching ON process, it appears that it is not ruled by a single time constant.

Figures 3.11 and 3.12 show digitised data of switching ON oscilloscope tracks, open circles, together with a single exponential fit, dotted lines, and a two-exponential fit, solid lines. The figures correspond to two properly chosen experimental recordings, but all the others gave completely similar results. It is fairly evident that the single exponential curve can't fit reasonably the data points, while a very good fit is obtained by the two-exponential curve. In fact, a $\hat{A}^2$ value 100 times lower is obtained in the latter case (see the insert in Figures 3.11 and 3.12). This result gave us an indication that two competing physical mechanisms are intervening in restoring the orientational order in the LC layers.

A Model for the POLICRYPS Dynamical Response

In order to understand the dynamical response of these gratings it is necessary to refer to their particular structure: inside a POLICRYPS, LC molecules are confined both from the polymer stripes and the cell glass walls; however, the first interaction seems much more important, for the a double reason:

1) the alignment is likely induced by the polymer (glass walls are just cleaned and not further treated)

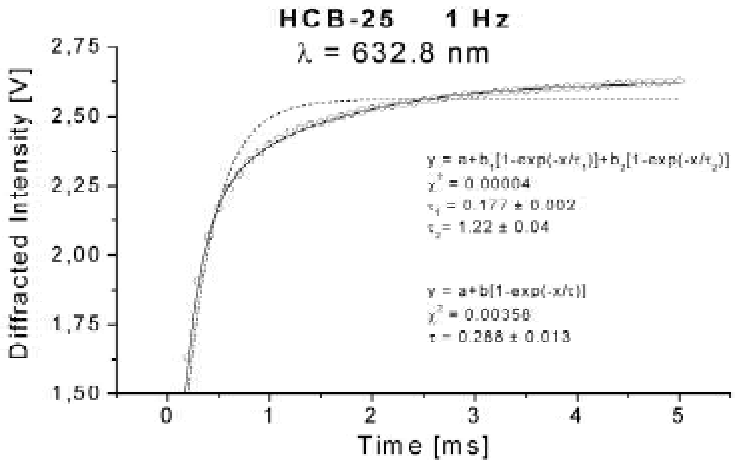

Figure 3.11. Analysis of optical response in the OFF-ON transition at 633nm: experimental data (open circles); single exponential fit (dotted line); two-exponential fit (solid line).

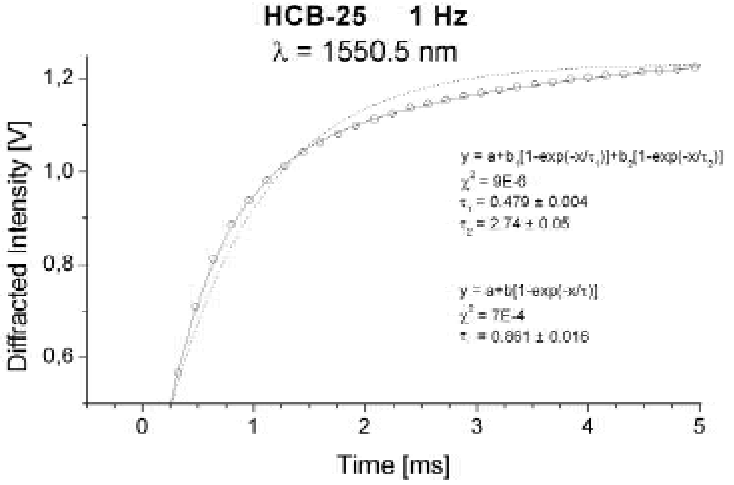

Figure 3.12. Analysis of optical response in the OFF-ON transition at 1550nm: experimental data (open circles); single exponential fit (dotted line); two-exponential fit (solid line).

2) the distance L between the polymeric walls is much shorter than the cell thickness d.

Because of these considerations, the behaviour of another sample with different features has been investigated: sample HCB-3 shows a smaller pitch and a bigger thickness (see Table 3.2). Infrared light was not used, because the pitch of this new sample was too small to allow the Bragg diffraction in the IR; however the response times does not seem to be strongly dependent on wavelength.

The thickness of the liquid crystal film does not exceede 30% of the nominal pitch ($L \sim 0{:}40\,\mu m$ for sample HCB-25 and $L \sim 0{:}18\,\mu m$ for sample HCB-3), proportionally to the LC concentration in the mixture. These values for L are theoretical maxima, assuming a complete material separation during the fabrication process; thus we expect shorter actual values.

By an external voltage one can create an electric field E perpendicularly to the LC director, which is orthogonal to the polymer stripes; thus, the situation is quite similar to the classical configuration for a Fréederiksz transition experiment [26]. In the case of strong anchoring, the Fréederiksz threshold field is given by:

$$E_0 = \frac{\pi}{L}\sqrt{\frac{k}{\varepsilon_0 \Delta\varepsilon}} \tag{3.2}$$

while the reorientation time constant is

$$\tau_E = \frac{\eta}{\varepsilon_0 \Delta\varepsilon}\frac{1}{(E^2 - E_0^2)} \tag{3.3}$$

where L is the distance between the anchoring surfaces, k is the elastic constant (in our geometry, the bend one, $k = 8{:}4 \cdot 10^{-12}$N), $\Delta\varepsilon$ is the LC dielectric anisotropy ($\Delta\varepsilon = 11{:}5$), ε_0 is the vacuum dielectric constant and η the viscosity ($\sim 10^{-2}$ Pa$\cdot$s). Putting Equation (3.2) into Equation (3.3) and setting $E = 0$, the expression for the relaxation time constant

is obtained:

$$\tau_r = \frac{\eta L^2}{k\pi^2} \tag{3.4}$$

Note that in the previous formulae τ is the usual exponential time constant, that is related to the experimentally measured 10-90% response time by means of the relation $t_{10-90} = 2.2\tau$.

Of course, the situation is much more complicated than in the simple homeotropic LC cell, because we cannot observe directly the director reorientation, but only the effect produced by the reorientation on the optical response of the grating. Nevertheless, these formulae are useful to understand the experimental behaviour of our samples.

Switching off Dynamic

The switching off dynamic is ruled by the electrical reorientation of the liquid crystal director. First, I experimentally determined the minimum voltage required to obtain a complete switching off; then I increased stepwise the voltage up to reach a saturation in the fall time curve (Figure 3.13). As expected, due to the different thickness of the LC layers, the complete switching off field for sample HCB-25 was lower than for sample HCB-3. For both samples the higher electric field corresponds to a faster response time, but in sample HCB-3 the response dependence on the applied field was much more important than in sample HCB-25. For the former I measured a variation in the range 50 ÷ 650 μs, while for the latter I observed times within the narrower interval 30 ÷ 170 μs (see Table 3.5).

	Fall Time [μs]		Rise Time [μs]	
	min	max	min	max
Sample HCB-25	30	170	180	1040
Sample HCB-3	50	650	130	280

Table 3.5. Response time ranges

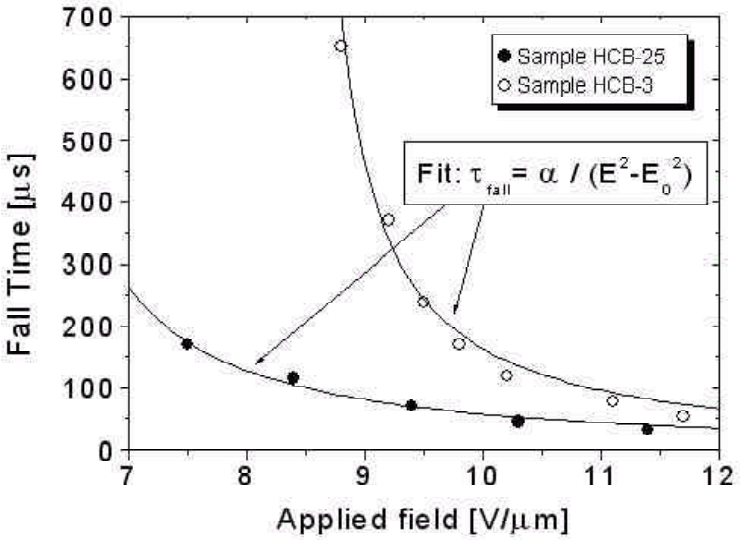

Figure 3.13. Fall time dependence on the applied field, experimental points and fit.

By means of a fitting procedure, we also verified that the fall time dependence on the electric field is well described by equation (3.3). From the fit we can calculate the rotational viscosity °, according to equation (3.3), and obtain the values $0{:}17 \S 0{:}02 Pa¢s$ and $0{:}22 \S 0{:}02 Pa¢s$ for the sample HCB-25 and HCB-3, respectively. These values differ by one order of magnitude from the value provided in literature for 5CB: ° should be » $10^{i2} Pa¢s$. This difference can be due to the presence of impurities, like polymeric clusters that affect the LC domains. For the threshold fields E_0 in the two samples, we found the values $5{:}9 \S 0{:}3 V=¹m$ and $8{:}37 \S 0{:}04 V=¹m$, respectively. The ratio of these fields, 1:4, is quite different from the value of 2:2, calculated by using the maximum allowed width of the LC layers. In fact, if we put our E_0 fitted values in equation (3.2), we get for the width L of the LC stripes, the values $0{:}15¹m$ (= $0{:}11¢¤$) and $0{:}11¹m$ (= $0{:}18¢¤$), both much less than 30% of the grating pitch ¤.

Even adopting a simplified model, it seems reasonable to infer that the pitch fraction really occupied by the liquid crystal is strongly depen-

dent on the fabrication procedure; in particular, the different result in the two samples can be related to the different control of the set-up mechanical stability ensured during the curing process: larger vibrations producing wider irradiated areas and broader polymer layers.

Switching on Dynamic

Unlike the switching off, the switching on process is not ruled by the electric field, but only by the elastic torque induced by the surface anchoring; this torque drives the relaxation of the LC director towards the zero-field orientation. Nonetheless, contrary to an intuitive expectation, also the rise time was found to depend on the pulse shape: in Figure 3.14, the non linear dependence of the rise time on the pulse duration is shown for different amplitudes; in Figure 3.15, the same experimental data are reported versus the pulse amplitude for different pulse durations, showing an almost linear behaviour. In this case, that is for switching ON, the sample HCB-25 showed the largest variation of the response time ($180 \div 1040^{-1}s$), while sample HCB-3 rise time changed only in the range $130 \div 280^{-1}s$ (Table 3.5). Hence, our experimental results indicate that some kind of "memory" of the electric field that has been applied still remains for a while when only the elastic restoring torques are effective. In our opinion, the observed behaviour can be explained by assuming that a partial anchoring breaking and restoring, ruled by a surface viscosity, happens at the LC-polymer interface. Indeed, we don't expect that the interfacial region is very thin, i.e. of the order of few molecular layers. On the contrary due to the curing process, a fraction of the LC molecules remains partially embedded in the adjacent polymer stripes, close to the border, still retaining a reduced mobility. Moreover, the curing interference pattern has not a rectangular profile, but instead a $\cos^2$ one, thus we expect a reduced number of polymeric links close to the LC-polymer border. Finally, the degree of spatial stability of the pattern does certainly affect the width and softness of the interfacial region. Therefore, let us depict the consequent scenario. When the electric field

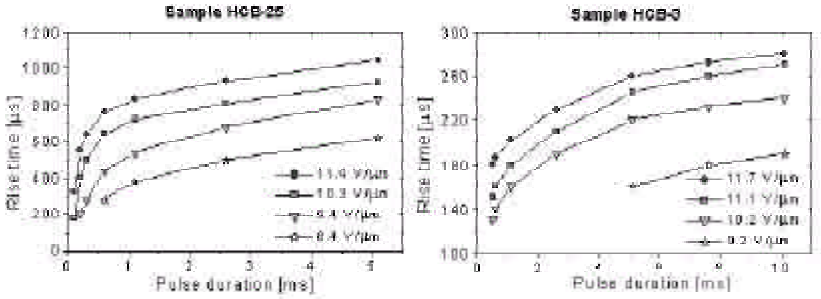

Figure 3.14. Rise time dependence on the pulse duration for different pulse amplitudes.

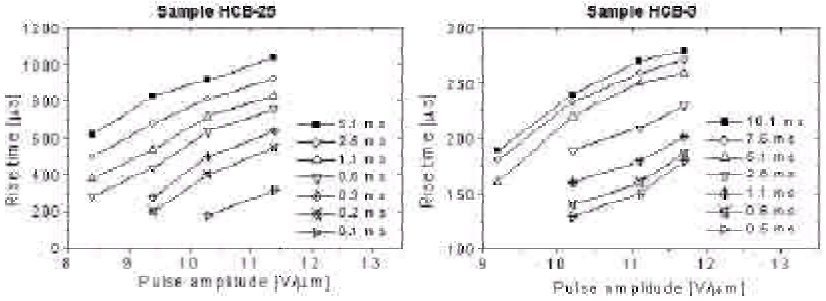

Figure 3.15. Same experimental points; here rise time is reported versus pulse amplitude for different pulse durations.

is switched on, surface and bulk molecules reorient with a different viscosity, corresponding to different time constants. Bulk response is faster and is responsible for the strong reduction of the diffraction efficiency; the response of the surface layer is slower but its influence on the optical signal is almost negligible because this layer is much thinner. When the electric field is switched off, the boundaries play the main role in the reorientation process, thus in determining the response dependence on the pulse shape. Short and/or weak electric pulses are not able to affect significantly the reorientation of the director in the surface layer; only bulk molecules reorient and both ("o" and "off") transitions are ruled by a simple Fréederiksz transition model with strong anchoring, according to the equations (3.3) and (3.4). Putting in the last equation the data obtained from our fit, we obtain for the elastic relaxation time of the two samples the values $110 \pm 20^{1}s$ and $68 \pm 7^{1}s$ respectively, which could be considered as limiting values in the case of a perfect interface and infinite anchoring energy. Latter values are obviously smaller than the smallest measured relaxation times.

For long and/or strong pulses, also the molecules in the interfacial region are partially reoriented. These molecules are affected by a higher surface viscosity and need more time to resume the initial orientation than the bulk ones. At the removal of the electric field, the molecular director in the bulk undergoes a first quick reorientation towards the intermediate orientational state held by the director at the surface; then, with a slower time constant, the director at the surface will relax towards the unperturbed state and the bulk director will follow it adiabatically. The final result is that the overall relaxation time is a mix of the bulk and surface time constants, which depends on the intermediate state of reorientation reached by the director at the surface under the effect of the electric field.

This hypothesis can also account for the quite complex shape of the relaxation optical signal. As said before, experimental curves cannot be described by a single exponential function [15]. A good fit is obtained only by using a double exponential or some kind of sigmoid curve (Fig-

ure 3.16): all these functions have a common general shape, with a fast growing part, followed by a very slow saturation tail. We guess this can be connected to the different bulk and surface viscosity values.

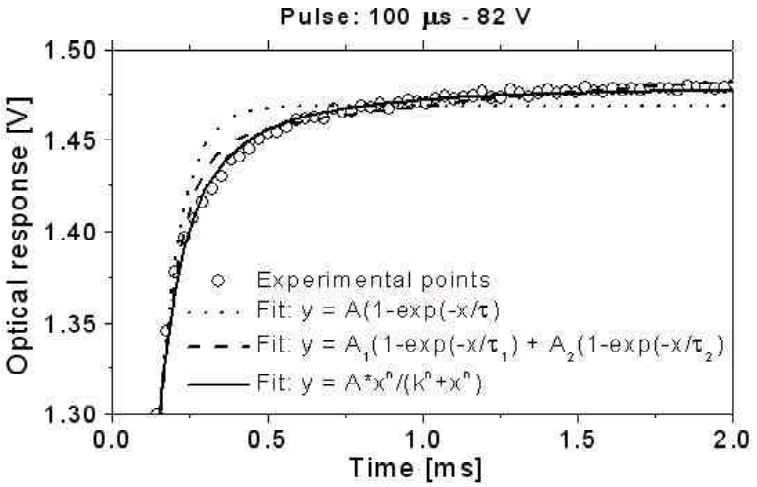

Figure 3.16. Diffracted beam optical signal (circles) during the off-on transition; lines show different fitting curves.

Finally, from an application point of view, we underline that, by choosing short driving pulses and a proper voltage, it is possible to get simultaneously both response times in the range 50 ¥ 150 ¹ s. Furthermore, as mentioned above, the large value of the bulk viscosity found in the LC stripes determines the limiting values for achievable response times: optimisation of the fabrication process will have a positive effects also in lowering the viscosity, hence on the switching dynamics.

3.4 Summarizing

We performed an electro-optical characterization of the first produced POLICRYPS samples using red light and NIR light in the telecom C-band. We wanted to make a comparison among POLICRYPS perfor-

mances at the two wavelengths, in particular observing how and how much performances were degrading at NIR wavelength. Obtained results are not only interesting but also very useful because they prove that this new LC-polymer composite can be conveniently exploited for photonic applications in the telecom field, once they have been optimised for use at telecom wavelengths. Our results together with a careful theoretical analysis, now in progress with Montemezzani theory, can give the needed feedback to the POLICRYPS producer for its optimisation in view of the wanted applications.

POLICRYPS grating with diffraction efficiency over 90%, good angular selectivity, and time response in the microsecond range, can be very soon obtained in the C-band, still maintaining a very good optical transparency with almost negligible scattering losses.

We showed how both switching off and switching on times strongly depend on amplitude and duration of the applied electric pulses. This was not expected for the elastic off-on transition and has been explained by assuming an essential role of the interfacial region between the LC and the polymer stripes, without a well-defined and sharp border, exhibiting a surface viscosity higher than the LC bulk one.

Though both rise and fall response times can change in a wide range, it was already possible for those first batch and not-optimised samples, to get values in the range $50 \div 150\ \mu s$, by means of a proper choice of the driving pulse shape. These results are very attractive for many possible applications of a key component, like a fast switchable Bragg grating, in telecom devices. Moreover, they can be the starting point for fundamental studies on bulk and surface elastic interactions in liquid crystalline composite materials.

Chapter 4

Photonics of Periodic Structures

To realize the continuously increasing performance demands for communication systems, like Wavelength Division Multiplexing (WDM), more and more stringent requirements are imposed on laser, like a narrow linewidth, low threshold, high speed and a dynamic single-mode (DSM) operation. Several laser structures have been designed to achieve single mode operation and between them the most promising seems to be Distributed Feedback (DFB) laser operation.

In general, the resonator structure of a laser provides the feedback necessary for the build-up of oscillations. If the medium shows a spatial variation of the refractive index, this feedback mechanism can be distributed inside the medium: the feedback is provided by backward Bragg scattering, and moreover the grating-like nature of the device provides a filter mechanism which restricts the oscillation to a narrow spectral range.

In the early 1970s work on distributed feedback laser began. This work was part of the research toward Dinamic Single Mode semiconductor lasers. Considered approaches include Cleaved Coupled Cavity lasers, external mirror or external cavity lasers, short cavity lasers, injection locking through light injection, DFB lasers [27] and Distributed Bragg Reflector (DBR) lasers. Among those alternatives, DFB lasers have prevailed as the monst cost-effective approach. At the present, distributed feedback laser diodes are the preferred optical transmitters in most advances optical communication systems, because of their single-

mode stability and their possible low-noise operation. However, early fabricated devices often became unstable at rather low power levels.

For several reasons liquid crystals seem to be useful material to realise the distributed feedback lasing: they are self-assembling, no external force is needed to organize the system in a periodic structure; they are easy to integrate in fiber as fiber sensor; their optical properties can be changed with the temperature and external fields, leading to a tunability of the lasing; and nevertheless they are cheap. Because of their birefringence and periodic structure, cholesteric liquid crystals (CLC) generete a distributed feedback. Due to this distributed feedback, low threshold mirrorless lasing has been observed in dye doped and pure cholesteric liquid crystals.

In this chapter the photonics of periodic structures is discussed, with a special regard to cholesteric liquid crystals.

4.1 Photonic Bandgap Materials

Because of the periodic arrangement of its atoms and molecules, a crystal presents a periodic potential to an electron propagating through it. The lattice might introduce band gaps into the energy structure of the crystal, so that electrons are forbidden to propagate with certain energies in certain directions. In analogy a photonic bandgap (PBG) may appear in the spectrum of propagating electromagnetic modes in periodic structures [28][29], in which the periodic "potential" is due to a lattice of macroscopic dielectric media instead of atoms. A photonic device already in common use is the "quarter wave-stack": a mirror composed of alternating layers of different dielectric materials. Light of the proper wavelength is scattered at the layer interfaces, and if the spacing is right, the multiply-scattered waves all interfere destructively inside the material, and the light is completly reflected.

We will see, in the next section, that within the bandgap, the wave is evanescent and decays exponentially, so that the density of states (DOS)

within the gap vanishes in large structures. Since the rate of spontaneous emission is proportional to the DOS, spontaneous emission is suppressed within the gap.

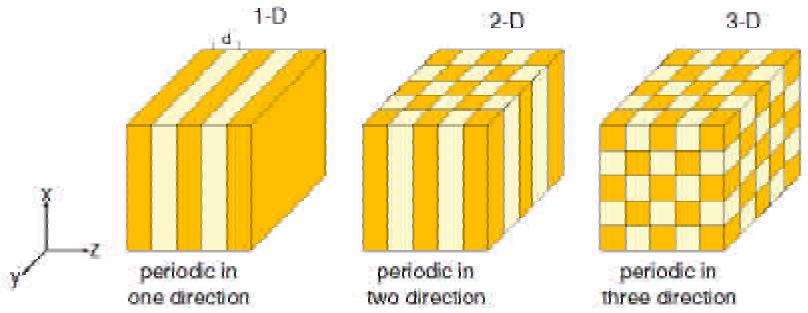

Figure 4.1. Simple examples of one-, two, and three-dimensional photonic crystals. The different colours represent materials with different dielectric constants.

Let us consider the most simple photonic crystal (PC), a one-dimensional system consisting of alternating layers of material with dielectric constants, ε_a and ε_b, and layer thicknesses a and b (Figure 4.1). The refractive indices are

$$n_a = \sqrt{\varepsilon_a}, \text{ and } n_b = \sqrt{\varepsilon_b}$$

The traditional approach to those systems is to study the multiple reflections that take place at each interface for a plane wave propagating through the material. By the way, we will use a different approach which is easily exportable to the liquid crystal systems.

We assume the material is both dispersionless and lossless, it is periodic in the z direction, and homogeneous in the transverse x ¡ y plane. We index all the wavefunctions along this plane by k_q, and k_z the wave vector in the z direction. In the layering direction, because of the periodicity, wavefunctions are Bloch waves and stop bands exist. To simplify we consider a light propagating normal to the plane, $k_q = 0$. The

time-independent Maxwell's equation is in the scalar form,

$$\frac{\omega^2 \varepsilon(z)}{c^2}\tilde{A}(z) + \frac{d^2}{dz^2}\tilde{A}(z) = 0$$

where $\varepsilon(z)$ is a function with period $d = a + b$. The wavefunction $\tilde{A}(z)$ represents the electric or magnetic field and has the Bloch form

$$\tilde{A}(z) = e^{izK} u_k(z)$$

where K is the Bloch wavevector and u_k is a periodic function of period d. The dispersion relation, $\omega(k)$, is determined by the equation

$$\cos Kd = \cos(k_a a)\cos(k_b b) - \frac{1}{2}\left(\frac{k_a^2 + k_b^2}{k_a k_b}\right)\sin(k_a a)\sin(k_b b) \quad (4.1)$$

(for further calculations see [29]) where

$$k_a = \frac{n_a \omega}{c}, \text{ and } k_b = \frac{n_b \omega}{c}$$

We can identify two conditions. If the right member of equation (4.1) has an absolute value less than or equal to the unity, the value of K is real, so propagating modes are allowed. Band-edge state occur when $Kd = m\pi$ so that $\cos(Kd) = \pm 1$. At the band edges the wavefunctions are standing waves. Inside the bandgap, equation (4.1) yields a complex wavevector K corresponding to a decaying wave. The density of states (DOS) diverges as the band edge is approached as an inverse square root and vanishes inside the bandgap. The standing waves at the lower and upper edges have the same value of K but are mutually orthogonal.

We will see in the next section, directly applied to the cholesteric liquid crystals, that the density of states is

$$DOS \propto \frac{dk}{d\omega}$$

which is the reciprocal of the group velocity. The DOS has its largest value at modes closest to the edges of the band, where the line is the narrowest and the dwell time is the greatest. This reflects the accumu-

lation of energy inside the sample. Thus, the band-edge resonance is favourable for lasing.

4.2 Cholesteric Liquid Crystal

As said in the first chapter, chiral liquid crystal are built up of chiral molecules, or are mixtures where at least one of the components is chiral. In chiral nematics, usually called *cholesterics*, there is a tendency of forming a helicoidal structure superimposed on the nematic order.

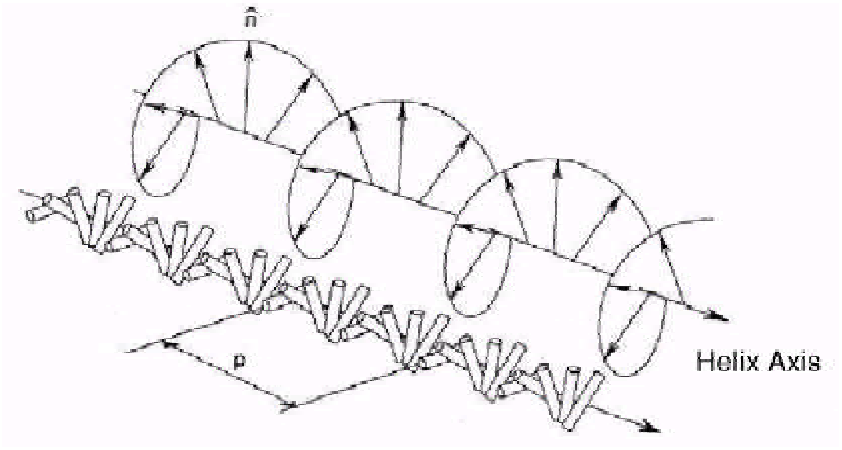

Figure 4.2. Definition of the pitch p in a cholesteric liquid crystal.

When molecules become distorted in a helical structurel, the optical axis is not along (like in nematics) but perpendicular to the local director. The distance along the helix axis corresponding to a $360^{\pm}$ rotation of the director is denoted as the pitch p of the material. It is needed to distinguish between right and left handed materials from the sense of director rotation around the helix axis. Figure 4.2 shows the molecular ordering in the cholesteric phase. Since $\mathbf{b} = \mathbf{¡b}$, the true period of the cholesteric phase correspond to p=2, i.e. a $180^{\pm}$ rotation of the director.

If the director field describes a right-handed screw along the z-axis, in a right handed coordinate frame the director components may be written has

$$\begin{aligned} n_x &= \cos\frac{2\pi}{p}z \\ n_y &= \sin\frac{2\pi}{p}z \\ n_z &= 0 \end{aligned}$$

By definition, p is positive for right handed and negative for left handed materials. The quantity

$$q = \frac{2\pi}{p}$$

is called the *helical vector*.

4.2.1 Light Propagation in Cholesteric Liquid Crystals

By simple considerations on cholesteric liquid crystals it is possible to demonstrate that they act like a photonic crystal.
Maxwell's equations provide the basic relationships that must be satisfied by the optical field,

$$\nabla \times E = -\frac{\partial B}{\partial t}$$

$$\nabla \times H = \frac{\partial D}{\partial t}$$

and letting $B = \mu_0 H$ and $D = \varepsilon_0 \varepsilon_r E$ gives

$$\nabla^2 E - \nabla(\nabla \cdot E) = \frac{\varepsilon_r}{c^2}\frac{\partial^2 E}{\partial t^2} \qquad (4.2)$$

We now introduce the periodic modulation of the molecular director along the z direction:

$$\hat{b} = \hat{i}\cos qz + \hat{j}\sin qz$$

$$\hat{A} = -\hat{i}\sin qz + \hat{j}\cos qz$$

In the $(\hat{b}, \hat{A})$ reference system of the molecular director the dielectric tenson is diagonal,

$$\varepsilon_r = \begin{pmatrix} \varepsilon_q & 0 \\ 0 & \varepsilon_\perp \end{pmatrix}$$

If we assume that the field is

$$E = E(z)\, e^{i(\omega t - kz)} \tag{4.3}$$

where $E(z)$ is in the $x - y$ plane, we have that $\nabla \cdot E = 0$, thus we can simplify the Maxwell equation (4.2) eliminating the $x - y$ dependence,

$$\frac{\partial^2 E}{\partial z^2} = -\frac{\omega^2}{c^2}\varepsilon_r E \tag{4.4}$$

Replacing equation (4.3) into (4.4), after few calculations we get

$$E''(z) - 2ikE'(z) - k^2 E(z) = -\frac{\omega^2}{c^2}\varepsilon_r E(z) \tag{4.5}$$

Labeling E_q the $E(z)$ projection on $\hat{b}$, and $E_\perp$ among $\hat{A}$,

$$E(z) = E_q \hat{b} + E_\perp \hat{A} \tag{4.6}$$

introducing it into equation (4.5), we resolve the equations separately on the two directions[10]:

$$\left(-q^2 + \frac{\omega^2}{c^2}\varepsilon_q - k^2\right) E_q = -2ikqE_\perp \tag{4.7}$$

[10] To realize this passage consider that $\hat{b}' = q\hat{A}$, $\hat{A}' = -q\hat{b}$, $\hat{b}'' = -q^2\hat{b}$, $\hat{A}'' = -q^2\hat{A}$.

$$\left(-q^2 + \frac{\omega^2}{c^2}\varepsilon_\perp - k^2\right) E_\perp = 2ikqE_\parallel \tag{4.8}$$

Now we replace

$$q = \frac{2\pi}{p}$$

$$k = \frac{2\pi n}{\lambda_0}$$

$$\frac{\omega}{c} = \frac{2\pi}{\lambda_0}$$

where p is the cholesteric pitch, λ_0 is the wavelength of light in free space and n is the effective refractive index[11]. If we also let

$$\Phi = \frac{\lambda_0}{p}$$

equations (4.7) and (4.8) become

$$\left(\Phi^2 - \varepsilon_\parallel + n^2\right) E_\parallel = 2in\Phi E_\perp \tag{4.9}$$

$$\left(\Phi^2 - \varepsilon_\perp + n^2\right) E_\perp = -2in\Phi E_\parallel \tag{4.10}$$

Extracting $E_\parallel$ from equation (4.9) and replacing it into equation (4.10), after some algebra we obtain the equation

$$n^4 - \left(2\Phi^2 + \varepsilon_\parallel + \varepsilon_\perp\right) n^2 + \Phi^2 - \varepsilon_\parallel\Phi^2 - \varepsilon_\perp\Phi^2 + \varepsilon_\parallel\varepsilon_\perp = 0$$

$$n^2 = \Phi^2 + \bar{\varepsilon} \mp \sqrt{\delta^2 + 4\bar{\varepsilon}\Phi^2} \tag{4.11}$$

where

$$\bar{\varepsilon} = \frac{(\varepsilon_\parallel + \varepsilon_\perp)}{2}$$

is the *average dielectric constant*, and

$$\delta = \frac{(\varepsilon_\parallel - \varepsilon_\perp)}{2}$$

[11] $\lambda = \lambda_0/n$ is the wavelength in the $\hat{b}, \hat{k}$ space.

is the *dielectric anisotropy*. We call the two solutions of equation (4.11)

$$n_+^2 = \Re^2 + \varepsilon_\perp + \sqrt{\Delta^2 + 4\varepsilon_\perp \Re^2}$$

$$n_-^2 = \Re^2 + \varepsilon_\perp - \sqrt{\Delta^2 + 4\varepsilon_\perp \Re^2}$$

If $\Re \neq 0$, we have

$$n^2 = \Re^2 + \varepsilon_\perp \left(\Delta + 2\frac{\varepsilon_\perp \Re^2}{\Delta} \right)$$

$$n_+^2 = \varepsilon_\parallel + \Re^2 \left(1 + \frac{2\varepsilon_\perp}{\Delta} \right)$$

$$n_-^2 = \varepsilon_\perp + \Re^2 \left(1 - \frac{2\varepsilon_\perp}{\Delta} \right)$$

If $\Re$ goes to zero, the two refractive indices are

$$n_+^2 = \varepsilon_\perp + \Delta = \varepsilon_\parallel \quad \Rightarrow \quad n_+ = \sqrt{\varepsilon_\parallel}$$

$$n_-^2 = \varepsilon_\perp - \Delta = \varepsilon_\perp \quad \Rightarrow \quad n_- = \sqrt{\varepsilon_\perp}$$

Substituting in equations (4.9) and (4.10), we see that the eigenmodes are two plane polarized waves, one parallel to the director $\mathbf{b}$ and the other to $\mathbf{k} \times \mathbf{b}$. With the superscript $(+)$ we indicate forward propagating modes, and with $(-)$ backward ones.

If $\Re \gg 0$, that is the cholesteric pitch is long compared to the wavelength, the eigenmodes are given by

$$\left(1 + \frac{\varepsilon_\perp}{\Delta} \right) E_\parallel^+ + i\frac{\sqrt{\varepsilon_\perp}}{\Re} E_\perp^+$$

$$\left(1 - \frac{\varepsilon_\perp}{\Delta} \right) E_\perp^- + i\frac{\sqrt{\varepsilon_\perp}}{\Re} E_\parallel^-$$

or

$$\sqrt{\varepsilon_\parallel} E_\parallel^+ + i\frac{\Delta}{\Re} E_\perp^+ \tag{4.12}$$

$$p_{\overline{\varepsilon}_q} E_\perp^- = -i\frac{\pm}{\eta} E_q^- \tag{4.13}$$

That is, the two eigen modes are two elliptically polarized waves. If we take $E_\perp^+$ from equation (4.12) and we place it in equation (4.6) we find

$$E^+ = E_q^+ \left[\hat{b} \cos(\omega t - kz) + \frac{\eta p_{\overline{\varepsilon}_q}}{\pm} \hat{A} \sin(\omega t - kz) \right]$$

which is a wave propagating through the $+z$ direction, left-circularly polarized (with positive helicity), opposite to the handedness of the cholesteric, which is right-handed. Likewise,

$$E^- = E_\perp^- \left[\frac{\eta p_{\overline{\varepsilon}_\perp}}{\pm} \hat{b} \sin(\omega t - kz) + \hat{A} \cos(\omega t - kz) \right]$$

which is a right-circularly polarized (with negative helicity), with the same handedness of the cholesteric, propagating through the $-z$ direction. In this way we have expanded the field in a set of forward (E^+) and backward (E^-) propagating modes.

To understand why cholesteric liquid crystals can be considered as unidimensional photonic crystal we have to focalize on their behaviour in the vicinity of the region where n^2 becomes negative. In fact, imaginary n means that there is no propagation, hence one can expect strong reflection of one mode here. The end points of this reflection band are given by the condition,

$$n_i^2 = \eta^2 + \varepsilon - \sqrt{\pm^2 + 4\varepsilon\eta^2} = 0$$

which is realized when $\eta = p_{\overline{\varepsilon}_q}$ and $\eta = p_{\overline{\varepsilon}_\perp}$; remembering that $\eta = \lambda_0/p$, the reflection occur when

$$p\sqrt{p_{\overline{\varepsilon}_\perp}} < \lambda_0 < p\sqrt{p_{\overline{\varepsilon}_q}}$$

or

$$pn_o < \lambda_0 < pn_e$$

By the existence of this reflection band (see Figure 4.3) we can consider cholesteric liquid crystals like photonic crystals.

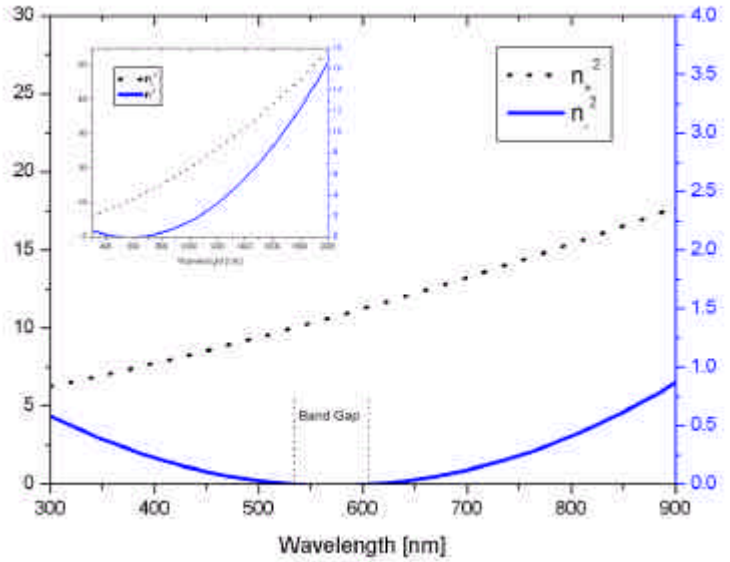

Figure 4.3. n^2 versus wavelength for the two eigenmodes, for a cholesteric liquid crystal: $p = 350nm$, $n_e = 1{:}7464$ and $n_o = 1{:}5211$.

Band-edge Modes

We will show that at the band edges one of the two modes in not propagated anymore:

- if $\omega = \frac{p}{\sqrt{\varepsilon_\perp}}$, then $n_i = 0$. Equation (4.10) is automatically satisfied, equation (4.9) gives $E_q^i = 0$. Since $k = 2\pi n/\lambda_0 = 0$, the solution is

$$E^i = E_?^i \hat{k} e^{i\omega t} \tag{4.14}$$

The field is always parallel to $\hat{k}$ and oscillating in time: it is a non-propagating mode, since we have lost the dependence from z.

From equation (4.11) we found $n_+^2 = 2(\varepsilon + \delta^2) \Rightarrow n_+ = \varepsilon_q + 3\varepsilon_\perp$. Introducing this into equation (4.9)

$$E_\perp^+ = -2i\sqrt{\frac{\varepsilon_\perp}{\varepsilon_q + 3\varepsilon_\perp}}E_q^+$$

and the solution is

$$E^+ = E_q^+\left[\cos(\omega t - kz) + 2\sqrt{\frac{\varepsilon_\perp}{\varepsilon_q + 3\varepsilon_\perp}}\sin(\omega t - kz)\right]$$

which is again left-circularly polarized (whit positive helicity), opposite to the handedness of the cholesteric.

- if $\delta = \sqrt{-\varepsilon_q}$, then $n_- = 0$. Equation (4.9) is automatically satisfied, equation (4.10) gives $E_\perp^- = 0$. Since $k = 2\pi n/\lambda_0 = 0$, the solution is

$$E^- = E_q^-\hat{b}e^{-i\omega t} \tag{4.15}$$

The field is everywhere parallel to $\hat{b}$ and oscillating in time: it is a non-propagating mode.

Once again from equation (4.11) we found $n_+^2 = 2(\varepsilon + \delta^2) \Rightarrow n_+ = 3\varepsilon_q + \varepsilon_\perp$. Introducing this into equation (4.9)

$$E_q^+ = -2i\sqrt{\frac{\varepsilon_\perp}{3\varepsilon_q + \varepsilon_\perp}}E_\perp^+$$

and the solution is

$$E^+ = E_\perp^+\left[-2\sqrt{\frac{\varepsilon_\perp}{3\varepsilon_q + \varepsilon_\perp}}\hat{b}\sin(\omega t - kz) + \hat{A}\cos(\omega t - kz)\right]$$

which is again left-circularly polarized (whit positive helicity), opposite to the handedness of the cholesteric.

It is interesting to see what happens when the pitch gets much shorter than the wavelength of light, $p \ll \lambda_0$, that is $\delta \gg 1$. From equation (4.11), if $\delta \gg \varepsilon$

$$n^2 \simeq \left(\frac{p}{\pi}\delta\right)^2$$

Let us start from the root

$$n_+ = \sqrt{\varepsilon_\perp} + \delta$$

From equation (4.9) we get

$$E_\eta = iE_\xi$$

so the field is

$$E^+ = E_\xi \left[-\beta \sin(\omega t - kz) + \alpha \cos(\omega t - kz) \right]$$

which is left-circularly polarized, opposite to the handedness of the cholesteric, with wavevector

$$k_+ = \frac{2\pi \sqrt{\varepsilon_\perp}}{\lambda_0} + \frac{2\pi\delta}{\lambda_0} = k_A + q$$

Now, substituting k, β and α we get the solution

$$\begin{aligned} E^+ = E_\xi \; & -\tfrac{1}{2}[\cos qz \sin(\omega t - qz - k_A z) + \sin qz \cos(\omega t - qz - k_A z)] \\ & + \tfrac{1}{2}[\cos qz \cos(\omega t - qz - k_A z) - \sin qz \sin(\omega t - qz - k_A z)] \end{aligned}$$

$$\therefore \; E^+ = E_\xi \left[-\tfrac{1}{2}\sin(\omega t - k_A z) + \tfrac{1}{2}\cos(\omega t - k_A z) \right] \qquad (4.16)$$

This is circularly polarized light, propagating with speed $c/\sqrt{\varepsilon_\perp}$, independent from the cholesteric pitch.
Similarly, for the root

$$n_- = \sqrt{\varepsilon_\perp} - \delta$$

from equation (4.10) we get

$$E_\xi = iE_\eta$$

and the field is

$$E^- = E_\eta \left[\beta \sin(\omega t - kz) - \alpha \cos(\omega t - kz) \right]$$

which is left-circularly polarized. Since $n_i < 0, k < 0$,

$$k_i = \frac{2\pi\sqrt{\varepsilon}}{\lambda_0} - \frac{2\pi\delta}{\lambda_0} = k_A - q$$

Now, substituting k, b and A we get the solution

$$\begin{aligned} E^i = E_q \; & f - i[\cos qz \cos(\omega t + qz - k_A z) + \sin qz \sin(\omega t + qz - k_A z)] \\ & + j[\sin qz \cos(\omega t + qz - k_A z) - \cos qz \sin(\omega t + qz - k_A z)]g \end{aligned}$$

$$\Rightarrow E^i = E_q \{i\cos(\omega t - k_A z) - j\sin(\omega t - k_A z)\} \qquad (4.17)$$

The normal modes in equations (4.16) and (4.17) are left and right circularly polarized waves, travelling with speed $c=\sqrt{\varepsilon}$, independent from the cholesteric pitch. That may be combined to give plane polarized light. Thus, for $\delta \ll 1$ the light essentially sees an isotropic medium, with dielectric constant ε.

Density Of States (DOS)

If we have a finite sample with lenght L, we need to have[12]

$$kL = \frac{2\pi n}{\lambda_0} L = N 2\pi$$

or

$$\frac{n(\lambda_0)}{\lambda_0} L = N$$

where N is an integer. We call $\Delta\lambda_0$ the wavelength change needed to get the next allowed mode:

$$\frac{\partial}{\partial \lambda_0}\left(\frac{n(\lambda_0)}{\lambda_0} L\right) \Delta\lambda_0 = dN = 1$$

[12] In order to have allowed modes satisfying boundary conditions

We define the density of states D^0 (DOS) as the number of states in a wavelength interval,

$$D^0 = \frac{1}{¢_{,0}} = \frac{@}{@_{,0}} \mu \frac{n(_{,0})}{_{,0}} L \P$$

where $D^0 d_{,0}$ is the number of states in the wavelength interval $d_{,0}$. If we excite light uniformly at all wavelengths, the density of states tell us how probable it is to have light (lasing) at a particular wavelength. It is more conventional to define the density of states so that the number of states is $Dd°$, then, since $d° = ¡ \frac{2¢}{c=_{,0}^2} d_{,0}$, we have

$$D = ¡ \frac{2_{,0}^2}{c} D^0 = ¡ \frac{2_{,0}^2}{c} \frac{@}{@_{,0}} \mu \frac{n(_{,0})}{_{,0}} L \P$$

$$\frac{D}{L} = ¡ \frac{2_{,0}^2}{c} \cdot \frac{1}{_{,0}} \frac{@n}{@_{,0}} ¡ n \frac{1}{_{,0}^2} ,$$

and

$$\frac{Dc}{L} = n ¡ _{,0} \frac{@n}{@_{,0}}$$

If we consider the non-propagating mode

$$n^2 = ®^2 + ¯ ¡ \frac{p}{±^2 + 4¯®^2}$$

The derivative, $@n=@_{,0}$, is

$$2n \frac{@n}{@_{,0}} = 2n \frac{@n}{p@®} = \frac{1}{p} \left(2® ¡ \frac{1}{2} \frac{p}{±^2 + 4¯®^2} 8¯® \right)$$

$$) \frac{@n}{@_{,0}} = \frac{®}{np} \left(1 ¡ \frac{p}{±^2 + 4¯®^2} 2¯ \right)$$

$$) \frac{@n}{@_{,0}} = \frac{®}{p \sqrt{®^2 + ¯ ¡ \frac{p}{±^2 + 4¯®^2}}} \left(1 ¡ \frac{p}{±^2 + 4¯®^2} 2¯ \right)$$

$$) \, _0\frac{@n}{@ \, _0} = \sqrt{\frac{®^2}{®^2 + ¯ \; ¡ \; \sqrt{±^2 + 4¯®^2}}} \; \left[1 ¡ \sqrt{\frac{2¯}{±^2 + 4¯®^2}} \right]$$

and

$$\frac{Dc}{L} = \sqrt{®^2 + ¯ \; ¡ \; \sqrt{±^2 + 4¯®^2}} \; ¡ \; \sqrt{\frac{®^2 \; 1 ¡ \sqrt{\frac{2¯}{±^2 + 4¯®^2}}}{®^2 + ¯ \; ¡ \; \sqrt{±^2 + 4¯®^2}}}$$

The essential feature is the fact that for one of the modes at the band edges n goes to zero , and therefore $@n=@ \, _0$, and hence the density of states diverges.

Finally we note that, since $d^o = ¡ \, c=_0 d \, _0$,

$$D = ¡ \frac{^2_0}{c} \frac{@}{@ \, _0} \left(\frac{n(\, _0)}{ \, _0} L \right) = \frac{@}{@^o} \left(\frac{n(\, _0)}{ \, _0} L \right) = \frac{@}{@^o} \frac{1}{2¼} k(^o) \, L = L \frac{@k}{@ !}$$

that is the density of states is inversely proportional to the group velocity

$$v_g = \frac{@ !}{@k}$$

At the band edge, the phase velocity

$$v_p = \frac{!}{k}$$

is infinite, while the group velocity is zero.

Non Propagating Modes

We will now show why in the reflection band, light with the same handedness as the cholesteric is reflected while light of the opposite handedness is transmitted. Let's consider right circularly polarized light travelling in the +z direction:

$$E^r_{+z} = E_0 \left[\cos \left(! t ¡ kz + Á_{+z} \right) ¡ \sin \left(! t ¡ kz + Á_{+z} \right) \right]$$

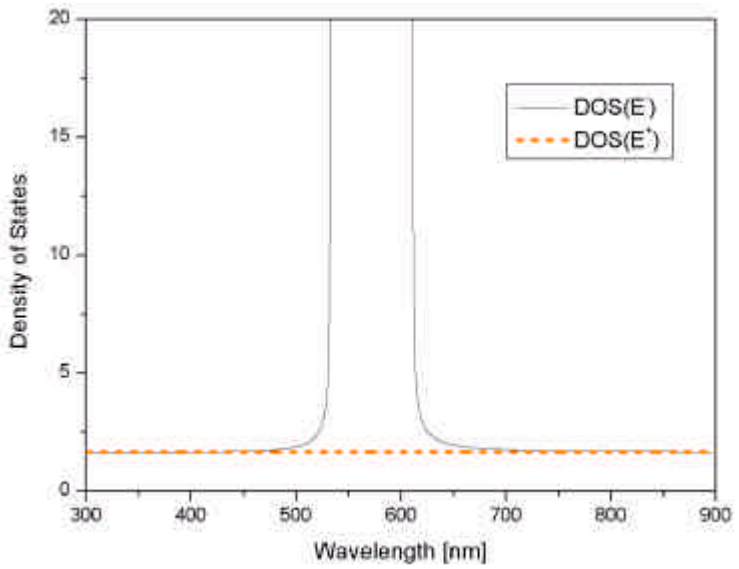

Figure 4.4. Density of states versus wavelength for the propagating mode (E^+) and non-propagating mode (E^i).

One can imagine the electric field vector tracing out a right handed helix, which is rotating clockwise when looking towards the source of light. Then consider the field

$$E^r_{iz} = E_0 \left\{ \cos\left(!t + kz + Á_{iz} \right) + \sin\left(!t + kz + Á_{iz} \right) \right\}$$

that is right circularly polarized light travelling in the ¡z direction. If both modes are present, after some algebra, we have

$$E^r_{+z} + E^r_{iz} = 2E_0 \left\{ \cos(kz) + \sin(kz) \right\} \cos\left(!t + \frac{Á_{+z} + Á_{iz}}{2} \right),$$

which is in the form of the non-propagating modes of equations (4.14) and (4.15). Hence, we can think of the non-propagating modes as super-positions of forward (+z) and backward (¡z) propagating modes with the same handedness of the cholesteric.

Therefore in the reflection band, light with the same handedness as the cholesteric is reflected while light of the opposite handedness is transmitted.

Handedness and Helicity

The concepts of handedness and helicity might be confused: handedness is associated with space alone, while helicity is space and time. In fact helicity is associated with the sign of angular momentum projected onto the propagation direction. Consider a vector field given by

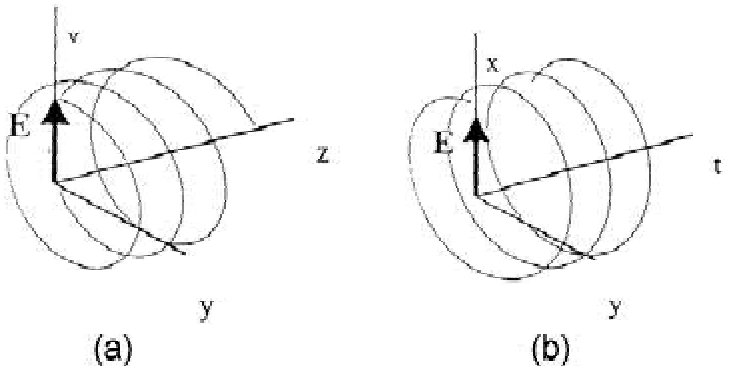

Figure 4.5. (a) Right handed polarization (b) Negative helicity.

$$\vec{E} = \hat{i}\cos(\omega t - kz) - \hat{j}\sin(\omega t - kz)$$

At a fixed time (say $t = 0$), as function of position z, $\vec{E}$ traces out a right handed helix, similar to a right handed screw. This is right polarized light. If you are looking so that light is coming towards you, the helix is rotating countclockwise as the spatial coordinates z increases.
At a fixed position (say $z = 0$), as function of time t, $\vec{E}$ traces out a left handed helix, similar to a left handed screw. This light has negative helicity (or left handed helicity). If you are looking so that light is coming

towards you, the helix is rotating clockwise as the temporal coordinates t increases.

- Right circularly polarized light has negative (left handed) helicity.
- Left circularly polarized light has positive (right handed) helicity.

4.2.2 Unwinding of the Cholesteric Helix

The cholesteric pitch can be controlled by temperature or by means of external fields.

The dependence on the temperature strongly changes among different substances; generally the pitch decreases with increasing temperature, and this causes the medium to twist harder. Hence, by a temperature variation one can drive the pitch to an expected value of the pitch, and consequently of the reflection band.

It looks clear that cholesteric and nematic are not two different phases, they are thermodynamically the same phase, so there cannot be a phase transition between them. However, a particular interesting feature of cholesteric liquid crystals is the unwinding of the helical structure by means of an external magnetic or electric field, phenomenon known as *cholesteric to nematic phase transition*. If the external force is an electric field, there will be a torque on the director due to the coupling between the field and the dielectric anisotropy $\Delta\varepsilon$ of the medium. Let's consider the case of a cholesteric helix perpedicular to the confining glass plates, and an electric field E parallel to the helix axis. In the case of positive anisotropy the director wants to align along the field, increasing E the pitch p increases and the helical structure unwinds till a certain value E_c, above which the helix is completely unwound and the liquid crystal (even if it is made of chiral molecules) is a nematic. Because of the unwinding continuously changes the effective birefringence, the reflection band can be tuned by use of an external electric field.

Chapter 5

Mirrorless Lasing

Multi wavelenght sources, for WDM and DWDM systems, should meet basic requirements such as a precise alignment with standardised wavelengths, a tuneable and selectable bandwidth and a sophisticated wavelength tuning setting according to application. Several kind of solutions are now under investigation [1], like wide-tunable semiconductor laser or multiwavelength arrays of common semiconductor laser or distributed feedback lasers.

Cholesteric Liquid crystals are one of the elect material to realise Distributed Feedback Laser: they are self-assembling, no external force is needed to organize the system in a periodic structure; they are easy to integrate in fiber as fiber sensor; their optical properties can be changed with the temperature and external fields, both magnetic and electric, leading to a tunability of the lasing; and nevertheless they are cheap.

In the previous chapter, properties of CLC connected to their birefringence and periodic structure have been shown. It has been expained how they can generate a distributed feedback. Due to this distributed feedback, low threshold mirrorless lasing has been observed in dye doped and pure cholesteric liquid crystals.

In order to optimize the lasing conditions for a telecom application, we have studied the dependence of the lasing threshold on dye concentration and sample thickness, and we have carried out the possible physical process responsible for the observed behaviour.

In this chapter a brief survay is given on how to interpretate the phenomenon of mirrorless lasing in period structures by means of the coupled wave theory, and the special application to dye doped cholesteric liquid crystals is explored in details.

5.1 The Coupled Wave Theory of Distributed Feedback Laser

The coupled wave theory developed by Kogelnik [8] can be used to analyse the lasing action in a periodic structure [34].

In general, the resonator structure of a laser provides the feedback necessary for the build-up of oscillations. If the medium shows a spatial variation of the refractive index, this feedback mechanism can be distributed inside the medium: the feedback is provided by backward Bragg scattering, and moreover the grating-like nature of the device provides a filter mechanism which restricts the oscillation to a narrow spectral range. In Figure 5.1a, a diagram shows two waves, represented by arrows, one which travels to the left and the other to the right. At each wave travels in the periodic structure, it receives light at each point along its path by Bragg scattering from the oppositely traveling wave. This creates a feedback mechanism which is distributed throughout the length of the periodic structure: with sufficient feedback, there will be condition for oscillation.

The model proposed by Kogelnik and Shank in 1972 [34] is that of a self-oscillating device there are no incoming waves, and the internal waves start with zero amplitudes at the device boundaries (see Figure 5.1b). The boundary conditions for the wave amplitudes are then

$$R\left(-\frac{1}{2}L\right) = S\left(-\frac{1}{2}L\right) = 0 \tag{5.1}$$

where L is the length of the device.The coupled wave equations (2.11), derived in chapter two, describe wave propagation in the Distributed

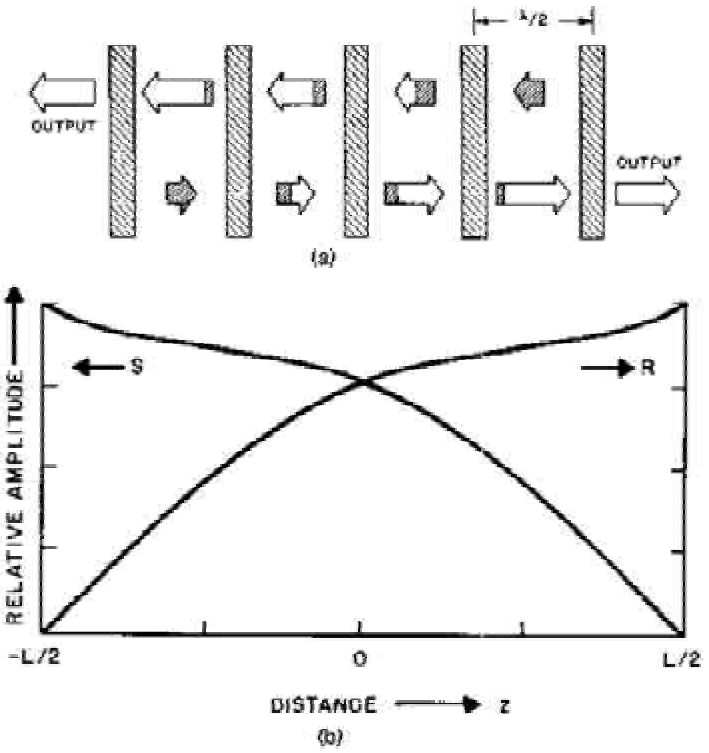

Figure 5.1. Laser Oscillation in a periodic structure: (a) the feedback mechanism; (b) plot of the amplitudes of left traveling wave S and right traveling wave R versus distance.

Feedback structure. These equations, together with the boundary conditions (5.1), specify the electromagnetic field in the DFB laser. The corresponding solutions yields oscillation states, namely the modes of the periodic structure.The general solutions to the coupled wave theory are in the form

$$R(z) = r_1 e^{\circ z} + r_2 e^{i \circ z}$$
$$S(z) = s_1 e^{\circ z} + s_2 e^{i \circ z}$$

with the complex propagation constant ° obeying the dispersion relation

$$°^2 = .^2 + \left(®^2 ¡ ¡^3\right)^{¢}$$

Because of the symmetry of the device

$$r_1 = §s_2$$
$$r_2 = §s_1$$

The boundary conditions provide a further set of relations between the coefficients, namely,

$$\frac{r_1}{r_2} = \frac{s_1}{s_2} = ¡e^{°L}$$

Using these results Kogelnik and Shank described the longitudinal field distribution of the modes of a DFB structure in the form

$$R = \sinh\left(° z + \frac{1}{2}L\right)^{¶}$$
$$S = §\sinh\left(° z ¡ \frac{1}{2}L\right)^{¶}$$

So, there is a set of modes which correspond to a discrete set of eigenvalues °:

5.2 Mirrorless Lasing in CLC

Due to chirality, the direction of the average molecular orientation varies linearly with the position, giving rise to a helicoidal structure. As a consequence of the periodicity of the helical cholesteric structure and the birefringence of the liquid crystal, for a range of wavelengths, the propagation along the helix axis is forbidden for one of the normal modes. Hence, incident light with a wavelength in this band and with the same helicity as the cholesteric is strongly reflected (Figure 5.2). Adding a fluorescent dye (Figure 5.3a), with emission in the reflection band, and pumping the mixture we see that the fluorescence is inhibited

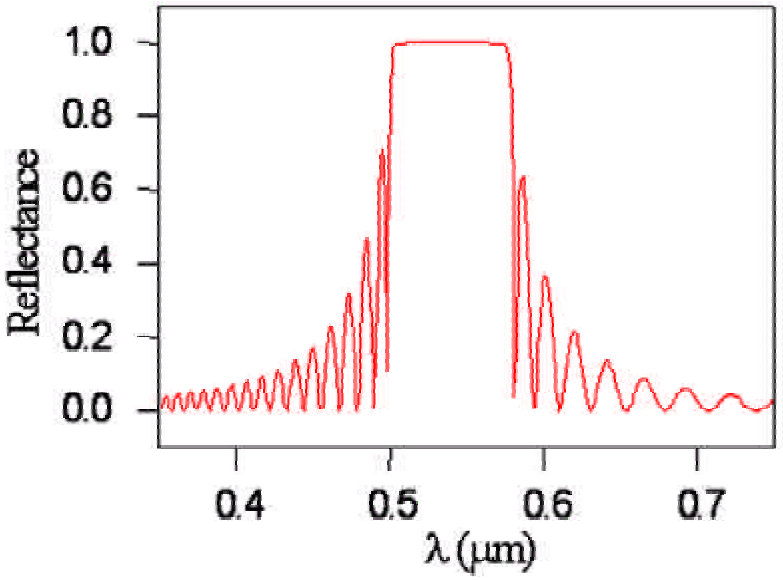

Figure 5.2. Reflection Band for a Cholesteric Liquid Crystal.

inside the reflection band, but it is enhanced at the band edges and mirrorless lasing can occur (Figure 5.3b) with low threshold [35][36]. In this systems cholesteric liquid crystals act as a distributed cavity and the dye as active material. We can talk about a Cholesteric Liquid Crystals DFB laser.

The possibility of lasing in CLC was first proposed by Goldberg and Schnur [37] and Il'chishin [35] in the first years of the '70. After few months from their publications Kogelnik and Shank [34] explained the CLC lasing by means of the DFB theory. After a decade a second interpretation, based on the photonic band-gap description was given: in 1987 Yablonovitch and John proposed that in certain dielectric structures with sufficiently large index contrast a PBG may exist in the spectrum of the electromagnetic propagating waves [28].

Nowadays mirrorless lasing has been observed and demonstrated in one dimensional dye-doped CLC [36][39][38], in pure CLC [40][41], chiral ferroelectric smectic materials [42], polymeric CLCs [43], and in

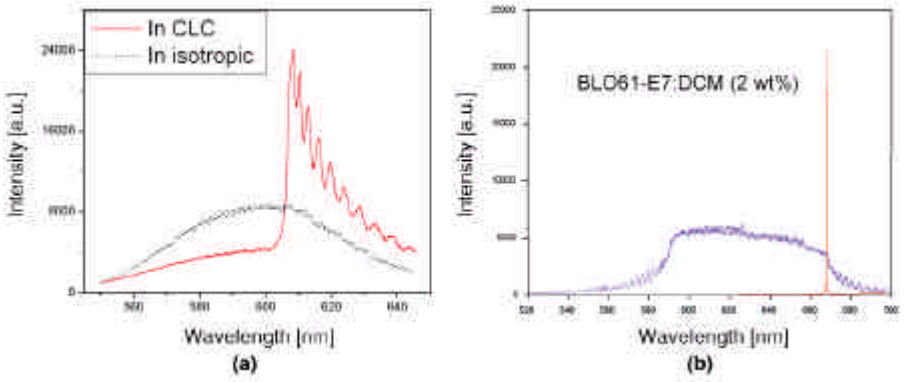

Figure 5.3. (a) Spontaneous emission: supression in the reflection band and enhancement at band edge; (b) Stimulated emission, Distributed Feedback low threshold lasing.

Cholesteric Liquid Single Crystal Elastomers [39]. In 2002 mirrorless lasing was also demonstrated in the three dimensional cholesteric blue-phase II [44].

5.3 Materials and Setup

The liquid crystal used in this study was a mixture consisting of 78wt% cholesteric BLO61 and 22wt% nematic E7 (EM Industries). The mixture was doped with the laser dye DCM (4-(dicyanomethylene)-2-methyl-6-(4-dimethyl-amino-styryl)-4-H-pyran), see Figure 5.4, with concentration in the range of 0:1wt% to 3:0wt%.
A glass cell, with windows treated to produce homogeneous alignment, was filled with this mixture. On cooling slowly from the isotropic phase, the sample showed a defect-free planar texture. The material has a right-handed helical structure, with a reflection band between 545nm to 608nm that overlaps the maximum of the fluorescence spectrum of dye. For the study of the dependence of lasing threshold on dye con-

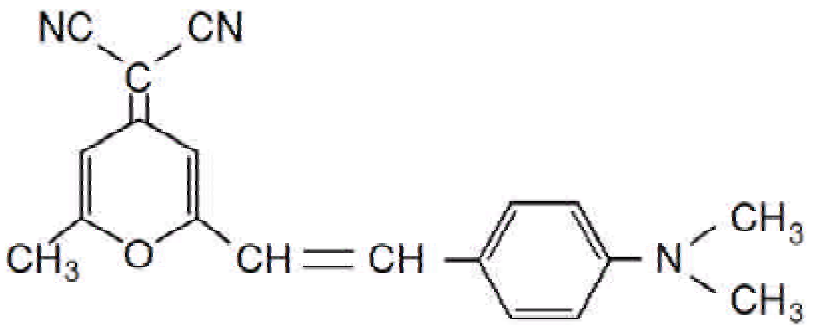

Figure 5.4. DCM Dye

centration, the thickness of the CLC sample in the cell was $23\,\mu m$. For the study of the dependence of lasing threshold on sample thickness, a wedge-shaped cell, with thickness ranging from $5\,\mu m$ to $50\,\mu m$, was used. The dye concentration for the wedge cell was $0.5 wt\%$. The cells were pumped either by a Q-switched Nd-YAG laser delivering $7.5 ns$ pulses, or a mode-locked Nd-YAG laser delivering $40 ps$ pulses, at $532 nm$. Two polarizers and a half wave plate were placed along the pumping beam to control the pulse energy. Part of the pumping beam was collected on an oscilloscope to measure its energy, the rest was focused on the sample using a $f = 20 cm$, $2.5 cm$ diameter lens; the beam diameter on the sample was $25\,\mu m$. Laser emission was characterized with a TRIAX550 (Jobin-Yvon Spex) spectrometer and recorded with an i-Spectrum intensified CCD detector. The defined spectral region was scanned ten times during a single measure, and the signal was subsequently averaged. The spectral resolution of the system was $0.03 nm$. Measurement were all made at room temperature.

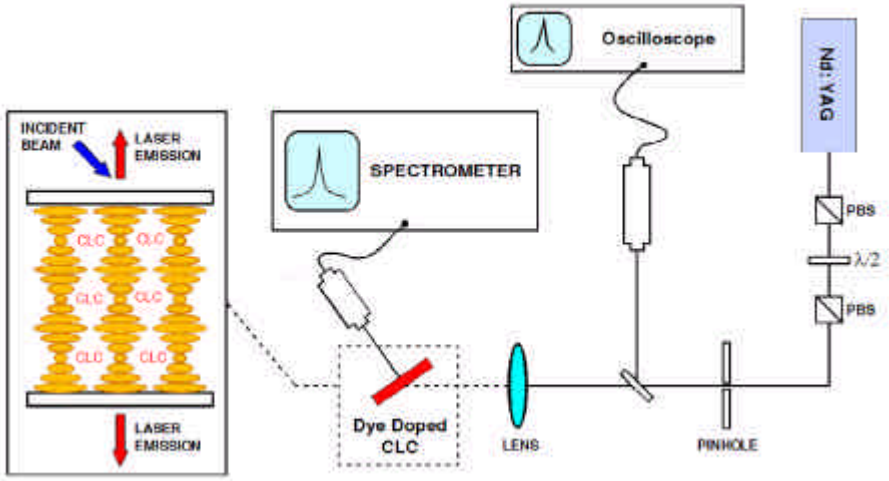

Figure 5.5. Experimental Set Up

5.4 Threshold Measurements

In our well-aligned dye-doped CLC samples, the lasing peak with the lowest lasing threshold is at the low energy edge of the reflection band. We measured the intensity of this lasing peak when it was stable; measurements were averaged over 10 pulses. Figure 5.6 shows typical behaviour of laser intensity as function of pump energy. The intensity was measured at the laser peak at $608{:}6\mathrm{nm}$. The lasing threshold, determined from the intersection of the two straight line fits to the intensity below and above threshold, is $64{:}0\mathrm{nJ}$ for this sample, as shown.

5.4.1 Threshold Dependence on Dye Concentration

The threshold dependence on dye concentration is shown in Figure 5.8. The threshold exhibits similar behaviour with both nanosecond and

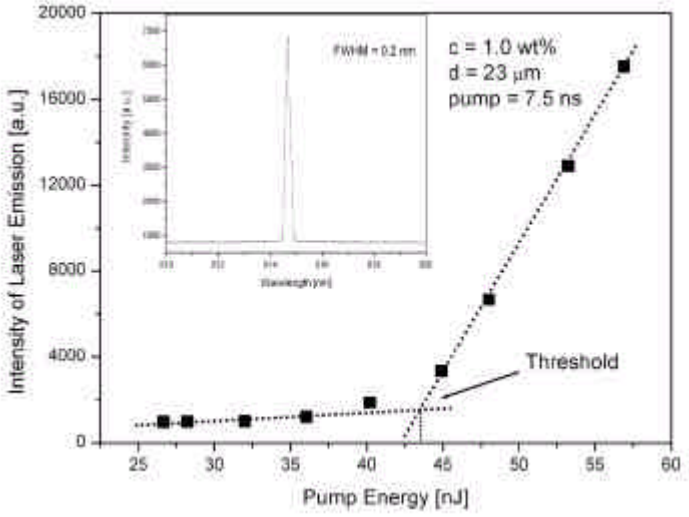

Figure 5.6. Intensity of CLC laser emission as function of pump energy.

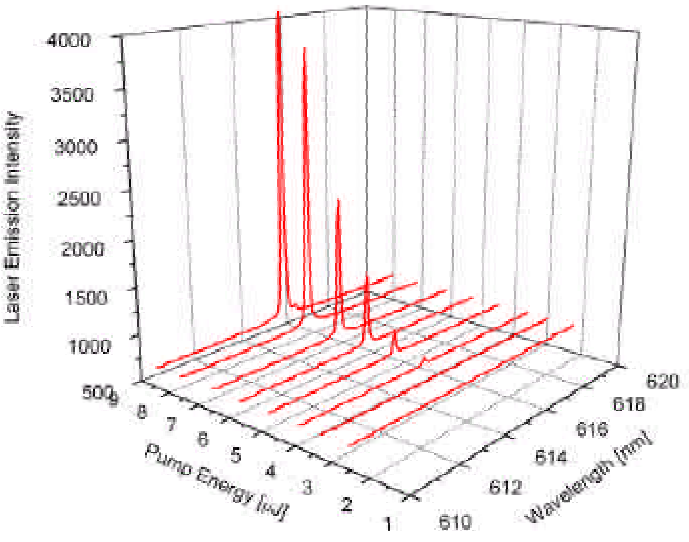

Figure 5.7. A 3D example of CLC lasing, typical linewidth are of the order of 0:5nm.

picosecond pump. At both the low (0:1wt%) and high (3:0wt%) ends of the concentration range, thresholds are significantly higher.

In order to lase, the medium has to provide gain greater than the gain threshold to overcome loss. Since nominally the gain is proportional to dye concentration, there can be no lasing if the dye concentration is below the concentration corresponding to the gain threshold. The lasing threshold therefore diverges as this critical dye concentration is approached from above.

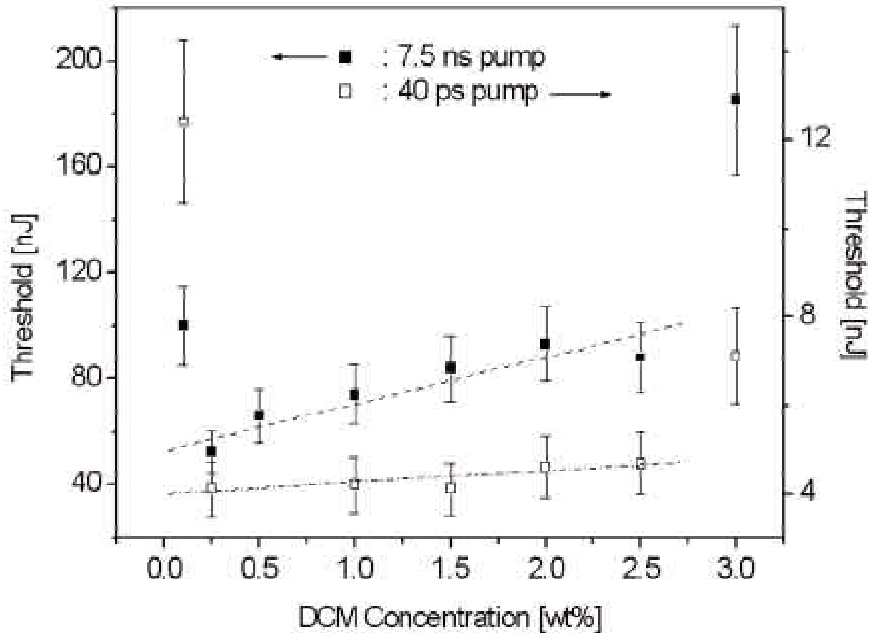

Figure 5.8. Dependence of lasing threshold on dye concentration with nanosecond and picosecond pump pulses. The dotted lines are linear fits in the concentration region of 0:25wt% to 2:5wt%.

At high dye concentration the liquid crystal mixture becomes saturated with the dissolved dye. Above a certain concentration, dye crystals, coexisting with the liquid, can exist in the medium. At 3:2wt% concentration, dye crystals can be clearly seen in the mixture under a

microscope in the form of grains. The scattering and absorption of both pump beam and lasing beam by these dye crystals are likely the cause of the observed strong increase of the lasing threshold at high dye concentrations.

In the intermediate dye concentration region, between $0{:}25wt\%$ and $2{:}5wt\%$, the lasing threshold increases linearly with dye concentration. This increase is likely due to quenching of the fluorescence by the dye. The dye concentration in conventional dye lasers using DCM as active medium is typically of the order of $10^{-4}[M]$ while in our samples, the DCM concentration is of the order of $10^{-2}[M]$. At these relatively high concentrations, bimolecular process involving dye molecules, such as excimer formation, are likely important, resulting in quenched fluorescence as shown in Figure 5.9.

The fluorescence spectra were measured for samples with different dye concentrations. With the same experimental conditions (pump energy, pump position, spectrometer parameters), the fluorescence intensity at $608{:}5nm$ is quenched, by a factor $2{:}6$, when the dye concentration is increased from $0{:}5wt\%$ to $2{:}5wt\%$. Correspondingly, the lasing threshold is increased, by a factor of $1{:}6$. This quenching of the fluorescence, together with the shifting of the emission peak to longer wavelengths (Figure (3.2)) is characteristic of excimer formation. DCM molecules are polar, due to the electron-acceptor (-CN) and the electron-donor (-N) groups attached to the conjugated molecular skeleton. The molecular dipole moment is $6{:}1D$. The excited state of DCM is even more polar, with a dipole moment of $26{:}3D$ [31]. An excited DCM molecule and a ground state DCM molecule can form an excimer due to charge transfer interaction (Figure 5.10). The excimer can decay by returning to an excited DCM and a ground state DCM, or by emission of a photon or by dissociation. In the latter two cases, the excited population of DCM molecules is quenched. Using a picosecond pump and a streak camera, we measured the fluorescence decay at $608nm$ as shown in Figure 5.11. For dye concentration of $0{:}5wt\%$, the decay curve was fit well by a single exponential, with a lifetime of $1{:}25ns$. This is the

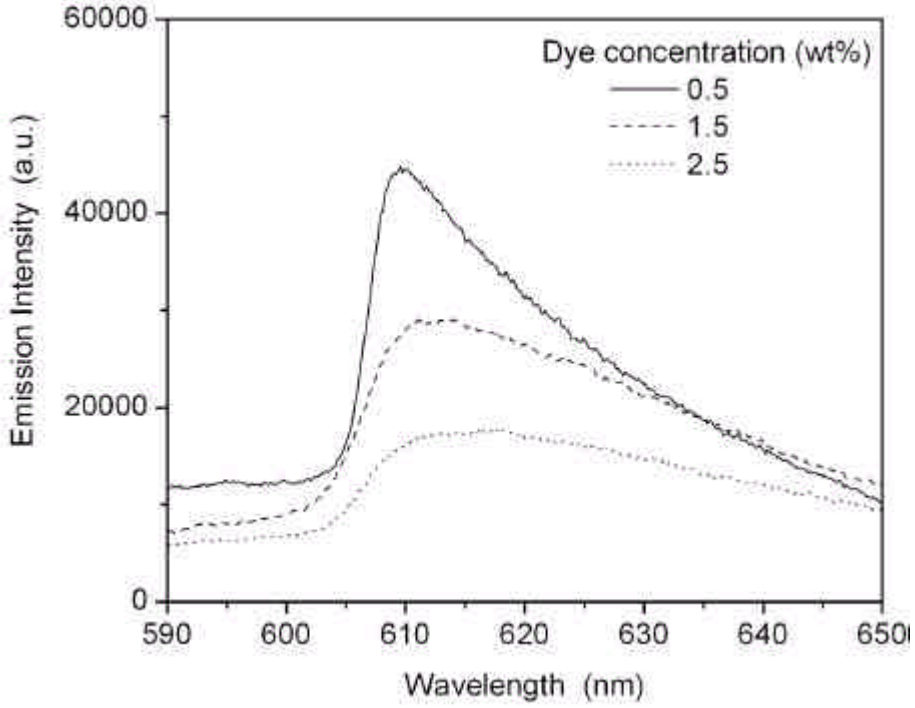

Figure 5.9. Fluorescence quenching: fluorescent emission for different dye concentrations. The pump pulsewidth is 7.5ns.

typical lifetime of an excited DCM molecule. For dye concentration of 2:5wt%, the decay is double exponential, with lifetimes of 1:20ns and 0:32ns. The much shorter-lived excited state species, with a lifetime 0:32ns, is the DCM excimer.

In the intermediate dye concentration region from 0:25wt% to 2:5wt%, the threshold energy increases from 4:13nJ to 4:72nJ for picosecond pump, while it increases from 53nJ to 95nJ for the nanosecond pump. The less pronounced dependence of lasing threshold on dye concentration for the picosecond pump is consistent with the picture of fluorescence quenching by excimer formation. Since the lifetime of excimer is 320ps, the excimer can only form once after 40ps pump, while the

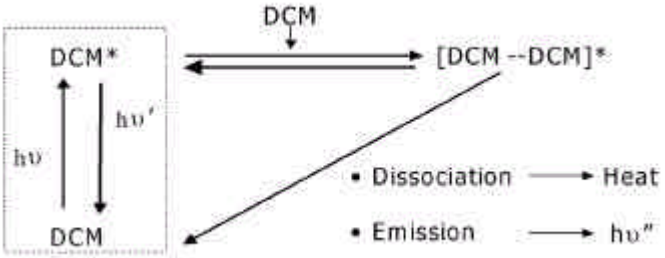

Figure 5.10. Excimer formation and decay. DCM*: excited DCM molecule, [DCM–DCM]*: DCM excime. The dotted frame shows the process when dye concentration is low.

quenching process can likely repeat a number of times during the 7:5ns pump pulse.

5.4.2 Threshold Dependence on Cell Thickness

The lasing threshold as function of sample thickness has been measured at the fixed dye concentration of 0:5wt%. The results are shown in Figure 5.12. The threshold behaviours are the same for both nano- and picosecond pump pulses: with increasing cell thickness, the threshold decreases to reach a minimum, and then gradually increases. In addition, with increasing cell thickness, the lasing wavelength blue-shifts several nanometers, towards the expected band edge for a semi-infinite sample.

The observed behaviour suggests competition between processes with opposite thickness dependence. In order to understand this, we make comparison with the threshold of a typical Fabry-Perot (F-P) cavity laser. The threshold gain constant of a F-P cavity laser is [32]:

$$\circ_{th}^{F\,i\,P} = ® \; i \; \frac{\ln(r^2)}{d}$$

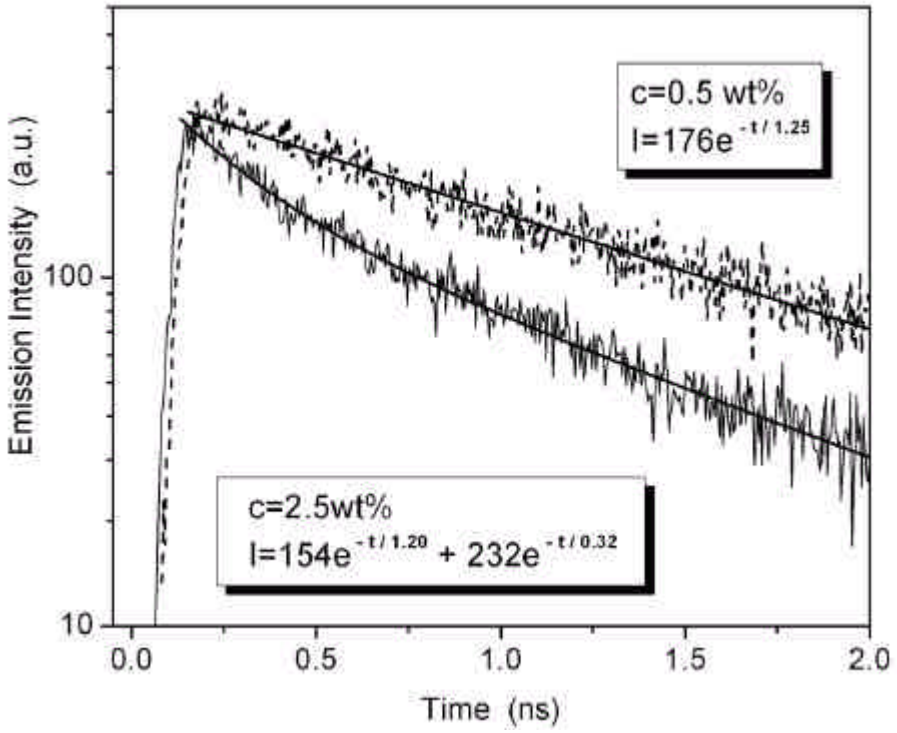

Figure 5.11. Fluorescence decay at 608nm with DCM concentrations of 0:5wt% and 2:5wt%. The pump pulsewidth is 40ps.

where ® is the absorption coefficient, r is the reflection coefficient of the mirrors and d is the cavity length. The gain must therefore compensate for both absorptive and cavity losses to achieve lasing. The threshold pump energy is [32]

$$E_{th}^{F\,i\,P} = A \circ {}_{th}^{F\,i\,P} d$$

where A is a constant related to the pump properties. It is straightforward to show that in a F-P cavity, the maximum value of the density of states (DOS) is related to the reflection coefficient by

$$DOS_M = \frac{1 + r^2}{1 \; i \; r^2}$$

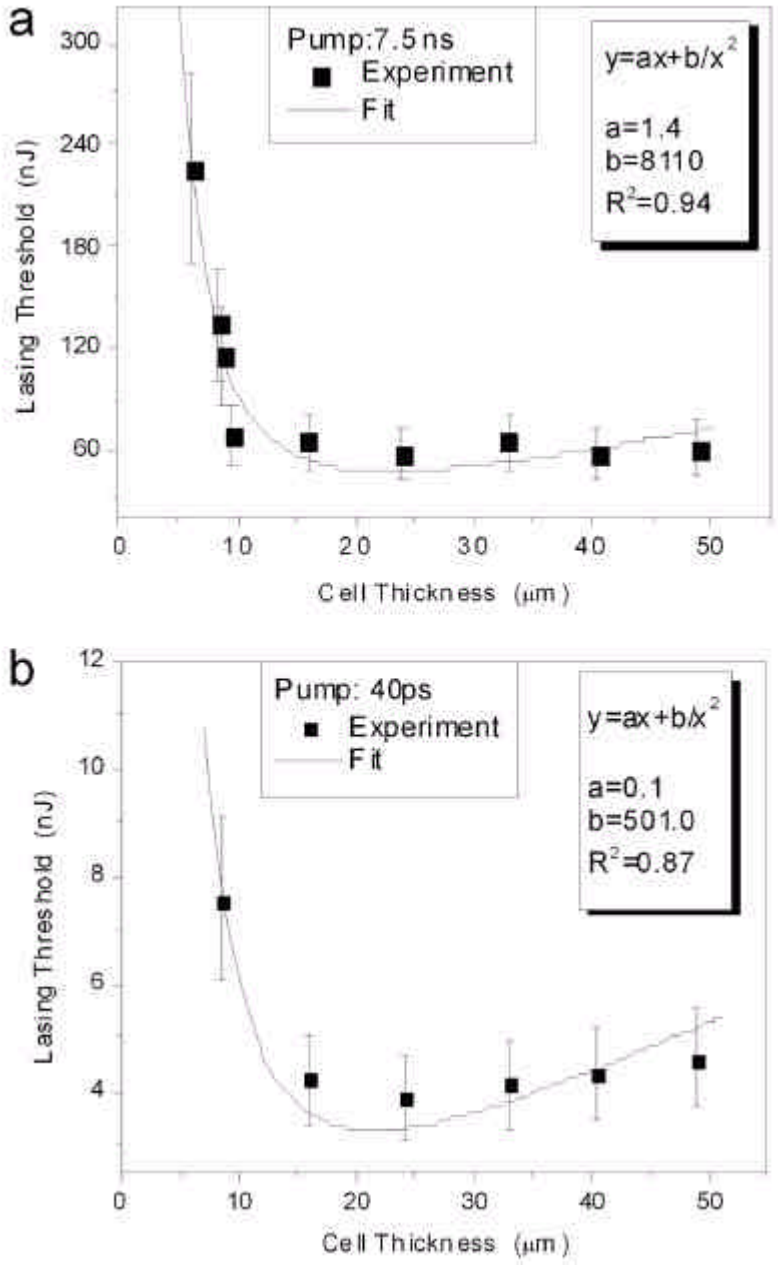

Figure 5.12. Lasing threshold as function of sample thickness. (a) nanosecond pump (b) picosecond pump

and it follows that

$$\ln r^2 = \ln \frac{1 - DOS_M}{1 + DOS_M} \approx -\frac{2}{DOC_M}$$

for large DOS_M. In CLC, the salient optical properties of the system are contained in the DOS. In analogy with the F-P laser, we write the threshold gain constant of the CLC laser as

$$\alpha_{th}^{CLC} = \alpha + \frac{2}{DOS_M \cdot d}$$

where α is the absorption coefficient. We have calculated the DOS for cells with different thicknesses shown in Figure 5.13. The highest DOS

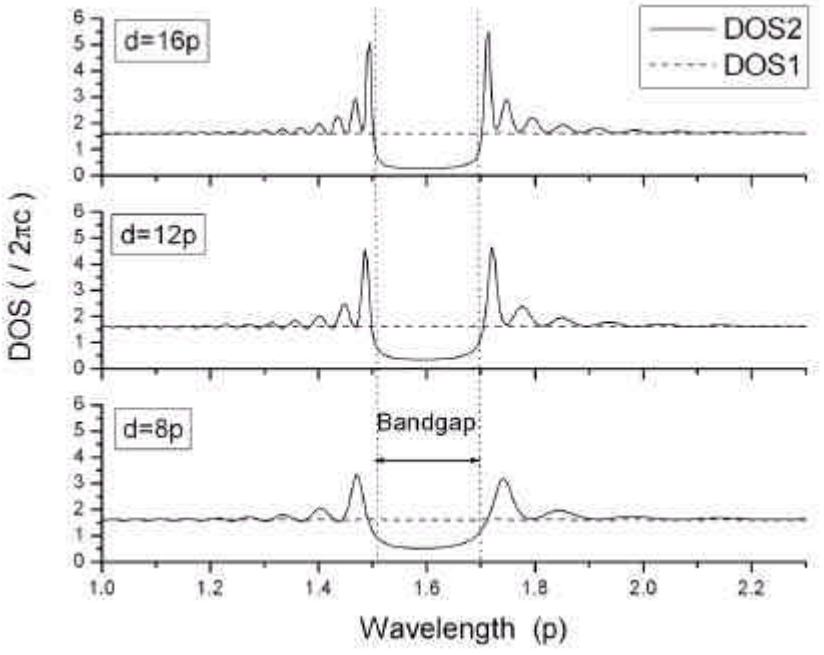

Figure 5.13. Calculated DOS for the two normal modes as a function of cell thickness. The dotted lines are the reflection band edges of a semi-infinite sample.

peak is close to the reflection band edge and lasing occurs at this wavelength. We have found that here $DOS_M = cd^2$, where c is a fitting

constant. This result is similar to the one of Dowling [33], who analytically calculated the DOS as function of sample thickness in a dielectric medium with alternating refractive indices. We then write for the pump energy at lasing threshold:

$$\begin{aligned} E_{th}^{CLC} &= B\,\alpha_{th}^{CLC} d \\ &= B\left(\alpha + \frac{-}{DOS_M d}\right) d = B\left(\alpha + \frac{-'}{d^3}\right) d \\ &= (B\alpha)\, d + \frac{(B-')}{d^2} \end{aligned}$$

This describes the dependence of lasing threshold on sample thickness d. Fitting experimental data to this expression a good agreement is found, as shown in Figure 5.12. The first term accounts for absorption loss, while the second term accounts for the cavity loss. For a distributed feedback laser without absorption losses, Kogelnik and Shank found that the threshold gain constant $\alpha_{th} = c'/d^3$, c' is a constant related to material and lasing wavelength, and d is the cavity length [34]. Thus the dependence of threshold on cavity length agrees with our results.

5.5 A Cholesteric Liquid Crystal DFB Laser

It has been clearly demonstrated the possibility to have lasing with periodic structures, and moreover it has been demonstrated the easy utility of CLC for this application. They are self-assembling, no external force is needed to organize the system in a periodic structure; they are easy to integrate in fiber as fiber sensor. Their optical properties can be changed with the temperature and external fields, acting on the pitch of the cholesteric, leading to a tunability of the lasing. Nevertheless cholesteric liquid crystal are cheap.

In order to optimize the lasing conditions for a telecom application, the dependence of the lasing threshold on dye concentration and sample thickness has been studied. The possible physical process responsible

for the observed behaviour has been carried out in terms of molecular dynamics inside the LC and density of states.

5.6 Perspectives

Both the devices presented in this thesis exploit the periodicity of the soft material they are made of: in the Active Bragg grating this periodicity is realized through a polymerization process, while in the DFB laser it is self-assembly. Both are easy to integrate in fibers because they are realized with soft material. The performances of both can be driven by a temperature change, or by an external electric force.

Often conclusions of a project, as this thesis, merge with perspectives,and probably that is why scientific research excite passion in scientists.

The next steps of the project will be aimed at realizing a *tunable distributed feedback laser inside a dye-doped activeBragg grating working at the NIR range*. In this way, the exploited index modulation will not be the one of the cholesteric liquid crystal, but the grating one. In Figure 5.14 it is shown a possible configuration of the device: the grating will be written inside the core of a fiber. This means that the strating syrup will be constituted not only from the photoinitiator, the monomer and the nematic liquid crystal, but also from the dye. The fiber core will be filled of this syrup and then illuminated with an interference pattern of curing UV radiation. With a reflection grating the index variation will be parallel to the fiber axis. If the fluorescent dye spectrum is in the reflection band, pumping the fiber the fluorescence will be inhibited inside the reflection band, and enhanced at the band edges. Mirrorless lasing will occur.

I will make some discursive considerations on the design of the device. If the molecules orient like in the studied POLICRYPS, that is perpendicuar to the polymer discs, the incoming light will not see an index mismatch. One solution can be to insert the fiber in a solenoid and to use

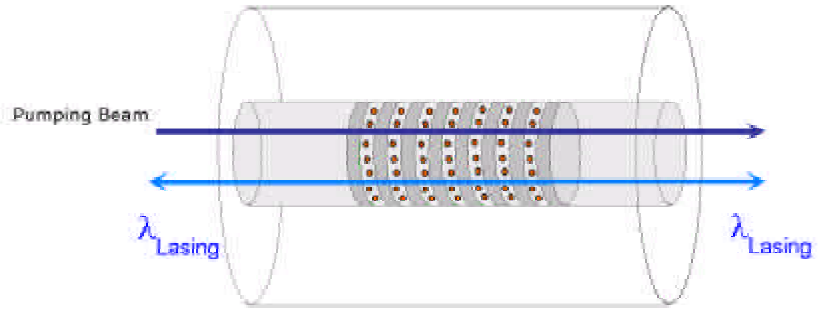

Figure 5.14. An integrated distributed feedback laser realized with a dye doped POLICRYPS grating working in reflection.

a liquid crystal with negative anisotropy: in this way, the magnetic field generated by the solenoid will orient the molecules parallel to the discs, and the incoming light will see the index modulation. The strength of the field will also be responsible of the lasing tuning.

If the field is applied, the refractive index modulation will occur: the higher and the lower index value will be n_e and $n_{polymer}$. The reflection band edges and the bandwidth will now depend on the liquid crystal orientation and on the index mismatch between the liquid crystal and the polymer:

$$\lambda_{lower} = 2pn_{polymer}$$

$$\lambda_{upper} = 2pn_e$$

$$\Delta\lambda = 2p(n_e - n_{polymer}) = 2p\Delta n$$

where λ_{lower} is the lower band edge, λ_{upper} is the upper band edge, and $\Delta\lambda$ is the bandwidth. If the lasing is asked to be in the C-band, $\lambda \approx 1550nm$, the reflection band upper edge should be $\lambda_{upper} \approx 1550nm$. If we suppose $n_e \approx 1{:}57$, then $p \approx 500nm$, which is a reasonable value. Varying the field, the effective index seen from the signal changes, hence the lasing wavelength can be tuned.

Nevertheless, the problem to realize a device with such features is that it does not exist an organic dye fluorescing in the Telecom bands yet,

from 1300 to 1600nm. The next challenge will be to overcome this obstacle. The use of metallo-mesogens, with heavy metal atoms or metallic complexes, will be explored for this purpose. Organic molecules having large ¼ conjugated systems constitute the majority of the used dyes. The presence of donor and acceptor groups or of ionic charges increases the absorbance and generally produces a great red shift of the absorbance band. Compounds with very large ¼ conjugated systems may have absorbance maximum up to 1000 ¥ 1100nm. Moreover, it's well known that such compounds may show further large red shift upon complexation with transition metal ions. The idea is to introduce in the new POLICRYPS DFB LASER design some compounds of this class including transition metal ions that have the absorbance maximum in the 1100 ¥ 1300nm region, so that they show fluorescence, if present, at higher wavelength range. To conduct this new line of research a strong collaboration with chemistry groups is foreseen, in particular with the group of Prof. A. Roviello at the Department of Chemistry of the University of Naples Federico II, already collaborating with us in the frame of the Centre of Competences in New Technologies (POR-Campania).

Chapter 6

Conclusions

The physics of two new electro-optical devices has been shown: an active Bragg grating realized with a composite liquid crystal and polymer material, and a distributed feedback laser realized with cholesteric liquid crystals.

An electro-optical characterization of the first produced POLICRYPS samples has been performed, using red light and NIR light in the telecom C-band. Results are not only interesting but also very useful because they prove that this new LC-polymer composite can be conveniently exploited for photonic applications in the telecom field, once they have been optimised for use at telecom wavelengths. POLICRYPS grating with diffraction efficiency over 90%, good angular selectivity, and time response in the microsecond range, can be obtained very soon in the C-band, still maintaining a very good optical transparency with almost negligible scattering losses.

Both switching off and switching on times strongly depend on amplitude and duration of the applied electric pulses. This was not expected for the elastic off-on transition and has been explained by assuming an essential role of the interfacial region between the LC and the polymer stripes, without a well-defined and sharp border, exhibiting a surface viscosity higher than the LC bulk one. This result can be the starting point for fundamental studies on bulk and surface elastic interactions in liquid crystalline composite materials.

Though both rise and fall response times can change in a wide range, it was already possible for those first batch and not-optimised samples, to get values in the range $50 \div 150^{1}s$, by means of a proper choice of the driving pulse shape. These results are very attractive for many possible applications of a key component, like a fast switchable Bragg grating, in telecom devices.

It has been clearly demonstrated the possibility to have lasing with periodic structures, and moreover it has been demonstrated the easy utility of CLC for this application. They are self-assembling, no external force is needed to organize the system in a periodic structure; they are easy to integrate in fiber as fiber sensor. Their optical properties can be changed with the temperature and external fields, acting on the pitch of the cholesteric, leading to a tunability of the lasing. Nevertheless cholesteric liquid crystal are cheap. The dependence of the lasing threshold on dye concentration and sample thickness has been studied. The possible physical process responsible for the observed behaviour has been carried out in terms of molecular dynamics inside the LC and between dye molecules.

The coupled wave theory, developed by Kogelnik and his coworkers in the 70's, has been introduced to explain the physics of both the devices. Through this theory it is possible to relate the diffraction efficiency of thick gratings with their design prameters; analogously, the theory can be used to explain the distributed feedback dynamics inside the periodic structures.

Appendix A - HPDLC

Polymer Dispersed Liquid Crystals (PDLCs) are composites systems in which droplets of liquid crystals are dispersed in a polymer matrix. By applying an electric field, and by choosing appropriate optical constants of the materials, the PDLC can be switched from a scattering state to a non-scattering state: this effect is due to the refractive index matching between the liquid crystal and the polymer when the field is ON, and to the mismatch of the refractive indices in absence of field. PDLCs are formed from a homogenous mixture of pre-polymer and liquid crystal. As the polymer is cured, the miscibility gap between the LC and the host increases and the LC separates as a distinct microdroplet phase. If a photopolymer system is used, the photo polymerization can be optically controlled and it is possible to record holographic gratings in the PDLC. This gratings are called HPDLC. The result of the writing process is a grating made by a periodic distribution of small LC droplets, randomly oriented, embedded in a polymeric matrix, with a higher concentration of the LC component in the dark fringes. The interference pattern usually generates also a periodic gradient of the droplet size distribution: larger droplets are in general located in the dark fringes of the interference pattern, whereas smaller ones are located in the directly irradiated areas. Due to the mismatch between polymer and LC refractive index, the spatial modulation of the droplet density and size results in a small modulation of the average refractive index.

H-PDLC gratings can be proposed as active elements for a number of telecom photonic devices based on the Bragg grating functionality. Of course, matching the requirements of optical communication systems demands their optimization for working at the telecom wavelengths, typically in the NIR range: in this spectral region, gratings should show high diffraction efficiency (DE), angular selectivity, low losses, low driving voltages and fast switching times. In this appendix

a small introduction to PDLC and PDLC gratings is given in order to understand the main differences with POLICRYPS gratings.

A.1. PDLC

There are different methods used to realize PDLCs [9]. The most common is colled Polymerization Induced Phase Separation (PIPS). It starts from a homogeneus mixture of a low molecular weight liquid crystal and a fluid prepolymer. The typical structure of liquid crystal droplets dispersed in a polymer matrix is due to the phase separation, induced during the polymerization process, between the LC and the polymer. The polymerization process may happen in different ways, depending on the used materials. If the polymer is an epoxy resin, it needs a curing material to start polymerization, which is achieved through a condensation reaction. Similarly, using UV curable adhesives as prepolymers, the polymerization can be induced by absorption of ultaviolet light. In both instances, as the polymerization starts the liquid crystal solubility decreases and the separation between the two phases (the one of the polymer and the one of the LC) starts. The first droplets appear. As the polymerization goes on, the droplets grow incorporating an increasing amount of LC, until the polymer congealment fixes the droplets size and shape inside the matrix. The size and the density of the droplets depend on the polymer viscosity, rate of diffusion and solubility of the LC in the polymer, on the curing temperature, concentration of the curing material and the stating mixture. Driving the rate of polymerization and the temparature, one can controll the microscopic properties of PDLC, and as a consequence its macrocopic properties.

The physical properties of a PDLC strictly depend on the droplets properties, including the LC molecular director distribution inside the droplet. This can be calculated through a minimization of the free energy. By this precedure one founds that several director configurations are possible, depending on the boundary condition. For example, for spherical droplets, in the one elastic constant approximation, and ne-

glecting the changes in the value of the order parameter induced by the surface, one can found these two common solutions:

- in case of tangential anchoring, the director $\mathbf{n}$ tends to orient tangential to the droplets meridians (see Figure 6.1a), in a configuration called *bipolar*;
- with normal anchoring, the director $\mathbf{n}$ orients parallel to the droplet radius (see Figure 6.1b), in a *radial* configuration.

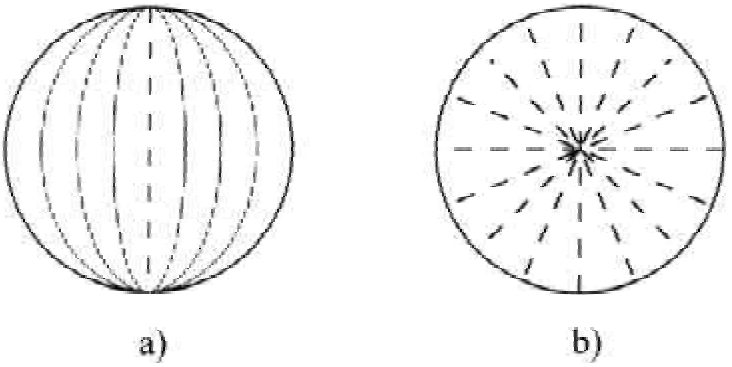

Figure 6.1. Two possible director configurations in a droplet (a) bipolar (b) radial.

In general it is possible to associate to each droplet a vector $\mathbf{N}_d$, called the *droplet's director*, which describes the average orientation of the molecular director inside the droplet[13]. Similarly, the droplet's order parameter S_d describes the average fluctuations of $\mathbf{n}$ with respect to $\mathbf{N}_d$. Usually the droplet shape is not exactly spherical but like elliptic: when no external force is applied, the director $\mathbf{N}_g$ stays along the major axis of the droplet. The application of an elctric field changes the director configuration in the droplets, reorienting $\mathbf{N}_g$ parallel to the field $\mathbf{E}$

[13] This is not possible in the radial configuration, where the director distribution is isotropic.

(supposing a positive dielectric anisotropy); once that the field has been switched off, elastic forces will reorient N_g again along the ellipse axis.

To reorient LC droplets inside a polymer matrix higher electric fields are required, higher than in a simple LC cell. In fact, being encapsulated in a polymer matrix, the effective field applied to the droplet is very different from the external one. By simple consideration on the classical problem of an isolated spherical droplet in a uniform field, the local field on the droplet can be related to the external one

$$E_{LC} = E_P \frac{3}{2 + \frac{"_{LC}}{"_P}}$$

where $"_{LC}$ and $"_P$ are respectevely the dielectric constant of the liquid crystal inside the droplet and the polymer. At low frequency, $! \; ! \; 0$,

$$E_{LC} = E_P \frac{3}{2 + \frac{¾_{LC}}{¾_P}} \qquad \text{(A.1)}$$

where the complex definition of the dielectric permittivity $" = "^0 + i¾=!$ has been taken into account. Since the conductivity of the LC is generally much more bigger than the polymer, $¾_{cl} \; À \; ¾_p$, from equation (A.1) it results that the local field on the droplet is weaker than the external one.

In a LC cell, the applied voltage, over that the *Freédericksz transition* is visible, is independent on the cell thickness. In PDLC the critical field E_c, needed to have reorientation, is not inversely proportional to the cell thickness, but to the average droplets radius ½,

$$E_c = \frac{\{}{½}$$

It means that the smaller is the radius, the stronger are the elastic forces. The average field in the cell is

$$V = Ed$$

If the LC density in the polymer matrix is small, the average field correspond to the field in the polymer, so the critical value of the voltage is

$$V_c = \frac{d}{3}\left(2 + \frac{\varepsilon_{cl}}{\varepsilon_p}\right)\frac{\{}{\xi}$$

The threshold value of the applied voltage is inversely proportion to the droplet radius ξ and directly proportional to the thickness d of the polymer matrix.

The optical properties of PDLC are dominated by light scattering, due the droplets size which is closed to the light wavelength ($\approx 1\mu m$). For equal particles uniformly dispersed in the polymer matrix, the scattering coefficient β_s may be set proportional to the square of the index mismatch,

$$\beta_s = \cdot(\Delta n)^2$$

where $\Delta n = n_p - n_d$ is the difference between the polymer and the droplet refractive indices. The optical field attenuation in traveling through such medium is described by a differential equation

$$\frac{dE}{dz} = -\frac{\beta_s}{2}E$$

It means that after crossing the cell thickness d, the field is

$$E(d) = E(0)\,e^{-\frac{\beta_s}{2}d}$$

and the transmitted intensity is

$$I(d) = I(0)e^{-\beta_s d} = I(0)e^{-\cdot d(\Delta n)^2}$$

This equation relates the intensity I to the walk d inside the PDLC.

The single droplet refractive index depends on the orientation of the droplet director N_g with respect to the propagating direction and the light polarization. When no electric field is applied, the droplets are randomly oriented. The average value of Δn can be as large as $0{:}1$ or more, because of the LC high anisotropy: that gives strong light scat-

tering. Under electric field, the droplets director will be oriented in the same direction, and the rediation will see the same effective refractive index. If this is chosen closed to the polymer one, the index mismatch approaches to zero, the scattering losses decrease and the PDLC shows high light transmission.

A.2. PDLC Holographic Gratings

If a photopolymer system is used, the photo polymerization of the starting mixture can be optically controlled and it is possible to record holographic gratings in the PDLC. This gratings are called *Holographic Polymer Dispersed Liquid Crystals* (HPDLC). The result of the writing process is a grating made by a periodic distribution of small LC droplets, randomly oriented, embedded in a polymeric matrix, with a higher concentration of the LC component in the dark fringes. The interference pattern usually generates also a periodic gradient of the droplet size distribution: larger droplets are in general located in the dark fringes of the interference pattern, whereas smaller ones are located in the directly irradiated areas. Due to the mismatch between polymer and LC refractive index, the spatial modulation of the droplet density and size results in a small modulation of the average refractive index. The physic of the switchable diffraction is easy: without field incident light sees, on average, the ordinary and extraordinary refractive indices of the liquid crystal. This average index differs from the polymer index, and hence produces an index modulation forming a phase grating (Figure 6.2a). When a strong electric field, whose amplitude is well above the Fréedericksz threshold, is applied normal to the cell substrates, the director of all the LC domains will reorient parallel to the field (Figure 6.2b). In this situation, an impinging light at quasi-normal incidence sees the ordinary refractive index of the LC, independently of the light polarisation direction, and if this index is equal to the polymer one, the H-PDLC appears as an optically homogeneous material: the grating disappears.

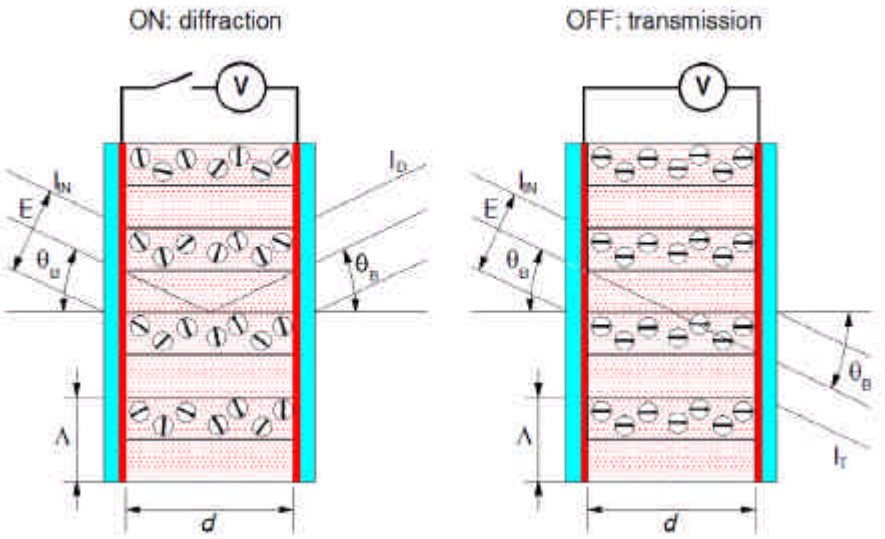

Figure 6.2. H-PDLC operating mode

A.3. A Comparison with POLICRYPS

- From a morphological point of view, the biggest difference between H-PDLCs and POLICRYPS is the following: in the former, in the UV-illuminated regions, a light-induced phase separation process creates LC droplets embedded in a polymer matrix, while the dark regions remain in the form of isotropic LC-polymer mixture. In the latter material, no phase separation happens within the illuminated regions, instead, under particular conditions, it happens between the illuminated and non-illuminated regions, so that one component (for example polymer) is almost totally confined within illuminated regions and the other component (for example LC) within non-illuminated regions.
- In order to be attractive for telecom applications a switching grating must be transparent in both the ON and the OFF states. This

constraint imposes an upper limit to the size of the droplets in the PDLC; in fact droplet size of the order of the light wavelength gives rise to significant scattering losses. For this reason, nano-PDLC with droplet size of the order of 100nm have been developed in the last years by different authors[10][11]. Nano-PDLC may show a very high diffraction efficiency and good transparency having however as a drawback a quite large driving voltage, increasing with decreasing droplet size.

- The writing process is more complicated for POLICRYPS grating, where a complete separation occurs. This process is more sensible to small noises, lake vibrations of the writing set-up. Moreover HPDLC have been written both in transmission and reflection, while POLICRYPS only in transmission.
- The switching field is bigger in H-PDLC of a factor 2 ¥ 2:5 with respect to POLICRYPS
- While POLICRYPS are highly dependent from the light polarization (because of the molecules orientation between the polymer stripes), on the other hand HPDLC are theoretically polarization independent, but experimentally this does not seem.

Appendix B - Ellipsometry

In order to be applied in photonic devices for telecom applications, soft materials, polymers and in particular liquid crystals, need to be optically characterised at the working wavelengths, typically in the Near IR region (NIR). Unfortunately, for most of these materials very few data are available in literature, especially in the NIR range. Moreover, because of the nature of these media, it is often necessary to make measurements on samples consisting of complicated multilayer stacks, including anisotropic, inhomogeneous, absorbing, and/or depolarising films. Recently, different ellipsometric techniques have been proposed to fulfil this task: the most versatile, sensitive and well-established technique is Spectroscopic Ellipsometry (SE) [47][48]. SE and its further extensions, as the Generalised Ellipsometry (GE) and the Muller Matrix Ellipsometry (MME), have been applied also to the systematic investigation of anisotropic thin ($< 10^{1}\,m$) [49] and thick ($< 50^{1}\,m$) [23] films of LC materials. However, ellipsometric measurements may pose serious problems of results reliability, due to the high complexity of usual LC containing samples. In fact, a typical LC cell is a multi-layer structure with its first layer formed by a very thick glass plate ($0{:}4 \text{ ¥ } 1mm$), and then it contains coating films, surfactant layers, inhomogeneous structures like the electrodes of Indium Tin Oxide (ITO). The presence of interface roughness and the strong anisotropy exhibited by LC, eventually with optical axis varying along the stratification direction, complete a picture not easy to analyse.

B.1. Theory

Standard Spectroscopic Ellipsometry is based on measurement of two physical quantities: the relative phase change, ¢, and the relative amplitude change, ^{a}, suffered by incident light when reflected (or trans-

mitted) by a layered structure. These two parameters are linked to the reflection (or transmission) coefficients, which are themselves related to the optical response of the surface: the Ψ's and Δ's spectra depend on the refractive indices of the layers, on their thickness and, in the case of anisotropic films, on the orientation of their optical axis (of course, they depend on any physical parameters that affect the optical behaviour of the material, for instance on temperature). By the adoption of the 2×2 Jones matrix formalism, it is possible to extend ellipsometry application to anisotropic media (Generalized Ellipsometry). In this way it is possible to generalise the Standard Ellipsometry parameters, Δ and Ψ, suffered by incident light after transmission or reflection by a sample, to the case when a change occurs in light polarisation. The six GE parameters, Δ, Ψ, Δ_{ps}, Ψ_{ps}, Δ_{sp}, Ψ_{sp}, are linked to the Jones matrices of reflected (J_r) or transmitted (J_t) beam through the following equations:

$$\begin{aligned} \tan\Psi\, e^{i\Delta} &= \frac{J_{pp}}{J_{ss}} \\ \tan\Psi_{ps}\, e^{i\Delta_{ps}} &= \frac{J_{ps}}{J_{pp}} \\ \tan\Psi_{sp}\, e^{i\Delta_{sp}} &= \frac{J_{sp}}{J_{ss}} \end{aligned} \qquad \text{(B.2)}$$

where $J = J^r; J^t$ and

$$J^r = \begin{pmatrix} r_{pp} & r_{sp} \\ r_{ps} & r_{ss} \end{pmatrix} \quad \text{and} \quad J^t = \begin{pmatrix} t_{pp} & t_{sp} \\ t_{ps} & t_{ss} \end{pmatrix}$$

with r_{pp}, r_{ss}, r_{ps}, r_{sp} (t_{pp}, t_{ss}, t_{ps}, t_{sp}) representing the reflection (trasmission) coefficients for p-, s-, and cross-polarizations respectively. In the isotropic case we have $n_x = n_y = n_z$ and the Jones matrix will be diagonal

$$J_r = \begin{pmatrix} r_{pp} & 0 \\ 0 & r_{ss} \end{pmatrix} \quad \text{and} \quad J_t = \begin{pmatrix} t_{pp} & 0 \\ 0 & t_{ss} \end{pmatrix}$$

equations (B.2) reduce to the first one and only two parameters are meaningful. We remark that off-diagonal elements in Jones matrices

represent the conversion of the p- and s- polarized light into s- and p-polarized respectively; those elements vanish also for anisotropic media in highly symmetric configuration, i.e. when the optical axis is oriented parallel or perpendicular to the plane of incidence [50].

However, the Jones matrix formalism is based on the assumption of a completely polarized light. When a significant amount of reflected or transmitted light becomes depolarized, it may be necessary to introduce the Mueller matrix representation. In this scheme, a 4×4 matrix connects the Stokes vectors representing the input and the output beam, as described in equation (B.3)

$$\begin{bmatrix} S_0 \\ S_1 \\ S_2 \\ S_3 \end{bmatrix}_{OUT} = \begin{bmatrix} M_{11} & M_{12} & M_{13} & M_{14} \\ M_{21} & M_{22} & M_{23} & M_{24} \\ M_{31} & M_{32} & M_{33} & M_{34} \\ M_{41} & M_{42} & M_{43} & M_{44} \end{bmatrix} \begin{bmatrix} S_0 \\ S_1 \\ S_2 \\ S_3 \end{bmatrix}_{IN} \tag{B.3}$$

We have analysed several liquid crystals. Experimental data were measured on a spectroscopic ellipsometer manufactured by the J. A. Woollam Company. A Variable Angle Spectroscopic Ellipsometer (VASE®) was used to perform measurements as a function of both wavelength and angle of incidence, in the spectral range from 300nm to1700nm. This instrument is equipped by an Autoretarder™, which utilizes patented technology to achieve maximum measurement accuracy. Data have been analysed using WVASE32™ software version 3.396. Once the experimental data are acquired (see Figure 6.3), it is necessary to draw up a multilayer optical model, which carefully describes the sample structure. Specific software generates theoretical data and unknown parameters, such as thickness or optical constants values, are adjusted in the optical model to better fit the experimental data. Parameters values are fixed once the iteration process minimizes the difference between experimental and model-generated data. The software determines the sample refractive index and eventually thickness, by means of a multiple fitting procedure. This procedure ends providing a numerical value for the discrepancy between experimental and generated data, called Mean Square

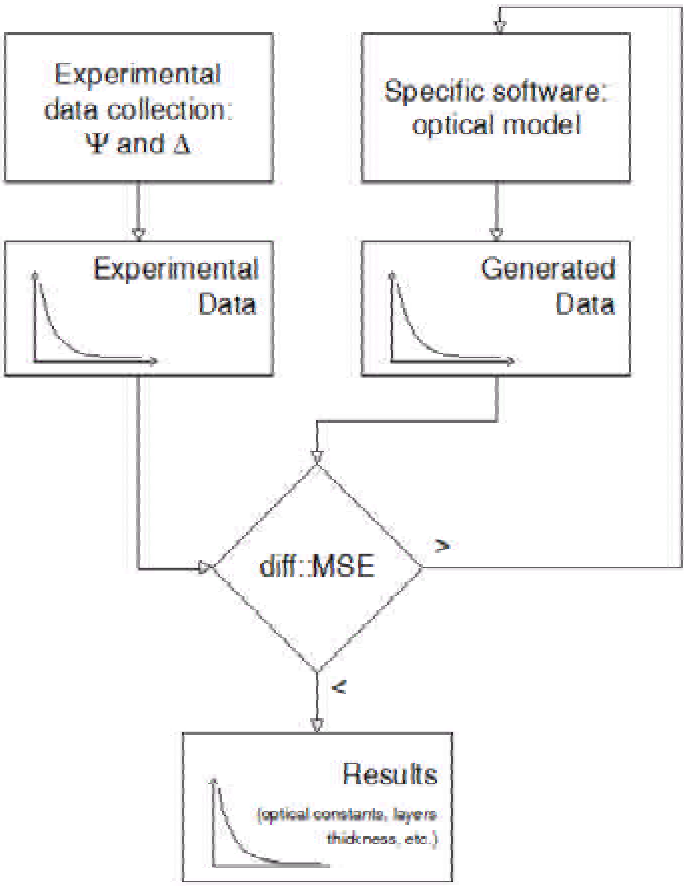

Figure 6.3. Spectroscopic GE Analysis Flow Chart

Error (MSE), which we used to check the goodness of the fit. The main possible drawbacks in SE, GE and MME analysis could be the dependence of final results on:

1) accuracy of the optical model,
2) starting points in fitting procedures,
3) statistical correlation between fit parameters.

B.2. A Measure on Liquid Crystal

The first sample investigated is a $12{:}4^1\,m$ thick layer of a nematic 5CB[14] nematic LC (provided by Merck) sandwiched between $0{:}4mm$ thick silica glasses[25]. The LC film was homeotropically aligned by using a very thin layer of DMOAP surfactant[15]. In this simple geometry, we could consider the off-diagonal elements of Jones matrices to be vanishing [50] and use SE technique in reflection. Due to the absence of any resonances in the examined spectral range, we can describe the ordinary and extraordinary indices of the nematic by using the simplest 2-parameter Cauchy formula (where the subscripts o and e stand for ordinary and extraordinary, respectively):

$$n_{o;e} = a_{o;e} + \frac{b_{o;e}}{\lambda^2} \qquad \text{(B.4)}$$

Trials made with the three parameter Cauchy formula did not give any significant difference in the obtained dispersion curves; furthermore, the third fitted parameter was always quite strongly correlated to the previous ones, especially the second one, decreasing accordingly the degree

[14] The same LC used to produce POLICRYPS gratings.

[15] The presence of the DMOAP film had a negligible influence on our sample measurements. Further measurements made just on a treated glass led to the determination of the DMOAP thickness corresponding to one molecular layer.

of confidence in the fit.

$$n_{o;e} = a_{o;e} + \frac{b_{o;e}}{\lambda^2} + \frac{c_{o;e}}{\lambda^4}$$

Starting from our experimental data we tried out different fit procedures.

- **FIT 1:** the film thickness d was held fixed to the above-mentioned value, previously obtained by empty cell measurements. Starting guess values for the fit parameters, $a_{o;e}$ and $b_{o;e}$, were found by a special routine of WVASE32™ software, namely a grid-based value pre-selection. This feature resulted to be extremely useful, a too far initial guess often producing unreliable results. Generated and experimental data, shown in Figure 6.4, are in good agreement apart a high frequency and small amplitude interference oscillation pattern, present in the generated curves that was never observed in actual measurements. These oscillations were finally recognised as an artefact of the simulation software, due to the glass plate expected interference. Lack of coherence of the lamp light does never allow this interference to be actually observed for a geometric path difference in the millimetre range (twice the glass plate thickness).

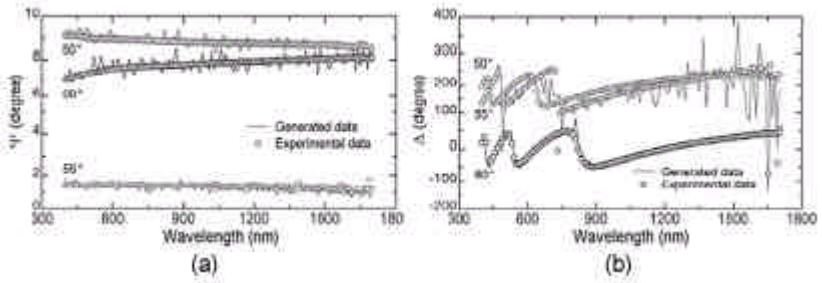

Figure 6.4. Spectroscopic ellipsometric measurements for the 5CB liquid crystal sample: ψ (fig.a) and Δ (fig.b) experimental data and respective generated curves (fit 1) for $50^{\pm}$, $55^{\pm}$ and $60^{\pm}$ incidence angles.

		Fit 1	Fit 2	Fit MM	K&M
n_e	a	1.6325	1.6452	-	1.637
		§ 0.0005	§ 0.0003	-	§0.002
	b [$^1m^2$]	0.0164	0.0193	-	0.0222
		§ 0.0002	§ 0.0002	-	§ 0.0006
n_o	a	1.5011	1.5124	-	1.50673
		§ 0.0002	§ 0.0002	-	§ 0.00008
	b [$^1m^2$]	0.0068	0.0086	-	0.01090
		§ 0.0001	§ 0.0001	-	§ 0.00003
¢n	a	0.1314	0.1328	0.1348	0.130
		§ 0.0007	§ 0.0005	§ 0.0002	§ 0.002
	b [$^1m^2$]	0.0096	0.0107	0.01007	0.0113
		§ 0.0003	§ 0.0003	§ 0.00006	§ 0.0006

Table 6.6. Comparison among 5CB dispersion Cauchy parameters obtained from different ellipsometric measurements and fit procedures and published data. Parentheses in n values indicate that were obtained by difference of the respective extraordinary and ordinary indices.

² **FIT 2**: a second fit was made including also the film thickness d amongst the fitted parameters. We obtained a fitted value for the thickness $d = 12{:}5\,^1m$, in good agreement with the empty cell value, and slightly different values for the a and b Cauchy parameters (Table 6.6).

Our experimental curves for ordinary and extraordinary refractive indices and the ones calculated on the base of data provided by Karat and Madhusudana [53]are shown in Figure 6.5: a quite good agreement with the literature is clearly obtained by fit 2, especially in the visible region. The curve displacement in the NIR region is not surprising. In fact, using our spectroscopic ellipsometer we obtained experimental data from the visible up to the NIR and we paid attention to take equally spaced data points in the whole range. On the contrary, the Karat and Madhusudana reference curve is only an extrapolation, built from refractive index values measured at three wavelengths in the visible region, through a Cauchy dispersion model (equation (B.4)).

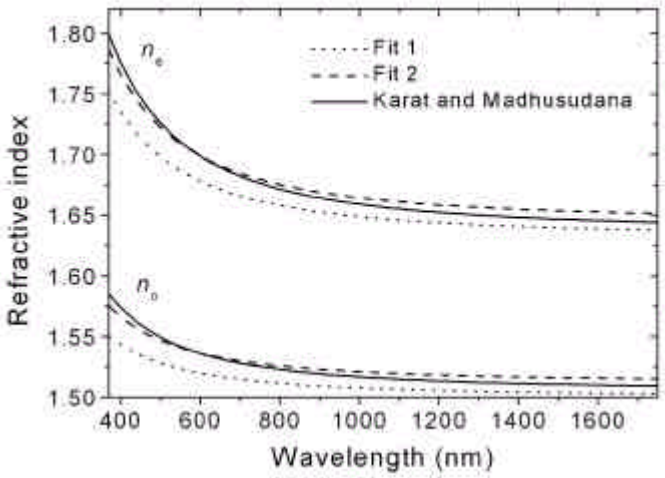

Figure 6.5. Ordinary and extraordinary refractive index dispersion for 5CB liquid crystal: the curves refer to two fitting procedures and one literature data set.

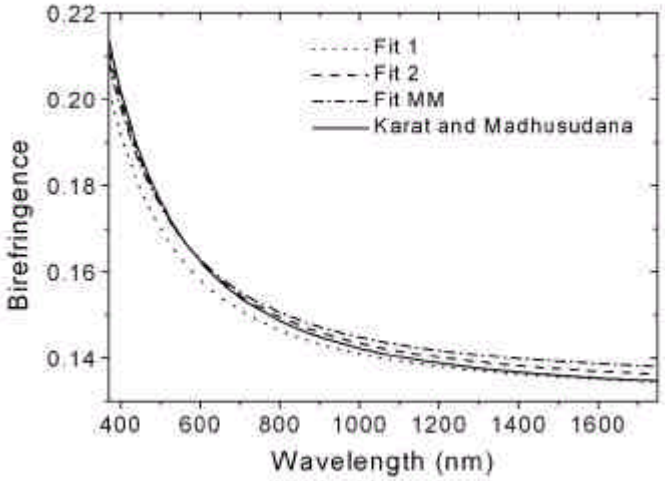

Figure 6.6. Birefringence dispersion for 5CB LC: the curves refer to three fitting procedures and one literature data set.

In order to verify our assumptions in the choice of the ellipsometric technique (small depolarization, zero off-diagonal elements) and at the same time to check the reliability of our fit results, we made an independent measurement of the birefringence Δn, by using transmission MME [5], also releasing the assumption of perfect homeotropic alignment of the LC film, and performing measurements at different sample orientation. Fit generated and experimental curves were in good accordance also in this case, and results were quite close to the previous ones (Table 6.6). The obtained dispersion curves for the birefringence are shown in Figure 6.6: fit 2 curve is almost coincident to the literature data, and very close to the one calculated from the MM transmission fit; fit 1 curve is again a little lower, with a relative displacement around $1 \div 2\%$.

Finally, we want to recall that refractive indices, hence also the birefringence, in nematic materials are very sensitive to the temperature, the closer you get to the clearing point T_C. Furthermore, next to T_C, the more meaningful dependence of the optical constants is on the physical parameter $T = T - T_C$ rather than on the absolute temperature T. This should be clear especially considering that a small impurity content in the sample can induce relatively large variations of T_C. Our samples were not controlled in temperature better than the whole clean room was, that is up to $\pm 1^{\circ}K$.

Bibliography

[1] *Roadmap towards the Optical Communication Age*, A European view by the HORIZON project and the ACTS Photonic Domain.

[2] P. G. de Gennes and J. Prost, *The Physics of Liquid Crystals*, 263 (Clarendon Press, Oxford, 1993).

[3] M. Born and E. Wolf, *Principles of Optics*, Pergamon (1980).

[4] L. Domash, G. Crawford, A. Ashmead, R. Smith, M. Popovich, and J. Storey, Proc. SPIE, 4107, 1 (2000).

[5] L. Lucchetti, S. Di Bella, F. Simoni, Liq. Cryst., 29, 515 (2002).

[6] P. Hariharan, *Optical Holography, Principles, Techniques and Applications*, Cambridge University Press (1984).

[7] J. A. Arns, W. S. Colburn, and S. C. Barden, *Proc. SPIE*, 3355, p. 866 (1998)

[8] H. Kogelnik, *Bell Syst. Tech. J.*, 48, 2909 (1969).

[9] F. Simoni, *Non Linear Optical Properties of Liquid Crystals and Polymer Dispersed Liquid Crystals*, World Scientific, River Edge, NJ, (1997)

[10] D. E. Lucchetta, R. Karapinar, A. Manni, and F. Simoni, J. Appl. Phys., 91, 6060 (2002).

[11] T.J. Bunning, L.V. Natarajan, V.P. Tondiglia, R.L. Sutherland, Annual Rev. Mat. Sci., 30, 83 (2000).

[12] R. Caputo, A. V. Sukhov, C. Umeton, and R. F. Ushakov, J. Exp. Theor. Phys., 91, 1190 (2000).

[13] R. Caputo, A. V. Sukhov, N. V. Tabirian, C. Umeton, and R. F. Ushakov, Chem. Phys., 271, 323 (2001).

[14] G. Abbate, A. Marino, F. Vita, Mol. Cryst, Liq. Cryst., Vol. 398, pp.269-280, (2003).

[15] G. Abbate, A. Marino, F. Vita, Acta Physica Polonica A, Vol. 103, No. 2-3, pp. 177-186, (2003).

[16] A. Marino, F. Vita, V. Tkachenko, R. Caputo, C. Umeton, A. Veltri, G. Abbate, Eur. Phys. J. E, 15, 47-52 (2004).

[17] Asquini, d'Alessandro, et all, Mol. Cryst. Liq. Cryst., Vol. 398, pp.223, (2003).

[18] Research Project of National Interest (PRIN 2000) by Italian Ministry of Education and Research, Devices for routing in optical networks using new liquid crystals materials and composites.

[19] R. Caputo et al., J. Opt. Soc. Am. B, (submitted).

[20] R. Caputo et al., App. Phys Lett., (submitted).

[21] T.K. Gaylord, M.G. Moharam, Proc. IEEE, 73, 894, (1985).

[22] G. Montemezzani, M. Zgonik, Phys. Rev. E, 55, 1035, (1997).

[23] G. Abbate, G. Del Gais, L. De Stefano, A. Marino, T. Wagner, Mol. Cryst, Liq. Cryst., Vol. 398, pp.249-258, (2003).

[24] J. N. Hilfiker, C. M. Herzinger, T. Wagner, A. Marino, G. Delgais, and G. Abbate, 455-456, 591 (2004).

[25] V. Tkachenko, A. Marino, F. Vita, F. D'Amore, L. De Stefano, M. Malinconico, M. Rippa, G. Abbate, Eur. Phys. J. E, 14, 185-192 (2004).

[26] S. Chandrasekhar, *Liquid crystal* s, Cambridge University Press, Cambridge, (1977).

[27] G. Morthier, P. Vankwikelberge, *Handbook of Distributed Feedback Laser Diodes*, Artech House Publishers, Boston (1997)

[28] E. Yablonovitch, Physical Review Letters 58, 2059 (1987).

[29] J.D. Joannopoulos, R.D. Meade, J.N. Winn, *Photonic Crystals, Molding the Flow of Light*, Princeton University Press (1995).

[30] J.M. Bendickson, J.P. Dowling and M. Scalora, Phys. Rev. 53, 4107 (1996).

[31] M. Meyer, J. Mialocq and B. Perly J. Phys. Chem. 94, 98 (1990).

[32] C.C. Davis, Lasers and Electro-Optics, 90 and 254-258 (Cambridge University Press, New York, 1996).

[33] J.M. Bendickson, J.P. Dowling and M. Scalora, Phys. Rev. 53, 4107 (1996).

[34] H. Kogelnik and C.V. Shank, J. Appl. Phys. 43, 2327 (1972).

[35] I.P. Il'chishin, E.A. Tikhonov, V.G. Tishchenko and M.T. Shpak, JETP Lett. 32, 27 (1981)

[36] V. I. Kopp, B. Fan, H. K. M. Vithana and A. Z. Genack, Opt. Lett. 23, 1707 (1998)

[37] L.S. Goldberg and J.M. Schnur, US patent 3,771,065 (1973).

[38] B. Taheri, A. Muñoz, P. Palffy-Muhoray and R. Twieg, Mol. Cryst. Liq. Cryst. 358, 73 (2001).

[39] H. Finkelmann, S. T. Kim, A. Muñoz, P. Palffy-Muhoray and B. Taheri, Adv. Mater. 13, 1069 (2001).

[40] B. Taheri, P. Palffy-Muhoray and H. Kabir, ALCOM Symposium. Chiral Materials and Applications, Cuyahoga Falls, Feb 18-19 (1999).

[41] A. Muñoz, P. Palffy-Muhoray and B. Taheri, Opt. Lett. 26, 804 (2001).

[42] M. Ozaki, M. Kasano, D. Ganzke, W. Haase and K. Yoshino, Adv. Mater. 14, 306 (2002).

[43] T. Matsui, R. Ozaki, K. Funamoto, M. Ozaki and K. Yoshino, Appl. Phys. Lett. 81, 3741 (2002).

[44] W. Cao, A. Muñoz, P. Palffy-Muhoray and B. Taheri, Nature Mater. 1, 111 (2002).

[45] L.V. Natarajan, R.L. Sutherland, T.J. Bunning, V.P. Tondiglia, Proc. SPIE 3292, 44 (1998).

[46] F. Vita, A. Marino, F. Simoni, D. E. Lucchetta, L. Criante, G. Abbate, *Near Infrared Characterization and Modelling of Nanosized H-PDLC Gratings*, manuscript.

[47] R. M. A. Azzam, N. M. Bashara, *Ellipsometry and Polarized Light*, North Holland Press, Amsterdam 1977, Second Edition 1987.

[48] H.G.Tompkins, W.A.McGahan, Spectroscopic Ellipsometry and Reflectometry, Wiley & Sons (1999).

[49] M. Schubert, B. Rheinlander, C. Cramer, H. Schmiedel, J.A. Woollam, C.M. Herzinger, B. Johs, J. Opt. Soc. Am. A 13, 1930 (1996).

[50] H. Touir, M. Stchakovsky, R. Ossikovski, M. Warenghem, Thin Solid Films, in press (2004).

[51] J.A.Woollam, B.Johs, C.M. Herzinger, J.N. Hilfiker, R. Synowicki, C. Bungay, Proc. SPIE, CR72, Part I 3-28 and Part II 29-58, (1999).

[52] J. N. Hilfiker, C. M. Herzinger, T. Wagner, A.Marino, G. Del Gais, G. Abbate, Thin Solid Films, 455-456, 591 (2004).

[53] P. P. Karat, N. V. Madhusudana, Mol. Cryst. Liq. Cryst., 36, 51-64, (1976).

Webgraphy

Even if they are not cited inside the text, there are many intresting web-site on liquid crystal photonic. A navigation through them could be a nice way to approch the liquid crystal world.

- Optics in Soft-Matter Group, Università degli Studi di Napoli Federico II, **http://people.na.infn.it/» abbate/gruppo/**
- Antigone Marino web-site, **http://people.na.infn.it/» antigone**/
- Liquid Crystal Institute, Kent State University, Ohio, USA, **http://www.lci.kent.edu/**
- Italian Liquid Crystal Society (SICL), **http://www.sicl.it/**
- International Liquid Crystal Society (ILCS), **http://www.ilcsoc.org/**
- Polymers & Liquid Crystals Virtual textbook, **http://plc.cwru.edu/tutorial/enhanced/files/textbook.htm**
- Professor E. Santamato web-site, **http://people.na.infn.it/» santamat/**
- Advanced Liquid Crystalline Optical Materials (ALCOM), **http://www.lci.kent.edu/ALCOM/ALCOM.html**
- On line information on Liquid Crystal, **http://liqcryst.chemie.uni-hamburg.de/lc/lc_info.ht**m

- Physics Web Links to Liquid Crystals, **http://bly.colorado.edu/links/physlink.html**
- Companies which produce LC's devices,
  http://www.spectraswitch.com
  http://www.meadowlark.com
  http://www.displaytech.com
  http://www.digilens.com
  http://www.jenoptik.de
  http://www.nemoptic.com
  http://www.calctec.com
- Internationa Telecommunication Union (ITU), **http://www.itu.int**

List of Figures

List of Tables

List of Abbreviations

BG	Bragg Grating
CLC	Cholesteric Liquid Crystal
DBR	Distributed Bragg Reflector
DFB	Distributed Feedback Laser
DSM	Dynamic Single Mode
DWDM	Dense Wavelength Division Multiplexing
EDFA	Erbium Doped Fiber Amplifier
FLC	Ferroelectric Liquid Crystal
H-PDLC	Holographic Polymer Dispersed Liquid Crystal
ITO	Indium Tin Oxide
LC	Liquid Crystal
LCD	Liquid Crystal Display
NIR	Near Infra Red
NLC	Nematic Liquid Crystal
PBG	Photonic Bandgap
PDLC	Polymer Dispersed Liquid Crystal
PIPS	Polymerization Induced Phase Separation
POLICRYPS	Polymer Liquid Crystal Stripes
SSFLC	Surface Stabilized Ferroelectric Liquid Crystals
UV	Ultra Violet
WDM	Wavelength Division Multiplexing